Investigation on Influence of Cross-sectional Shape on Behaviour of Concrete Filled Double Skinned Steel Tubular Short Columns

THESIS

Submitted in partial fulfilment

of the requirements for the degree of

DOCTOR OF PHILOSOPHY

by

Manigandan R

ID No. 2018PHXF0444P

Under the Supervision of

Prof. Manoj Kumar

BITS Pilani
Pilani | Dubai | Goa | Hyderabad

BIRLA INSTITUTE OF TECHNOLOGY AND SCIENCE,

PILANI

2023

BIRLA INSTITUTE OF TECHNOLOGY & SCIENCE

PILANI – 333 031 (RAJASTHAN) INDIA

CERTIFICATE

This is to certify that the thesis entitled "**Investigation on Influence of Cross-sectional Shape on Behaviour of Concrete Filled Double Skinned Steel Tubular Columns**" submitted by **Manigandan R.**, ID No. **2018PHXF0444P** for award of Ph.D. of the Institute embodies original work done by him under my supervision.

_____

Signature of the Supervisor

Name: **Prof. Manoj Kumar**

Designation: Professor

Date: 08/07/2023

DEDICATION

This thesis is dedicated to my mother, who made my
dream a reality

Acknowledgment

I express sincere gratitude and indebtedness to my guide, **Prof. Manoj Kumar**, Associate Professor, Department of Civil Engineering, BITS Pilani, Pilani Campus. He has been a constant source of inspiration throughout my work. The enthusiasm, moral support, and advice that he has given me will stimulate me to be the best in my endeavors. I sincerely acknowledge the help rendered by him at all times.

I express my deep appreciation to BITS Pilani for providing all the necessary facilities and support to complete the research work. My special thanks to **Prof. S. Bhattacharyya**, Vice-Chancellor of the University, and **Prof. S. K. Barai**, Director, BITS-Pilani, Pilani Campus, for allowing me to pursue my research work successfully. I also express my gratitude to **Prof. Shamik Chakraborty**, Associate Dean, Academic Research, and other faculty members of ARD for providing valuable support throughout the programme. I would like to take this opportunity to express my gratitude to Dr. G. Muthukumar and Dr. Rajesh Kumar, who are members of the Doctoral Advisory Committee (DAC), for their kind suggestions, motivation, and moral guidance and support throughout the program, both technically and personally. I would like to thank **Prof. Anshuman** (former HOD) and **Prof. Anupam Singhal,** HoD, Civil Engineering, for their support and motivation during difficult times**.**

I am also thankful to all my professors for their support and motivation throughout my studies at BITS-Pilani, Pilani Campus. Thanks to all the non-teaching staff of the Department of Civil Engineering, Mr. Ramesh Das (workshop), Mr. R. D. Soni, Mr. Jaspal, Mr. Suresh Saini, and Mr. Kamal for their constant co-operation throughout my work. I also thank all my friends and colleagues, especially Mr. Dhanesh Kumar, Mr. Hrishikesh N. Shedge, Mr. Danish Khaki, Mr. Kathir Vadivel, Ms. Srishti Khare, Mr. Farhan Mohammad

Khan, Mr. Jaya Kumar Bhaskar, and all others whose name are not here and have helped me during my Ph.D. Thanks to all BITS-Pilani faculty and staff members, Pilani Campus, for helping me at various times.

I express my hearty gratitude to my beloved mother and sister for their care and affection shown towards me on this journey. I owe thanks to my family members for their love, encouragement, and moral support, without which this work would have been impossible. My parents have always been supportive, and their encouragement in all my endeavors from the beginning has always inspired me. I am grateful to Almighty God, whose blessings this thesis has seen the light of day. May, I would cherish the happy moments spent at the BITS Pilani campus for my whole life.

Manigandan R.

Abstract

The scarcity of land available for construction and its skyrocketing prices have resulted in the vertical development of towns and cities. The high-rise structures are subjected to combined loading and necessitate high axial and lateral strengths. The conventional reinforced concrete (RC) columns subject to high axial and lateral loads necessitate a larger section area and a significant amount of steel. The Indian design code (IS 456, 2000) limits the maximum amount of steel in RC columns to 6% to avoid the congestion of steel bars; however, from practical considerations, the maximum amount of reinforcement is normally limited to 4%. To achieve the column's large axial and lateral strengths as well as to attenuate induced drift from wind and seismic loads, structural engineers prefer the use of composite sections in high-rise structures. Various composite sections are being used in columns of the high-rise structure, but concrete-filled steel tubular (CFST) columns are preferred for several advantages. In order to further increase the axial compressive strength of CFST columns without increasing the column's outer dimensions, concrete-filled double-skin tubular (CFDST) columns are used. Usually, circular section CFDSTs are used as they offer a better confinement effect to concrete; however, sometimes, it becomes essential to adopt a non-circular shape of the column due to geometrical constraints, aesthetic requirements, etc. The strength of a CFDST column width given dimensions can be increased by decreasing the aspect ratio of steel tubes; however, this technique of increasing the column's strength is helpful up to a specific strength limit only because steel tubes with the desired aspect ratio are not always readily available. This study proposes concrete-filled multi-skin tubular (CFMST) columns to address this issue. The new concept of the CFMST column suggested in this study is both innovative and cost-effective. To this end of the study, the structural behaviour of circular and square section columns with four inner square tubes is investigated.

Broadly the research conducted in this study is divided into two phases. The first phase of this study aims to evaluate the impact of outer and inner steel tube shapes and their aspect ratio on the structural response of CFDST column specimens experimentally and numerically. Experimental and numerical investigations are carried out to evaluate the structural response of concrete-filled multi-skin tubular columns in the second phase of this study. In this study, ABAQUS is used to create and analyze the CFDST specimens. The numerical results are compared with the experimentally observed data, and they are found to be reasonably close. The study found that the failure mode of the axially loaded CFDST columns with different sections was identical. The failure mode of these sections was a combination of local buckling in outer and inner steel tubes followed by crushing of concrete and slipping between the sandwiched concrete and outer steel tubes at the locations of outer tube local bucking. When the structural response of eccentrically loaded CFDST columns with circular, rectangular, and octagonal sections was compared, it was noticed that, in general, the geometric shapes of the inner steel tube and the magnitude of eccentricity have no significant effect on the failure mode of the column specimens. Though, the buckling pattern of the outer steel tube in CFMST columns under the concentric and eccentric load cases was almost similar to that of CFDST column specimens. However, the CFMST columns exhibited more bulging compared to the CFDST columns. On the other hand, the study has revealed that compared to CFDST columns, the CFMST columns are less sensitive to the eccentricity of the load.

Keywords: Concrete-filled double skin tube (CFDST); Concrete-filled multi-skin tube (CFMST); Experimental Testing; Eccentric Loading; Finite Element Analysis, Failure Mechanism, Parametric Sensitivity Analysis: Comparative Analysis.

Table of Contents

List of Figures

List of Tables

List of Symbols

a_o Side length of the external square steel tube

a_i Side length of the internal square steel tube

a Side length of octagonal steel tube

A_c Cross-sectional area of concrete

A_{ce} Nominal cross-sectional area of concrete

A_k cross-sectional area of the hollow section

A_{soc} Cross-sectional area of the outer tube and the sandwich

       concrete $(= A_{so} + A_c)$

A_s Cross-sectional area of steel

A_{si} Cross-sectional area of inner steel tube

A_{so} Cross-sectional area of outer steel tube

B_o Outer major axis width of inner elliptical steel tube

b_i Outer minor axis width of inner elliptical steel tube

C_1 Circular CFDST column

D_{oc} Outer dimension the octagonal steel tube

D_o Outer dimension (width/diameter) of outer

       elliptical/circular steel tube

d_i	Outer dimension (width/diameter) of inner elliptical/circular steel tube
E_c	Modulus of elasticity of concrete
E_s	Modulus of elasticity of steel
f_c	Cylindrical compressive strength concrete ($= 0.8\, f_{cu}$)
f_{ck}	Characteristic concrete strength ($f_{ck} = 0.67\, f_{cu}$ for normal strength concrete)
f_{cu}	Cube Compressive Strength of concrete
f_{si}	Yield strength of inner steel tube
f_{so}	Yield strength of outer steel tube
f_{scy}	Combined strength of steel and concrete
f_y	Yield strength of steel tube
L	Length of CFDST column
N_{ue}	Experimental ultimate compressive axial eccentric load
$N_{u/0,(Exp)}$	Experimental ultimate compressive axial concentric load
$N_{u,(FEM)}$	FE predicted ultimate compressive axial load
$N_{ue,(FEM)}$	FE predicted ultimate compressive eccentric load
t_o	Wall thickness of outer steel tube
t_i	Wall thickness of inner steel tube

σ	Stress values
ε	Strain values
ξ	Nominal confinement factor $\left(= \dfrac{A_{so}}{A_c} \cdot \dfrac{f_{yo}}{f_{ck}}\right)$
ψ	Hollow ratio of CFDST column$\left(= \dfrac{A_k}{A_C - A_k}\right)$
α	Real steel ratio $(= A_{so}/A_c)$
α_n	Nominal steel ratio $(= A_{so}/A_{ce})$
μ_c	Poisson's ratio of concrete core
μ_s	Poisson's ratio of steel tube

Chapter -1
Introduction

1.1.Background

Despite being the world's second most populous country, India's geographical landscape accounts for only 2.4% of the world's surface area. As a result, the limitation of the construction area has been the root cause of the vertical development of towns and cities. High-rise structures subjected to combined loading necessitate high axial and lateral strengths. The conventional reinforced concrete (RC) columns subject to high axial and lateral loads require a larger section area and demand a huge amount of steel. The Indian design code (IS 456, 2000) restricts the maximum amount of steel in RC columns to 6% to avoid the congestion of steel bars; however, from practical considerations, the maximum amount of reinforcement is normally limited to 4%. To achieve the column's large axial and lateral strengths and also to attenuate induced drift from wind and seismic loads, structural engineers prefer the use of composite sections in high-rise structures. A variety of composite sections are being used in columns of the high-rise structure; however, the concrete-filled steel tubular (CFST) columns are preferred as they are more efficient (Tiziano *et al.,* 2013). The steel tube in the CFST columns acts as longitudinal as well as transverse reinforcement and also serves as formwork. Since the steel in CFST columns is located in the outermost layer, farthest away from the column's centroid, it significantly increases the section's moment of inertia and column's moment resisting capacity. The concrete core in the CFST column not only adds stiffness and compressive strength to the tubular column but also reduces the potential for inward local buckling of steel tubes (Morino *et al.,* 2015). For a given axial load, the cross-section of the CFST column may be reduced by up to 40% compared to the conventional RC column (Goode, Kuranovas and Kvedaras, 2010). As a result, the CFST columns have excellent

structural performance and are more cost-effective than conventional RC columns due to lower material and labour costs (Zhao, Grzebieta and Elchalakani, 2002). In the CFST columns, the percentage of steel, commonly referred to as steel ratio, may be increased to achieve desired strengths as the increase in steel tube area in CFST columns not causes any practical difficulty during construction. Normally, the circular section CFSTs are used; however, in certain circumstances, it becomes essential to adopt a non-circular shape of the column due to geometrical constraints, aesthetic requirements, etc. The various well-established non-circular shapes of the CFST columns are square, octagonal, and elliptical, as shown in Fig. 1.1.

(a) Circular   (b) Square
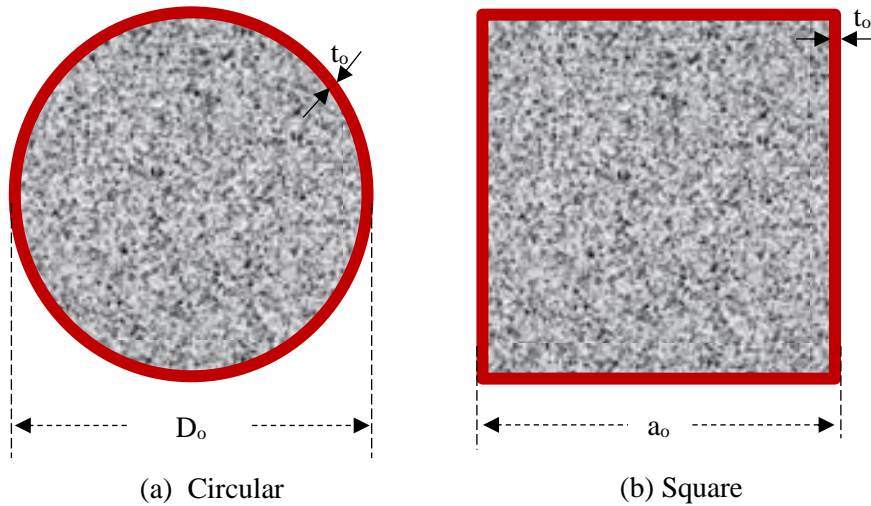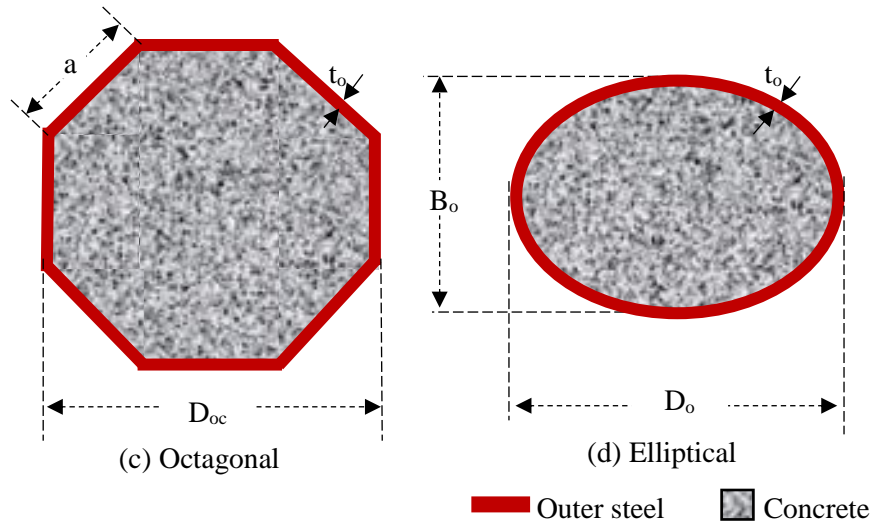
Fig. 1.1 A schematic view of CFST columns

    To further increase the axial compressive strength of CFST columns without increasing the column section, various steel elements, such as steel bars, I-section, steel tubes, and so on, are embedded in the infill concrete of CFST columns. The CFST columns, combined with the internal tube embedded in concrete, are called Concrete Filled Double Tube (CFDT) columns. The concrete filled within the internal tube of a CFDT column does not play a significant role in enhancing the column's strength; therefore, to reduce the self-weight of the column, the internal tube is left empty, and these columns are referred to as Concrete Filled Double Skin Tubular (CFDST) columns. Usually, CFDSTs with circular cross-sections are preferred due to a better confinement effect developed from the outer and inner tubes, as shown in Fig. 1.2 (a). Sometimes, it becomes essential to adopt a non-circular shape of the column due to geometrical constraints, aesthetic requirements, etc. The various well-established non-circular shapes of the CFDST columns are square, octagonal, and elliptical, as shown in Figs. 1.2 (b-d). For the regular polygonal cross-section (square, hexagonal, octagonal), the shape of the internal tube is normally selected as circular (Figs. 1.2 (b-c)); however, for the elliptical CFDST columns, the internal tube is taken elliptical in order

3

to achieve an equal confinement effect throughout the periphery of the column (Fig. 1.3d).

(a) Circular

(b) Square

(c) Octagonal

(d) Elliptical

Outer steel   Inner steel   Concrete
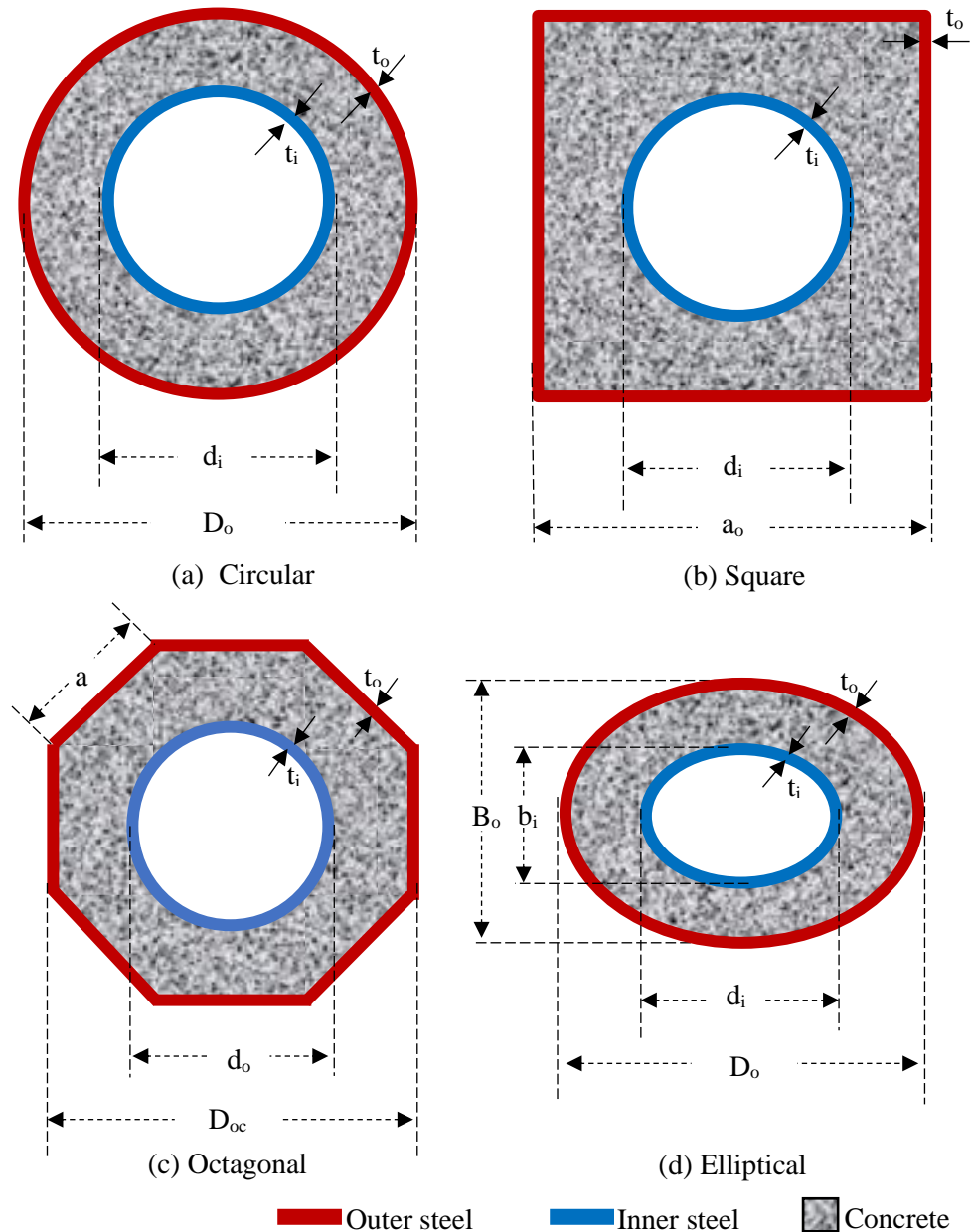
Fig. 1.2 Schematic view of CDFST columns

One of the most representative applications of concrete-filled tubular columns is the Goldin Finance 117 tower in China which has a total height of

597 m. In this tower, mega columns are located at the four corners of the building, and the section of columns is Hexagonal. Fig. 1.3(a) shows the Gaoyin Finance 117 tower, and the section of the mega column is shown in Fig. 1.3(b). The multi-cell steel tubular columns have a better confinement effect than traditional steel tubes. The use of the CFST section results in sufficient lateral resistance capacity against earthquake and wind loads (Yin *et al.,* 2022).
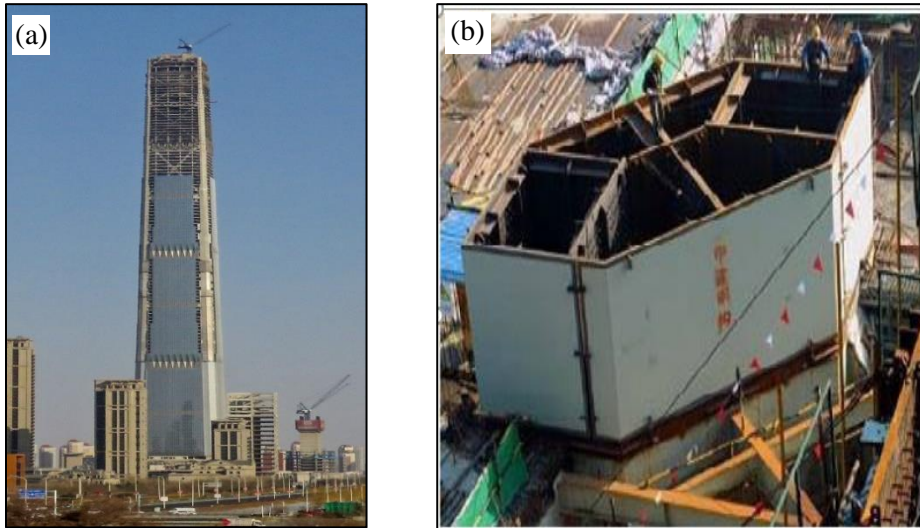
Fig. 1.3 Tianjin Goldin Finance 117 tower in China (under construction),
(a) Elevation

1.1.1. Concrete Filled Steel Tubular (CFST) Columns

The steel tube in the CFST Columns exerts lateral compressive pressure on the concrete, which is referred to as a lateral confinement effect. The magnitude of lateral confining pressure in CFST columns depends on the steel tube diameter-to-thickness ratio, column section shape, and steel grade. The lateral confining pressure boosts the compressive strength of infill concrete, which improves the compressive strength of CFST columns. In addition to axial strength, the lateral confinement effect enhances the ductility of the infill concrete (Zhao *et al.,* 2002) and increases the section stiffness (Gardner *et al.,* 1967; Elchalakani *et al.,* 2016). Furthermore, the drying shrinkage and creep of concrete infill in CFST columns are lower than in conventional RC columns.

5

With the advancements in concrete technology and steel manufacturing, in recent years, high-strength steel tubes filled with high-strength concrete are being used in Japan and Europe to increase the load-carrying capacity of CFST columns.

1.1.2. Concrete Filled Double Skinned Tubular (CFDST) Columns

The concrete filled between the outer and inner tube in CFDST columns behaves as a sandwich concrete and experiences lateral confining pressure from both tubes; consequently, the sandwiched concrete exhibits enhanced compressive strength (Morino and Tsuda, 2002). The existence of internal hollow steel tubes and the improved compressive strength of concrete significantly reduce the column size even for larger loads. In addition to contributing to column strength loads, the concrete core in CFDST columns effectively restrains and delays local buckling of the steel tubes. Additionally, the steel tubes act as longitudinal reinforcement, confining the concrete and controlling the damage to the concrete. The composite action between the outer and inner steel tubes and the sandwiched concrete increases the section modulus and bending stiffness of the CFST column, resulting in superior structural performance under axial loads for the CDST columns. Several studies have shown that when subjected to gravity loads in conjunction with seismic loads, CFDST columns outperform CFST columns (Guerrini *et al.*, 2015; Ukanwa *et al.*, 2018). Besides, CFDST columns have enhanced stability under external pressure, better damping characteristics, and improved cyclic performance (Han *et al.*, 2004; Yu, Ding and Cai, 2007; Tao *et al.*, 2008; Han *et al.,* 2010; Uy *et al.,* 2011). Additionally, CFDST columns are found to limit the overall inter-story drift ratio within the serviceability limit (Ding *et al.*, 2021). Furthermore, CFDST columns display better fire performance than CFST due to the inner steel tube being shielded by concrete as a low thermally conductive material during a fire (Lu *et al.,* 2007). The synergy between the steel tubes

and concrete core results in a more redundant section as a result column fails only when all three layers of materials fail.

The central opening of the section not only reduces the self-weight of the column but also provides spaces for facilities such as power cables, drainage pipes, and telecommunication lines where needed. The bare steel sections comprising outer and inner tubes only offer support for the initial construction before placing the infilled concrete. Furthermore, the CFDST columns do not need formwork in construction, and the concrete is directly placed between the outer and inner steel tubes. As a result, the CFDST members are found to be economical and quicker to construct compared to conventional RC members.

Although the CFDSTs were initially introduced as a modern construction technique for deep-water vessels to resist external pressure (Montague, 1975), however, owing to aforesaid advantages, the use of CFDST is widely spread worldwide in tall buildings where columns are subjected to lateral loads due to wind and earthquakes. CFDST columns are preferred in buildings because they keep the overall inter-story drift ratio within the serviceability limit (Ding *et al.*, 2021). Besides, due to high lateral resistance and better ductility, CFDSTs are also used in wind turbines to protect them from the high lateral wind load (Goode e*t al.,* 2010). Its application has extended to constructing the legs of off-shore structures to diminish stability concerns in hollow steel tubes (Wei *et al.*, 1995). Additionally, CFSTs are also used in transmission towers as they provide material and construction cost reserves (Li *et al.,* 2012). As a result of their superior physical characteristics, CFDSTs are increasingly being used as load-bearing structural components in the construction of modern skyscrapers and bridge piers around the world (Kawaguchi *et al.*, (2009); Uenaka *et al.,* (2010); Wang *et al.,* (2014); Zhang *et al.*, (2015)).

The compressive strength of a given size of CFST column can be increased by using high-strength materials, increasing the diameter of the inner

tube, and increasing the thickness of the outer and inner tubes. The strengths of materials and diameter on the inner tube cannot be increased beyond certain limits, and the thickness of the tube may be increased only up to the maximum available tube thickness.

1.1 Motivation

The RC columns designed for large axial loads and moments require large sections and a huge amount of longitudinal steel, which leads to congestion of longitudinal steel reinforcement. Sometimes, it becomes challenging to place the desired number of steel bars near the periphery of the column by maintaining a minimum clear spacing between the bars specified by design codes. According to IS 456 (2000), the spacing between the individual longitudinal bars should not be less than the diameter of a larger bar and also the nominal maximum size of coarse aggregate plus 5 mm, which sometimes becomes impossible, especially in small section columns. Therefore, when a large number of bars are to be accommodated in a column, it becomes necessary to bundle the bars into groups of two, three, or four. Normally, the longitudinal bars in the columns are bundled into a group of four bars, as shown in Fig. 1.4 as recommended by IS 456 (2000).
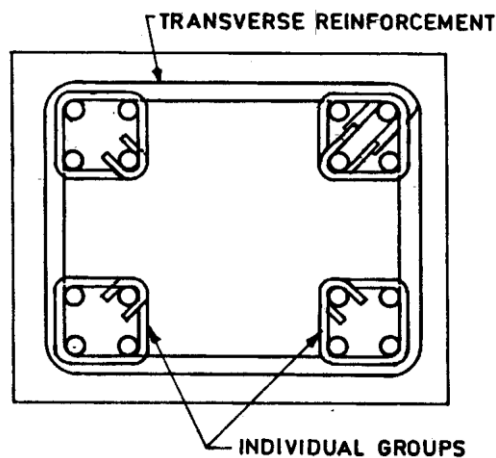
Fig. 1.4 A schematic view of Bundled bars in RC columns [IS 456, 2000]

Moreover, the code recommends that the bundled bars be enclosed within stirrups or ties and that the spacing of hoops not exceed half the column's least lateral dimension unless special confining reinforcement is provided according to IS 13920 (1993). Furthermore, IS 456 (2000) recommends the use of bundled bars for earthquake-resistant construction. Reinforcement detailing and column construction with bundled bars become time-consuming and tedious. For the ease of construction of the columns under high compressive loads, the present study proposes the use of CFST columns in conjunction with multiple inner hollow steel tubes in place of RC columns with bundled bars. Since the presence of an inner hollow steel tube in CFST columns introduce a skin to the CFST section, the CFST columns containing multiple internal steel tubes are referred to in this study as Concrete Filled Multi Skin Tubular (CFMST) Columns. According to practical engineering requirements, the geometric shapes of inner hollow steel tubes in the CFMST columns can be circular or square, and the number of internal steel tubes can be two or more (Zhao *et al.,* 2002). Analogous to bundled bar columns shown in Fig. 1.5, this study intends to consider four square shape inner tubes in outer circular and square section columns as shown in Fig.1.5. It is expected that there will be an excellent potential for CFMST members to be employed in various engineering projects over the upcoming decades. However, the lack of understanding of structural performance and relevant design specifications is one of the main issues hindering the broad application of CFMST members in practical engineering.
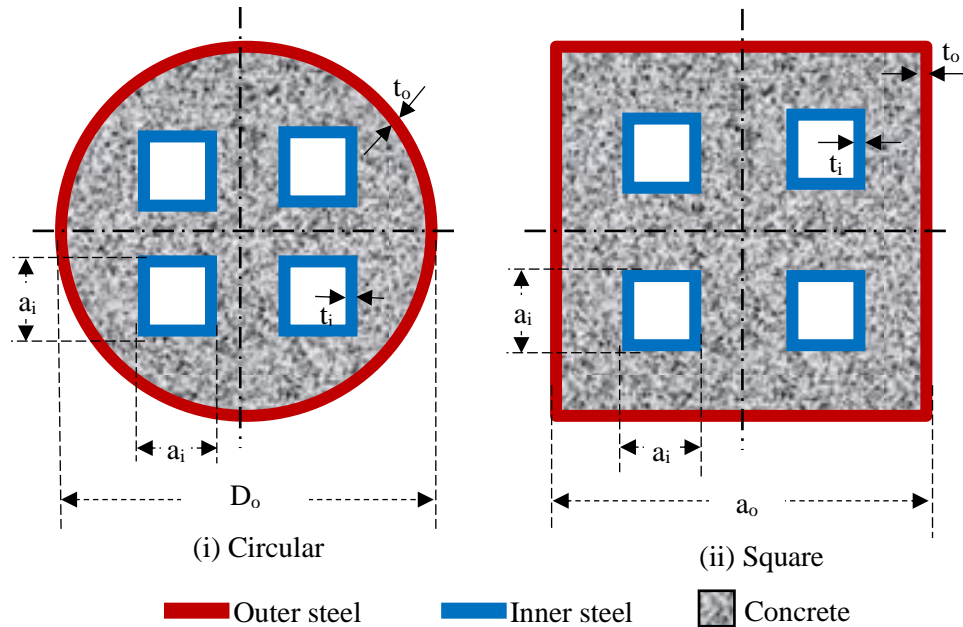
Fig. 1.5 A schematic view of CFMST column Sections

1.2 The problem statement in broad terms

The use of CFDST columns is increasing day by day since it has several merits over conventional RC and CFST columns. Although research on CFDST columns began in the 1980s, significant progress has been made and continues to be made in the last few decades. Following a thorough review of the literature on CFDST members, the gaps identified are listed below.

- Most studies on CFDST short columns under concentric and eccentric loads have been limited to circular and square shapes; thus, there is a need to investigate the structural response of axially and eccentrically loaded CFDST columns with other cross-section shapes.

- Only a few studies have been conducted to evaluate the effect of the inner steel tube's aspect ratio on the bearing capacity of CFDST columns of various sections. The effect of the inner tube's aspect ratio on the behaviour of the CFDST columns with different sections must be investigated in order to better understand the behaviour of CFDST columns under axial and eccentric loadings.

- The bearing strength of a conventional RC column of a given size may be increased with the use of bundled bars. Because building RC columns with bundled bars is a time-consuming and labor-intensive process, CFDST columns with high aspect ratio tubes are preferred over bundled bar columns. However, the strength of CFDST columns can be increased to a certain limit because steel tubes with the desired aspect ratio are not always readily available. To address this issue, concrete-filled multi-skin tubular (CFMST) columns are proposed in this study, and there is a need to investigate the structural response of CFMST columns.

1.3 Aim of the present investigation

The present research work primarily intends to explore and compare the structural behavior of CFDST columns with different geometries and configurations. The major objectives of the study are:

- To generate a database of experimental results for the CFDST column of various cross-sections under axial and eccentric loads.
- To develop a nonlinear finite element numerical model to assess the axial load versus deformation response of CFDST columns with different cross-sections under axial and eccentric loads and to validate the numerically obtained results with the experimentally observed data.
- To investigate the influence of shape and aspect ratio of outer and inner steel tubes on the structural response of axially and eccentrically loaded CFDST columns.
- To explore the structural behavior of the CFMST columns numerically under axial and eccentric loading conditions and to compare numerically obtained results with those observed experimentally.

1.4 Outline of the thesis

In order to study the structural behavior of CFDST columns with different cross-sections and to investigate the structural response of CFMST columns, the thesis is divided into seven chapters. The outline of the various chapters is discussed below.

Chapter 2: A detailed literature review on the behaviour of the CFST and CFDST columns with failure mode of local bucking under the axial and eccentric loading conditions with comparative numerical studies is given in this chapter.

Chapter 3: The characterization of material used in this study and types of tests conducted to obtain the material properties and experimental step-up of this study with the result of material properties is discussed in a detailed manner.

Chapter 4: Numerical investigation is carried out on CFDST and CFMST with different cross-sections. The detailed input parameters, such as element types, meshing, and methods to model the material properties, are briefly derived and discussed.

Chapter 5: Investigation of CFDST columns with different cross-sections under axial loads is done. The load-carrying capacity of the CFDST column with the mode of failure is discussed, and experimental results are compared with numerical analysis.

Chapter 6: Investigation of CFDST columns with different cross-sections under eccentric loads is done. The load-carrying capacity of the CFDST column with the mode of failure is discussed, and experimental results are compared with numerical analysis.

Chapter 7: Investigation of CFMST columns with circular and square cross-sections under axial and eccentric loads is done. The load-carrying capacity of the CFMST column with the mode of failure is discussed, and experimental results are compared with numerical analysis.

Chapter 8: This chapter concludes the thesis by providing significant finds and contributions along with the scope for future research work

1.5 Scope of the present investigation

- Designers may get confident in adopting CFDST columns subjected to axial and eccentric loads

- The researcher may get an overview of the different cross-sections of CFDST columns suitable for better performance under axial and eccentric loading conditions.

- The designer recommends using CFMST in place of RC columns with bundled bars to withstand heavy axial and eccentric loads.

Chapter – 2

Literature Review

2.1. Background

Concrete and steel are two of the most extensively used construction materials in modern engineering structures. Usually, these two materials work together as a structural element in engineering practice. The most common elements are reinforced concrete and steel-concrete composite structures. Steel-concrete composite structure refers to structures that use steel and concrete formed together into a component so that the resulting arrangement functions as a single item (Gardner and Nethercot, 2004).

A steel-concrete composite structure is a structural system that consists of one or more composite components. The typical composite components are composite beam, floor, and column. The origin of the composite beam, floor, and column dates back 100 years ago. With the development of construction technologies and research in composite structures, composite beams and floor systems were well accepted by the 1960s worldwide (Gardner and Nethercot, 2004a, 2004b). However, the development of composite columns fell far behind. Even in the 1990s, most of the steel bridges and buildings in the USA were constructed with composite beams or girders, but only a few were built using composite columns.

2.1.1. Experimental Studies on behaviour of CFST columns

The first experiment on the ultimate strengths of CFST columns was carried out by Klöppel and Goder (1957). Further tests on CFST short columns were conducted by Furlong (1967), who tested eight circular CFST columns and five square CFST columns under axial and eccentric loads. The depth-to-thickness ratio ranged from 29 to 98 of the tested CFST columns. They found that the steel and concrete components independently resisted the axial load applied to the CFST column. The influences of the steel tube thickness of CFST

columns were examined on the ultimate axial loads. Experimental results indicated that the thick-walled steel tube offered confinement to the concrete core in a CFST column. This confinement effect increased the concrete strength in circular CFST columns. A rectangular steel tube provided less confinement to the concrete core than a circular steel tube. The thin-walled steel tubes of CFST beam-columns locally buckled outward due to the restrains provided by the infilled concrete. It was suggested that a CFST column cross-section could be treated as a reinforced concrete section for determining the axial load-moment interaction diagrams.

Tests were conducted by Knowles and Park (1969) to investigate the effects of concrete confinement on the behavior of circular and square CFST beam-columns with various column slenderness ratios and depth-to-thickness ratios. They studied 12 circulars and 7 square CFST columns with depth-to-thickness ratios of 15, 22, and 59. Test results suggested that the confinement of the concrete core provided by the steel tube in a square CFST column increased the ductility of the concrete core but not much influenced its ultimate strength. On the other hand, confinement provided by the steel tube increased the compressive strength and ductility of the concrete core in a circular CFST beam-column. However, this confinement effect was shown to decrease with increasing column slenderness. This contributed to the fact that the column failed by buckling before the strain caused an increase in the concrete compressive strength. All CFST columns tested under axial load failed by column buckling. Local buckling was not observed in all tested CFST columns. The concrete failure appeared after the maximum load was reached. The straight-line interaction formula for eccentrically loaded CFST columns was conservative for short columns and unsafe for slender columns. It was concluded that the tangent modulus method gave a good prediction of the strengths of columns with L/D ratios greater than 11 but a conservative prediction for columns with L/D ratios less than 11.

15

The experimental behavior of pin-ended normal strength square CFST slender beam-columns under axial load and uniaxial bending was investigated by Bridge (1976). A series of slender column tests were performed to examine the effects of loading eccentricity, steel tube thickness, column slenderness ratios, and uniaxial bending on the behavior of the slender beam-columns. The test specimens were made of normal-strength steel tubes and concrete. Initial geometric imperfections at the mid-height of the specimens were measured. Test results revealed that the ultimate axial strength of CFST beam-columns increased with the steel tube thickness. Increasing the loading eccentricity ratio decreased the ultimate axial strengths of CFST beam-columns. In addition, increasing the column slenderness ratio reduced the ultimate axial strengths of CFST beam-columns. The maximum axial compressive strengths and axial load vs. deflection curves were compared with those predicted by an inelastic stability analysis technique developed by Roderick and Rogers (1969). His tests did not identify the local buckling of the steel tube walls for CFST slender beam-columns.

Shakir-Khalil and Zeghiche (1989) tested rectangular CFST slender columns in single curvature bending. These CFST columns were subjected to axial load and uniaxial bending. The axial load was applied at an eccentricity about the major or minor axis. Seven CFST slender beam-columns were tested for failure. One of these columns was tested under a concentric axial load. The slender beam-columns were constructed from cold-formed steel tubes and normal-strength concrete. The steel yield strengths varied from 343 MPa to 386 MPa, while the concrete compressive strength varied from 40 MPa to 45 MPa. Specimens were fabricated from 5 mm thick steel tubes so that their depth-to-thickness ratio was 24. Although the initial geometric imperfection was not measured in the study, the effects of initial geometric imperfection on the ultimate axial strengths of CFST beam-columns were recognized. Experimental results were compared with the design loads calculated by BS5400 (1979) and

16

finite element analysis. The experimental ultimate axial loads, axial load-deflection curves, and failure modes of rectangular CFST beam-columns were reported. It was observed that all tested CFST columns failed by overall column buckling. The local buckling of the steel tube walls was not observed in all tested columns. Shakir-Khalil conducted tests on normal-strength rectangular CFST slender beam-columns under uniaxial bending Shakir-Khalil and Mouli (1990). Three different rectangular CFST column cross-sections were used in their study such as $120 \times 80 \times 5$ mm, $150 \times 100 \times 5$ mm, and $250 \times 150 \times 6.3$ mm. The yield strength of the steel section varied from 340 MPa to 363 MPa, while the concrete compressive strength ranged from 35 MPa to 40 MPa. The test results showed that the ultimate axial strength of the CFST slender beam-columns significantly increased when a larger steel section was used. It was found that the steel tube walls were pushed out by the crushed concrete, which took the shape of the deformed steel section.

The behavior of circular and square CFST columns under axial and uniaxial bending was investigated experimentally by Matsui *et al.,* (1995). These columns were made of steel tubes with a yield strength of 445 MPa filled with 32 MPa concrete. The steel tube had a depth-to-thickness ratio of 33. Test parameters included concrete compressive strengths, buckling length, depth-to-thickness ratio, and loading eccentricity. A total of sixty columns were tested, including twelve hollow steel tubular columns under axial load. The columns were loaded through hemispherical oil film bearing so that they were pin ended in the bending plane. The design strengths calculated from AIJ (Architectural Institutive of Japan 1997), modified AIJ, and CIDECT (Committee International for the Development and the Study of Tubular construction) design methods were compared with experimental ultimate axial strengths. It was found that the AIJ design method yielded conservative predictions of the ultimate strengths of slender beam-columns. Test results indicated that increasing the loading eccentricity reduced the ultimate axial strengths of the

beam-columns. The effects of the loading eccentricity on the ultimate axial strengths of CFST beam-columns were shown to reduce with an increase in the column slenderness ratio. The mid-height deflection at the ultimate axial strength of the slender beam-column increased with an increase in the loading eccentricity. The axial load-moment-interaction diagrams obtained from tests were compared with those predicted by AIJ and CIDECT for circular and square CFST beam-columns. The beam-columns with a length-to-depth ratio greater than 18 could not attain the full plastic moment at the maximum load due to the overall column buckling.

Shams and Saadeghvaziri (1997) presented a state-of-the-art review of CFST columns. They highlighted the experimental and analytical studies on the design and behavior of CFST columns. The behavior of circular and rectangular CFST beam-columns under various loading conditions was discussed in their study. The effects of the cross-section shape, width-to-thickness ratios, and column slenderness ratios on the performance of CFST beam-columns were summarized. It was found that the confinement of the concrete core provided by the steel tube increased the strain on the concrete. It was observed that steel plates buckled outward on one of the sides of a column before the ultimate axial strength was reached. The remaining sides of a column cross-section were buckled after the ultimate load was attained. The steel plates were buckled outward on four sides of a column with large width-to-thickness ratios. In addition, local buckling of the steel tube occurred after crushing the concrete core.

The experimental study of axially loaded short CFST columns with a depth-to-thickness ratio ranging from 17 to 50 was undertaken by Schneider (Schneider, 1998). He tested fourteen specimens to examine the effects of steel tube shape and tube wall thickness on the ultimate axial strengths of CFST columns. All steel boxes of the specimens were cold-formed carbon steel and were seam welded and annealed to relieve residual stresses. The yield strength

of the steel section varied from 322 MPa to 430 MPa, and the compressive concrete strength ranged from 23 MPa to 30 MPa. Test results indicated that the post-yield strength and stiffness of circular CFST columns were higher than those of square or rectangular CFST beam-columns. Local buckling of circular steel tubes occurred at an axial ductility of 10 or more, while square and rectangular tubes buckled locally at a ductility ranging from 2 to 8. Circular steel tubes possessed higher post-yield axial ductility and strength than square or rectangular concrete-filled tube sections. All circular CFST columns displayed the strain hardening which occurred in rectangular CFST columns with $D_t/20$. The confinement provided by the steel tube only occurred after the axial load reached about 92% of the column yield strength. The yield load of a CFST column was found to increase significantly with decreasing the depth-to-thickness ratio.

Bridge and O'Shea (1994) studied experimentally the behavior of axially loaded thin-walled steel box sections with or without concrete infill. The width-to-thickness ratios of these sections ranged from 37 to 131, while the length-to-width ratios of the columns ranged from 0.8 to 3. The performance of thin-walled CFST short columns was compared with that of hollow steel tubular columns. The buckling modes for a wide range of width-to-thickness ratios were examined. It was observed that the concrete core prevented the inward buckling of the steel tube. This buckling mode significantly increased the strength of the steel tubes. They suggested that the effective width formula for clamped steel plates could be used to calculate the strength of thin-walled steel tubes with concrete infill. Local buckling of the steel tubes was found to reduce the ultimate strength of thin-walled CFST short columns under axial compression.

Experimental studies on the ultimate strengths of high-strength thin-walled square CFST slender beam-columns under axial load and uniaxial bending have been conducted by *Chung et al.,* (1999). These beam-columns

were made of steel tubes with a yield strength of 445 MPa filled with 88 MPa high-strength concrete. The width-to-thickness ratio of CFST slender columns was 39, while the length of the column ranged from 2250 mm to 3000 mm. The effects of the buckling length-depth ratio and eccentricity of the applied axial load on the behavior of CFST beam-columns were studied. They found that local buckling of slender columns under concentric or eccentric loading occurred after the ultimate axial strength was attained, while local buckling of short columns under concentric load occurred at the ultimate axial strength. The column with a smaller slenderness ratio had a higher ultimate strength.

O'Shea and Bridge (2000) conducted experiments to study the behavior of circular CFST short columns. These columns were tested under axial compression which was applied on either steel tube or both steel tube and concrete core at small eccentricities. The specimens had a length-to-diameter ratio of 3.5 and diameter-to-thickness ratios ranging from 60 to 220. The steel tubes were filled with high-strength concrete. The compressive strengths of the concrete cylinders were measured as 50 MPa, 80 MPa, and 120 MPa. Test results demonstrated that local buckling remarkably influenced the strength of hollow steel tubular columns. The bond between the steel tube and concrete was shown to be critical in determining the local buckling mode. The sufficient bond between the steel tube and concrete core prevents the buckling of the steel tube. In addition, the confinement of the concrete core provided by the circular steel tube was affected by the loading conditions. The effect of the confinement increased with increasing the axial load applied to the concrete core. Design methods were suggested for determining the strength of circular CFST columns subjected to various loading conditions. The strengths obtained from these design methods were compared with experimental strengths. A comparison was also conducted between the design method and Eurocode 4. They reported that Eurocode 4 provided conservative strength predictions for circular steel tubes

filled with concrete strength up to 50 MPa and subjected to axial load and bending.

Han *et al.,* (2002) investigated the influences of constraining factors and the depth-to-width ratios on the ultimate strength and ductility of axially loaded rectangular CFST columns. A total of 24 CFST columns were tested. The main variables examined in the test program were the constraining factor and depth-to-width ratio. The width of the steel tubes varied from 70 mm to 160 mm, while the depth of the steel tubes ranged from 90 mm to 160 mm. The short columns were constructed with steel tubes filled with high-strength concrete of 60 MPa. The steel yield strength varied from 194 MPa to 228 MPa. He reported that the axial strength and ductility of CFST columns decreased with an increase in the depth-to-width ratio but increased with an increase in the constraining factor. A confinement factor was proposed for determining the section performance of composite columns. Still, it did not consider the effects of b t ratios on the behavior of composite sections.

Zhang *et al.,* (2005) presented test results of 8 high-strength CFST beam-columns subjected to axial load and uniaxial bending. A 150×150 mm cross-section was used in the tests. Test parameters included column slenderness ratios, steel ratios, and loading eccentricity. Test specimens were made of high-strength concrete with a compressive strength of 94 MPa and steel tubes with yield strengths of 316 MPa or 319 MPa. Their test results indicated that increasing the column slenderness ratio and loading eccentricity reduced the ultimate axial strengths of CFST beam-columns. The ultimate axial strengths of CFST beam-columns decreased with increasing the steel ratio.

Han *et al.,* (2003) conducted several tests to study the behavior of rectangular CFST short columns under long-term sustained loading. They investigated the effects of steel ratios, long-term sustained load level, slenderness ratio, the strength of the materials, and depth-to-thickness ratio on the ultimate strengths of CFST columns. A theoretical model given in ACI

21

codes (ACI, 2014) was used to compare the predicted behavior of CFST columns under long-term loading. It was found that the axial strain due to long-term sustained loading affected the results and tended to stabilize after about 100 days of loading. The strength index decreased as the slenderness ratio, and the concrete strength increased when the slenderness ratio was less than 10. The maximum strength reduction due to long-term loading effects was approximately 20% of the strength under short-term loading. Han and Yang (Han *et al.,* 2003) developed a set of formulas for predicting the ultimate strengths of rectangular CFST short columns with long-term sustained loading effects.

Fujimoto *et al.,* (2004) examined the effects of high-strength materials on the behavior of circular and square CFST short columns under eccentric loading experimentally. They tested CFST short columns with a wide range of parameters, including the tubes' diameter-to-thickness ratio, normal and high-strength concrete, and normal and high-strength steels. Circular steel tubes used to construct these CFST columns were cold formed from a flat plate by press welding and seam welding. The length-to-diameter ratio of the specimens was 3.0. The depth-to-thickness ratios of these specimens range from 27 to 101. The yield strengths of the steel tubes were 283, 579, and 834 MPa, and the concrete cylinder compressive strengths were 25, 41, and 78 MPa. The applied axial load ranged from 13% to 59% of the ultimate axial load of the corresponding column obtained by the theoretical model. They reported that using high-strength concrete reduced the ductility of circular CFST beam-columns. Also, using high-strength steel tubes or steel tubes with a smaller diameter-to-thickness ratio increased the ductility of circular CFST columns. It was concluded that the confinement effect did not increase the moment capacity of square CFST columns. Local buckling must be considered in evaluating the strengths of square CFST columns with large width-to-thickness ratios.

22

The behavior of axially loaded circular CFST short columns with various concrete strengths was presented by Giakoumelis and Lam (Giakoumelis and Lam, 2004). The effects of the steel tube thickness, the bond strength between the concrete and the steel tube, and concrete confinement on the behavior of circular CFST short columns were examined. They tested 15 circular CFST short columns with concrete compressive strengths of 30, 60, and 100 MPa, and depth-to-thickness ratios varied from 23 to 31. The yield strength of the steel tube was either 343 MPa or 365 MPa. The diameter of the circular CFST short columns was 114 mm. The length of the beam-columns was 300 mm. They compared various design codes for circular CFST columns. They reported that Eurocode 4 provided accurate strength predictions for circular CFST beam-columns with normal and high-strength concrete. Their results indicated that the concrete strength considerably affected the bond between the steel tube and the concrete core.

Gupta *et al.,* (2007) conducted an experimental and computational on the behaviour of circular concentrically loaded concrete-filled steel tube columns. Eighty-one specimens were tested to investigate the effect of a steel tube's diameter and D/t ratio on the load-carrying capacity of the concrete-filled tubular columns. The effect on the grade of concrete, the volume of fly ash on concrete, and the confinement effect was investigated. Diameter to thickness ratio between $25 < D/t < 39$ and the length-to-tube diameter ratio of $3 < L/D < 8$ was investigated. The nonlinear finite element model was developed to study the load-carrying mechanism. The load-carrying capacity decreases with the increase in % the volume of fly ash up to 20%, but it again increases at 25% fly ash volume in concrete.

Fuyun Huang *et al.,* (2012) tested twenty-four rectangular CFST slender beam-columns with a depth-to-thickness ratio of 33 and concrete compressive strengths varying from 29 to 84 MPa. These beam-columns with a cross-section of 100×150 mm were constructed by cold-formed steel tubes. Specimens were

fabricated from 4.5 mm thick steel tubes so that their depth-to-thickness ratio was 33. The length of the column was 1855 mm. The yield strength of the steel tube was 379 MPa. It was observed that CFST columns with normal-strength concrete failed by the global buckling, while local buckling failure mode was found in the specimens with high-strength concrete. Test results were compared with various composite design codes to examine the validity of the design codes. It was concluded that the AISC-LRFD (2005) generally gave a good estimate of the ultimate loads of high-strength CFST columns, while the AISC-LRFD (1999) overestimated the ultimate loads of high-strength CFST columns.

Experiments on high-strength circular CFST slender beam-columns under axial load and bending were undertaken by Lee (Lee, Choi, and Park, 2017). They studied the effects of the diameter to- thickness ratios and loading eccentricity ratios on the axial load-deflection responses and axial load-moment interaction diagrams of CFST beam-columns. Their studies indicated that the confinement effect on the ultimate bending strength was insignificant for the beam-column with diameter-to-thickness ratios ranging from 40 to 100 and loading eccentricity ratios ranging from 0.2 to 0.5. In addition, the axial stiffness and flexural rigidity of a circular CFST column decreased with an increase in the diameter-to-thickness ratio. The ductility of normal-strength circular CFST beam-columns was higher than that of high-strength circular CFST beam-columns.

Uy *et al.,* (2011) conducted an experimental investigation on concrete-filled stainless-steel tubular short and slender columns with circular, square, and rectangular cross-sections. The ultimate axial strengths, failure modes, axial load-strain relationships, axial load-shorting curves, and axial load-deflection responses were measured in the tests. The experimental ultimate axial strengths of CFST columns were compared with the design strengths calculated using AS 5100 (2004), AISC (2005), Chinese code DBJ/T (2010), and Eurocode 4 (EN1993-1-4, 2004) for CFST columns. The authors concluded that AS 5100,

AISC, DBJ/T, and EC4 underestimated the ultimate axial strengths of concrete-filled stainless steel tubular columns under axial compression.

A test was undertaken by Xiong *et al.,* (2017) to investigate the behavior of 27 axially loaded CFST columns. Steel fibers were added to the ultra-high-strength concrete. The effects of ultra-high-strength concrete on the strength and ductility of the CFST column were studied. Test results demonstrated that the ultra-high-strength concrete increased the ultimate strengths of CFST columns but reduced the ductility of the columns because of the brittle nature of the ultra-high-strength concrete. However, the ductility and strength of CFST columns with ultra-high-strength concrete increased with an increase in the steel contribution ratio. The use of fiber-reinforced concrete in CFST beam columns resulted in similar behavior. The experimental ultimate axial strengths were compared with the design strengths calculated by Eurocode 4. It was shown that the EC4 accurately predicted the ultimate strengths of axially loaded ultrahigh strength concrete columns.

Abed *et al.,* (2013)carried out tests on 16 CFST short columns under axial load. The steel tubes were filled with normal and high-strength concrete having a compressive strength of 44 MPa or 60 MPa. The diameter-to-thickness ratios of 20, 32, and 54 were considered in the experimental investigation. The main variable parameters in the tests were the concrete compressive strength and diameter-to-thickness ratio. Test results indicated that the ultimate axial strength of circular CFST columns increased with an increase in the concrete compressive strength. The ductility of circular CFST columns decreased with an increase in the concrete compressive strength for larger diameter-to-thickness ratios. Increasing the diameter-to-thickness ratio reduced the stiffness and ultimate axial strength of axially loaded circular CFST short columns. The ultimate axial strengths measured from the tests were compared with the design strengths calculated by the theoretical equation, AISC code (2010), American Concrete Institute (ACI 2011) and Australian Standard (AS 2009) codes,

(Giakoumelis and Lam, 2004; Karthik and Mander, 2011, Mander *et al.,* 1988 and Eurocode-4 2005). They concluded that the equations Mander (1988) gave a good estimate of the ultimate loads of CFST columns while AISC, ACI, AS, and Eurocode 4 underestimated the ultimate loads of CFST columns by up to 43%. These design codes, except Eurocode 4 for CFST beam-columns, have not considered the effects of concrete confinement that significantly increase the strength and ductility of the concrete core. As a result, the ultimate loads calculated by these codes deviate considerably from experimental results.

2.1.2. Analytical study on CFST column

Neogi *et al.,* (1969) proposed a numerical model for predicting the elastoplastic behavior of pin-ended circular CFST slender beam-columns under eccentric loading. In the numerical model, the tangent modulus method was used to analyze axially loaded columns, while eccentrically loaded beam-columns were analyzed by assuming a displacement function. However, the effects of the concrete tensile strength and concrete confinement were not taken into account in their numerical model. As a result, their numerical model underestimated the ultimate strengths of circular CFST slender beam-columns. The load-deflection analysis procedure presented by Neogi *et al.,* (1969) can be used to develop strength envelopes by varying the loading eccentricity. However, it is not efficient when the loading eccentricity is large. Despite this, the axial load-moment interaction diagrams of circular CFST slender beam-columns have not been studied by Neogi *et al.,* (1969).

Tang *et al.,* (1996) proposed a confining pressure model for concrete in circular CFST columns. The model accounts for the effects of material and geometric properties of the column on the strength enhancement and the post-peak behavior. It was found that their model generally overestimated the lateral confining pressure in circular CFST columns (Liang 2009). Susantha *et al.,* (2001) proposed uniaxial stress-strain relationships for concrete confined by

various shaped steel tubes. Susantha *et al., (*2001) used the confining pressure model proposed by Tang et al. (1996) for circular CFST columns.

The nonlinear behavior of CFST short columns was discussed by Schneider (Schneider, 1998), who developed a nonlinear three-dimensional finite element model to analyze CFST columns. The model was generated using the finite element program ABAQUS. An eight-node shell element was employed to model the steel tube, while the concrete core was modeled using 20-node brick elements. The model considered the inelastic behavior of structural steel and concrete. The Prandtl-Reuss flow rule was used to determine the inelastic deformation of steel plates, while von Mises yield criteria were employed to define the yield surfaces. The results obtained from the finite element analysis were compared with experimental results. It was shown that the finite element model could predict the elastic and plastic behavior of CFST beam-column specimens. However, the ultimate axial strengths predicted by the finite element model were slightly higher than the test results.

Vrcelj and Uy (2002) presented a numerical model for simulating the load-deflection responses of high-strength square CFST slender beam-columns under axial load and uniaxial bending. They investigated the effects of compressive strengths, steel yield, and column slenderness ratios on the ultimate axial strength of high-strength square CFST slender beam-columns. However, their model did not account for the effects of confinement the steel box provided on the concrete core's ductility and progressive local buckling of thin steel plates under stress gradients. The axial load moment interaction diagrams of high-strength rectangular CFST slender beam-columns have not been studied by Vrcelj and Uy (2002).

Hu *et al.,* (2003) developed a finite element model for the nonlinear analysis of axially loaded CFST short beam-columns with confinement effect. They employed the general-purpose finite element analysis program ABAQUS to study the inelastic behavior of CFST beam-columns. Square and circular

concrete-filled sections with stiffened reinforcing ties were used in the nonlinear analysis. The steel tubes were simulated using an elastic-perfectly-plastic model with associated flow theory. In contrast, an elastic-plastic theory with the associated flow and isotropic hardening rule was used to model the concrete. The von Mises yield criterion was employed to define the steel tubes' elastic limit when subjected to multiple stresses. On the other hand, a linear. Drucker-Prager yield criterion was used to model the yield surfaces of the concrete because the concrete is usually subjected to triaxial compressive stress, and failure of the concrete is dominated by increasing hydrostatic pressure. Special nine-node interface elements modeled the concrete core and steel tube interaction. The finite element model was verified by experimental results. They concluded that the circular steel tube provided a good confining effect on the concrete core, especially when the width-to-thickness ratio of the steel tube was small and local buckling of the steel tube had not occurred. However, square CFST beam-columns did not provide a good confining effect on the concrete core, especially when the width-to-thickness ratio of the steel tube was larger and the steel tube was buckled locally outward. They proposed a confining pressure model for concrete in circular CFST beam-columns made of normal-strength steel and concrete. However, their confining pressure model overestimated the confining pressure in high-strength circular CFST columns with a depth-to-thickness ratio of less than 47 (Liang and Fragomeni 2009).

Chen *et al.,* (2016) investigated the post-local buckling behavior and ultimate strength of thin steel plates in rectangular CFST columns using the nonlinear finite element analysis method. In their investigation, an eight-node quadratic plate element based on the Mindlin plate theory was used to describe the local buckling displacement of the plate in the finite element analysis. The plate was divided into ten layers to treat the plasticity using the von Mises yield criterion with the volume approach. The effects of geometric imperfection, slenderness ratio, and residual stress on the post-local buckling strengths of

clamped steel plates were studied. Well-known Ramberg- Osgood formula was employed to model steel plates with residual stresses. They found that the residual stresses had considerable effects on the load-deflection behavior of clamped plates. The stiffness and ultimate strength of plates decreased by increasing the residual stresses. It is worth mentioning that the method developed by Liang and Uy (2000) is an efficient theoretical method for determining the initial local buckling loads and the post-local buckling reserve strengths of plates with imperfections.

Ellobody (2013) presented the design and behavior of circular CFST short columns under axial compression. They employed the finite element program ABAQUS to study the inelastic behavior of normal and high-strength circular CFST short columns under axial compression. The compressive strength of concrete ranged from 30 MPa to 110 MPa, covering normal and high-strength concrete. The finite element analysis was conducted on columns with a wide range of diameter-to-thickness ratios ranging from 15 to 80, covering non-compact and compact steel tube sections. The concrete confinement model proposed by Hu *et al.,* (2003) was used in the finite element analysis. The ultimate axial strengths and axial load-shortening curves for circular CFST columns were evaluated. The finite element results were compared with the test results provided by Giakoumelis and Lam (2004) and Sakino *et al.,* (2004). Parametric studies examined the effects of concrete compressive strengths, steel yield strengths, and diameter-to-thickness ratios. The ultimate axial strengths obtained from the finite element analyses were compared with the design strengths calculated using Australian, American, and European specifications. They reported that the design strengths obtained by Australian and American specifications were conservative.

Numerical models for the nonlinear inelastic analysis of circular CFST short columns under axial and eccentric loading were developed by Liang and Fragomeni (2009, 2010). The proposed constitutive material models for

confined concrete. The numerical models incorporated accurate constitutive models for normal and high-strength concrete confined by either normal or high-strength circular steel tubes. In their study, a circular CFST section was divided into fine fiber elements assigned with either steel or concrete material properties. Each element's coordinates and cross-section area were automatically calculated based on the geometry of the cross-section. Fiber stresses were calculated from fiber strains. Liang (Liang, 2009) developed the Secant method algorithms that were incorporated into the numerical models to iterate the neutral axis depth in a circular CFST beam-column section until the force equilibrium conditions were satisfied. The accuracy of the numerical models was examined by comparing the ultimate axial strengths, ultimate bending strengths, axial load-strain curves, and moment-curvature responses with corresponding experimental results. The accuracy and reliability of various confining pressure models proposed by Tang and Hu (Xi-min, Guanzao, and Bingguan, 1983; Hu *et al.,* 2003) and the authors were evaluated. It was found that the confining pressure models given by Tang *et al.,* (1996) and Hu *et al.,* (2003) overestimated the ultimate axial strengths of high-strength circular CFST columns. The comparison demonstrated that the confining pressure models proposed by Liang and Fragomeni (2009) provided reliable results for both normal and high-strength circular CFST columns under axial and eccentric loading. The verified numerical models were then utilized to investigate the fundamental behavior of circular CFST columns with various diameter-to-thickness ratios, concrete compressive strengths, steel yield strengths, axial load levels, and section shapes. They proposed new design models based on the numerical results for determining the ultimate axial and ultimate pure bending strengths of circular CFST beam-columns. They highlighted that the numerical models and formulas were effective simulation and design tools for circular CFST beam-columns under axial and eccentric loading.

An analytical model for determining the behavior of axially loaded circular CFST short columns was described by Choi and Xiao (Choi and Xiao, 2010). An analytical procedure for predicting the axial load-strain curves of circular CFST short beam columns was presented. Various modes of interaction between the steel tube and infill concrete under axial compression were discussed. The axial load-strain curves for circular CFST short columns under axial compression predicted by the analytical model were compared with experimental data. They found that the behavior of circular CFST short columns depended on the concrete strength and confinement of the concrete provided by the steel tube. The drawbacks of the analytical procedure are that the strain hardening of materials was not considered. Consequently, the procedure produced solutions that deviated considerably from the corresponding experimental results in the post-peak range of the axial load-strain curves.

The nonlinear inelastic behavior of high-strength circular CFST slender beam-columns was investigated by Liang (Patel, Liang and Hadi, 2012; Hassanein, Kharoob and Liang, 2013). He developed a numerical model based on the accurate fiber element method. The material constitutive material model proposed by Liang and Fragomeni (2009) for confined concrete was incorporated into the numerical model. The numerical model accounted for the effects of concrete confinement, initial geometric imperfection, and second order. The cross-section analysis of circular CFST beam-columns was discussed. In his numerical model, the deflected shape of circular CFST beam-columns was assumed to be a part of a sine curve. Computational algorithms based on the secant method were developed to adjust the neutral axis depth of the composite section.

In the axial load-deflection analysis, the deflection at the mid-height of a slender beam-column was gradually increased. The equilibrium of internal and external bending moments was maintained at the mid-height of the beam-column. In axial load-moment interaction strength analysis, the curvature at the

31

mid-height of the beam-column was gradually increased. The curvature at the column end was iteratively adjusted by the secant method to satisfy the moment equilibrium at the mid-height of the beam-column. The ultimate axial strengths, ultimate bending strengths, and axial load-deflection responses of circular CFST slender beam-columns under eccentric loading obtained from the numerical model were compared with experimental results available in the published literature. The numerical model was then utilized to investigate the effects of column slenderness ratio, loading eccentricity ratio, concrete compressive strengths, steel yield strengths, steel ratio, and concrete confinement on the behavior of high-strength circular CFST slender beam-columns in terms of axial load-deflection responses ultimate strengths, axial load-moment interaction diagrams and strength increase due to confinement effects. It was concluded that increasing the column slenderness ratio and eccentricity ratio significantly reduced the flexural stiffness and ultimate axial strength of eccentrically loaded circular CFST beam-columns. The deflections and displacement ductility of the columns increased with an increase in the column slenderness ratio. In addition, the stiffness and strength of circular CFST slender beam-columns increased with increasing the concrete compressive strength. It was noted that the steel yield strength did not influence the initial flexural stiffness of slender beam-columns. However, slender columns ultimate axial strengths increased significantly with the steel yield strength. Moreover, the flexural stiffness and ultimate strength were shown to increase significantly with increasing the steel ratio. The confinement effect was shown to decrease with increasing the eccentricity ratio and the column slenderness ratio.

Ellobody (2013) discussed the nonlinear behavior of fiber-reinforced concrete-filled stainless-steel tubular (CFSST) columns. A three-dimensional finite element model was developed using ABAQUS to analyze CFSST columns. The pin-ended axially loaded CFSST columns were considered in the

finite element model. The length of CFSST columns varied from short to slender. The effects of fiber-reinforced concrete confinement provided by a stainless-steel tube and the interface between the stainless-steel tube and fiber-reinforced concrete were also considered in the analysis. In addition, the initial geometric imperfection was incorporated into the finite element model. The finite element model had been validated against tests conducted by Ellobody and Ghazy (2012a) and Ellobody and Ghazy (2012b) on fiber-reinforced concrete-filled stainless steel tubular columns. The ultimate axial strengths, axial load-strain curves, and failure modes obtained from the finite element model were compared with experimental results. The finite element model accurately predicted the nonlinear behavior of fiber-reinforced concrete-filled stainless steel tubular columns. A parametric study was conducted to investigate the influence of the depth-to-thickness ratios, fiber-reinforced concrete compressive strengths, and column slenderness ratio on the behavior of fiber-reinforced concrete-filled stainless steel tubular columns. The parametric study indicated that increasing the concrete compressive strength drastically increases the ultimate axial strength for the columns with an L/ D ratio of less than six and a depth-to-thickness ratio of less than 50. The ultimate axial strengths obtained from the finite element model were compared with the design strengths calculated using Eurocode 4 for composite columns. It was shown that the EC4 predicted well the design strengths of axially loaded fiber reinforced CFST columns.

2.1.3. Experimental and Numerical Studies on behaviour of CFDST columns

Elchalakani, Zhao and Grzebieta, (2002) tested 8 CFDT stub columns (CHS outer and SHS inner) sandwiched with cold-formed steel tubes. The D/t ratio of the outer skin was 19 to 55, and the section slenderness ratio was 35 to 90. The b/t ratio of inner skin was 20 to 26, and the section slenderness ratio 23 was 31 to 33. The steel grade and concrete compressive cylinder strength were

33

400 to 500 MPa and 64 MPa, respectively. The axial compressive load was applied over the entire section. The author opined that CFDT stub columns performed satisfactorily up to very large deformations with ductile failure modes. The author did not observe any fracture in the outer or inner jackets. The following conclusions were mentioned too. i) Inward folding mechanism of the inner square tube maintained high capacity under very large deformations. ii) The AISC-LRFD rules for CFT columns were found suitable to predict the axial compressive capacity of CFDT up to section slenderness ratio 90. iii) EC4 rules for composite columns overestimate the enhancement of concrete strength and, in turn, the axial capacity of CFDT stub columns.

Zhao, Grzebieta, and Elchalakani (2002) carried out tests having 8 Concrete Filled Double Skinned Tubular columns (CFDST) stub columns, with a length of 375mm (SHS inner and SHS outer), five empty stub columns with tubes thickness ranging from 2.5 to 6mm, 5 CDFST beams, b/t ratio of outer tubes ranging from 16.7 to 25 and one sections with a b/t ratio 20. The nominal yield stress of steel was 450 MPa, and the cylinder strength of concrete infill was 71.3 MPa. He observed increased ductility and energy absorption for CFDST under compression. He also developed a theoretical model to predict the ultimate capacity of CFDST columns under compression and bending.

Han and Yao, 2004 tested 14 concrete-filled double-skin tubular (CFDST) stub columns, four beams, and 12 beam-columns. The column specimen lengths were from 360 to 900mm with a constant thickness of 3mm. The diameter of the outer tubes ranged from 120 to 300mm. The yield stress of the outer tube was 275.9 MPa. The inner tube diameter varied from 32 to 165 mm. The yield stress of the inner tube varied from 294.5 24 to 422.3 MPa. SCC in-fill of grade 40 MPa was used. He had established the load Vs. axial strain relationship for SHS stub columns. In addition to that, he observed enhanced strength and ductility for CFDST stub columns, beams, and beam-columns due to the composite action between the steel tubes and the sandwiched concrete.

Tao, Han, and Zhao (2004) conducted a series of tests on concrete-filled double-skin steel tubular (CFDST) of 14 stub columns and 12 beam-columns having both outer and inner tubes with circular hollow sections (CHS). For the stub columns, the length varied from 342 to 900mm. The thickness of the outer and inner specimens was kept at 3mm. The diameter of the outer tube varied from 114 to 300 mm, and that of the inner one varied from 48 to 165mm. The outer skin yield stress was from 276 Mpa to 295 Mpa. The inner skin yield stress varied from 294.5 Mpa to 396 Mpa. The hollow section ratio varies from 0 to 0.8, and the outer tube width-to-thickness ratio varies from 38 to 100. The beam-column length varied from 887 to 1770mm, and the slenderness ratio ranged from 28 to 56. The diameter of the outer tube was 114 mm, and that of the inner was 58 mm, with a constant thickness of 3mm. The outer and inner tube yield stress was 294.5 and 374.5MPa, respectively. The load eccentricities of the column were from 0 to 45mm. The column slenderness varied from 28 to 56. The author observed the following 1) local buckling did not occur before their ultimate strength was developed. 2) for specimens of larger D_o / t_{so}, earlier local buckling occurred. 3) hollowness ratio does not significantly influence the ductility of the CFDST specimens. 4) Ductility of CFDST specimens was as good as CFT specimens 5) The author also established the load versus axial strain relationship of the CFDST stub columns.

Han *et al.,* (2006) carried out 30 tests, including concrete filled double skin steel tubular (CFDST) 3 stub columns, three beams, and 24 columns with special emphasis on the behavior of CFDST (RHS inner and RHS outer) columns. Both outer and inner tubes were cold-formed rectangular hollow sections (RHS). The author compared the failure modes and load-deformation behavior of CFDST specimens with those of conventional concrete-filled steel tubular members and empty double-skin tubular members and predicted the load-carrying capacities with a simplified model in which a confinement factor was introduced considering the "composite action" between the outer steel tube

and the sandwiched concrete. The author finally concluded the following points.

1. The CFDST members behaved similar to the conventional CFST specimens.

2. Enhanced strength and ductility were observed for CFDST (RHS inner and RHS outer) stub columns, beams, and beams– columns due to the "composite action" between the steel tube and the concrete core.

3. Theoretical models were developed to predict the load versus deformation relationships for CFDST stub columns, beams, and beam columns, and good agreement was obtained between the predicted and experimental curves.

4. All predictions for beams and beam-columns were compared with test results, and reasonable agreement was achieved.

Kuranovas and Kvedaras (2007) prepared 24 specimens from circular hollow sections (CHS) of diameter 219mm, 5mm, and length of 438mm by centrifuging the concrete of 30 Mpa. The author concluded that more excess residual water when pressed out from double-layered elements, thus the water cement ratio (W/C), leading to lower porosity and greater density of concrete and, hence, the load–bearing capacity of H-CFST and H-ST members is increased.

Fujikura, Bruneau and Lopez-Garcia, (2008) investigated the Concrete-Filled Steel sandwich walls (CFS sandwich walls) concept for seismic applications in parallel with research conducted on the multi-hazard performance of concrete-filled steel tubes. The author concluded that CFSP sandwich walls as well as concrete-filled double-skinned tubes, could provide a cost-effective alternative to regular reinforced concrete construction, with faster construction time. The author also concluded that in concrete-filled double-skinned tubes, the outside skin at the periphery of the section provides strength and stiffness, the inside skin enhances ductility, and the concrete in

between provides local and overall stability to the system. The synergy between the tubes and the core results in a more redundant section which completely fails only when all three layers of material fail. This section controls concrete material failures such as spalling, breaching, or scabbing under shock load. This helps preserve the stability of the section and guarantees enough (axial) residual strength for a section at ultimate strength.

Uenaka *et al.,* (2010) investigated 12 specimens of concrete-filled double-skin tubular stub columns under axial compression. The outer diameter was 160mm, and the height was 450mm. The inner and outer tube diameters were 37.5mm, 75mm, and 112.5mm, respectively. The tube thicknesses in both cases were 1, 1.6, or 2.3mm. The D_o / t_o ratio ranged from 73.4 to 176.2, D_i/t_i ratio varied from 26.3 to 125.9, and the hollowness ratio ranged from 0 to 0.73. The yield stress of both outer and inner tubes was 221 to 308 MPa. The cylinder compressive strength of concrete was 18.7 MPa. The two main testing parameters were 1) inner-to-outer diameters ratio and 2) diameter-to-thickness ratio. The author concluded that the failure modes were controlled by the local buckling of the tubes associated with the shearing failure of the filled concrete. The experimental strength was mostly larger than the superposed estimation. The author also stated that no influence of the inner tube on the confinement effect could be found owing to complex biaxial compression.

Han, Li and Liao, (2011) carried out six tests, including Circular-CFDST, 2 CFDST specimens, and two references to conventional CFST specimens under concentrically sustained long-term sustained load. The specimens were tested under two stages, including the long-term service testing and ultimate load testing. CFDST and CFST reference specimens without experiencing long-term sustained loading were also tested for ultimate loads and compared. The author concluded that long-term deformation sustained loading decreases the ultimate strength of the CFDST column whilst increasing the corresponding deformation. Moreover, the loading effects on the ultimate strength and

corresponding deformation of the CFST and CFDST members were similar. The author, in conclusion, added that influences of changing steel strength and the diameter-to-thickness ratio of the inner tube on the strength index (SICFDST) of CFDST columns subjected to long-term sustained loading were moderate. However, (SICFDST) increases with the increasing hollow ratio. The author also proposed a formula for calculating the ultimate strength of CFDST columns under long-term sustained loading.

Li *et al.,* (2012) tested 12 specimens, including tapered concrete-filled double-skin steel tubular (CFDST) and two hollow CFDST stub columns under axial load. The failure mode of the tapered CFDST column was the outer tube's outward buckling and the inner tube's inward buckling with the crush of the sandwich concrete where the tubes buckled. It was similar to the straight CFDST column, while the failure occurred near the section with the smallest profile.

Dong and Ho (2012) tested a total of 10 specimens having external steel rings, out of which four normal strength CFSTs were with different spacing of the steel rings, four normal strength CFDSTs were with different spacing of the steel rings, and each one of CFST and CFDST without external rings under uni-axial compression load. The author concluded that the stiffness and elastic strength of CFDST columns are larger than CFST columns with a similar equivalent area. The strength of CFDST columns degrade more rapidly at high axial strain mainly because of the abrupt load transfer from the inner column during failure. The author developed a model for predicting the axial load-carrying capacity of confined CFST columns in which confining pressure provided by both the steel tubes and the ring confinement was considered.

Prabhavathy (2012) experimented with five double-skinned concrete-filled steel tubular (DSCFT) columns in-filled with self-compacting concrete (SCC), mix grade of M50 prepared with 15% replacement, of course, aggregate by silica fume and compared with another five (5) concrete-filled tube (CFT)

columns of the same area of steel (A_{st}) and outer diameter as in DSCFT columns with varying slenderness ratios. The author concluded that the DSCFT columns significantly reduce self-weight. The author also opined that DSCFT columns behaved relatively ductile and were found cost efficient than concrete-filled tube (CFT) columns.

Chang *et al.,* (2014) experimented with six specimens, including 4 CFSCT stub columns, one CFST, and one CFT column, having specimen properties of the length of 500mm, outside diameter, and inner steel tubes of 108mm and 114mm respectively, the thickness of tubes 2mm and, L / D ratio of 3.14 and grades of concrete 50 Mpa and 60 MPa. The author tested specimens under axial compressive load and compared the results with that obtained in the Finite element program ABACUS / Standard. The author noticed the failure modes of elephant foot buckling and outward buckling and finally concluded the following. a) the presence of the inner carbon steel tube of the CFCST column provides additional confining effects of the concrete core inside it and then leads to a higher column strength than that of CFST columns, b) the column strength increases as and when there is an increase in the diameter ratio, wall thickness ratio, yield strength ratio, and concrete strength.

Jin-kook kim (2013) conducted experiments on 23 specimens with the diameter of outer and inner tubes being 10 and 2mm, respectively. The concrete cylinder's compressive strength of 40MPa, and the outer and inner tube's yield strength was 690MPa and 245MPa. The hollowness ratio was 0.5. The specimens' outer diameter and height were 300 and 600mm, respectively. The author observed that the local buckling did not occur before their ultimate strength. Hence, D/t limitation in EC4 must be mitigated to 50%. The ductility of the HDSCF column is proportional to the thickness of the outer steel tube and can be assisted by a thicker inner steel tube when the outer steel tube is relatively thinner.

Yang *et al.,* (2015) investigated the experimental behaviour of CFDST subjected to local bearing forces. Sixteen specimens were prepared and tested with the included angle between the bearing member (BM) and compression member of 451 and 901. In contrast, the inner and outer steel tubes of the CFDST specimens are square hollow sections (SHS). The main parameters in the tests were: 1) outside width ratio between BM and compression member: from 0.4 to 0.6; 2) hollow ratio of CFDST: from 0 to 0.6; 3) wall thickness of outer steel tube: 3.05 mm and 3.95 mm; and 4) cross-section of BM: solid and hollow. The test specimens' failure pattern, load versus deformation curve, bearing capacity, and the corresponding deformation at bearing capacity are presented and analyzed. The experimental results show that CFDST specimens have a high bearing capacity and a good deformation-resistant ability while subject to local bearing forces.

Wang *et al.,* (2016) investigated the behavior of CFDST members under low-velocity lateral impact using ABAQUS. Strain and stress states of concrete and steel tubes in CFDST members are analyzed over the full loading range, followed by a parametric study investigating the influence of impact height, hollow ratio, nominal steel ratio, the diameter-to-thickness ratio of inner steel tube, and strength of materials on the impact force and global residual lateral deformation. Furthermore, the dynamic increase factor(DIF) of CFDST members under lateral impact is proposed, and the influence of the confinement factor on the dynamic increase factor (DIF) is analyzed. The results show that when the confinement factor is larger than 1.03, the dynamic increase factor needs to be considered to accurately estimate the dynamic resistance capacity of CFDST members subjected to lateral impact.

Zhang *et al.,* (2017) investigated on numerical behaviour of tapered concrete-filled double-skin steel tubular (CFDST) stub columns subjected to axially partial compression. A finite element analysis (FEA) model is developed to investigate the partial compressive behaviour of the CFDST

column. The full-range load versus deformation relations of tapered CFDST columns under partial and overall compression are both analyzed using the verified FEA model. A parametric study was conducted to investigate the ultimate strength of the column with various geometric and material parameters. It was found that the mechanism analysis, including failure modes, full-range analysis, and stress distribution, is performed using the verified FEA model. It was also found that, for the partially loaded tapered column, the confinement effect of concrete by the steel tube occurs at the beginning of the loading. The ultimate strength is mainly affected by the confinement provided by the outer steel tube. Moreover, the sandwiched concrete resists more loads in the partially compressed member than that in the overall compressed one.

The high-strength steel (HSS) has been used in steel–concrete composite constructions as it improves structural performance and reduces structural self-weight. Nassirnia *et al.,* (2018) investigated the experimental and numerical studies on the bending behavior of concrete-filled double-skin tubular (CFDST) beams using the HSS with a yield strength of 618 MPa. The results showed that the bending resistance of CFDST members was substantially increased, and the high-strength material was fully exploited. A parametric study was performed using the verified finite element model. In addition, the compatibility of various concrete classes and steel grades was discussed. The design methods from the current code of practice were also evaluated to predict the bending resistance of circular CFDST beams using an HSS tube.

Wang et al., (2018) investigated non-linear finite element (FE) analysis and design of circular and square CFDST stub columns with external stainless steel under axial compression. FE models were developed, and stainless steel's non-linear material property was considered. The behaviors of stainless steel composite columns are compared with that of columns with carbon steel tubes. Parametric studies were conducted to investigate the influence of the outer stainless steel tube strength, concrete strength, inner carbon steel tube strength,

and hollow ratio on the structural behavior of axially loaded columns in terms of loading and interaction performance.

Vernardos and Gantes (2019) investigated through a meticulous review of numerous experimental endeavors over 20 years. A summary of these tests and their pertinent results, followed by an exploration of their structural response and predominant failure mechanisms for different cross-section shapes and geometrical factors. The efficiency of the CFDST concept is subsequently quantified by means of a comparison between CFDST members and their components acting individually in terms of both ultimate strength and energy absorption. An extensive parametric analysis is finally carried out with respect to the influence of various key factors on axially-compressed CFDST stub members' structural performance.

Elchalakani *et al.,* (2019) investigated the characteristics of short CFDST columns under compression and the influences of the sandwiched concrete thickness, the yield stress of the outer tube, tube thickness of both the outer and inner components, and sandwiched concrete strength on the structural performance of circular short CFDST columns. a finite element analysis is conducted. The different steel and concrete models are adapted from previous research and verified by comparing their results with the experimental results. The best material models are presented and used in the parametric study, which examines several factors' effects on the CFDST columns' load-displacement relationships.

Liang *et al.,* (2019) investigated the experimental mechanical behaviour and working mechanism of CFDST with stiffeners. Totally 40 CFDST columns were prepared and tested under axial and eccentric loading. The test results indicated that the ductility of the CFDST specimens was improved greatly by the presence of stiffeners, which gave a lower load-bearing capacity owing to the reduction in the effective area of the inner concrete. Additionally, an

analytical-numerical model was developed to analyze the mechanical behaviour of the CFDST specimen.

Li and Cai (2019) investigated the compressive behavior of CFDST stub columns using high-strength steel using a finite element model. The material nonlinearity, the confinement effect, and the contact behavior were considered. A total of four largescale CFDST stub columns using HSS in the outer tube were tested under axial compression. A parametric study was carried out, such as the yield stress of steel, the hollow ratio, and the confinement factor. Furthermore, the feasibility of current design equations for CFDST columns using HSS was assessed. The results conclude that the HSS tube worked well with the sandwiched concrete, and the current methods could provide reasonable yet conservative predictions on the compressive strength of CFDST stub columns using HSS.

Hasan *et al.,* (2019) investigated a series of push-out tests on sixteen specimens of CFDST columns to explore the bond-slip behaviour between the cross-sectional elements (the inner steel tube, the outer steel tube, and the shell concrete). The primary test parameters involve (a) interface type (normal interface, interface with an internal ring, with reinforcing bars, and with shear studs); (b) concrete strength (high-strength concrete and normal strength concrete); (c) push-out type (push-out of the shell concrete and push-out of the inner tube). The results demonstrated that greater benefits arose in the bond strength once the reinforcing bars or internal rings were welded onto the inner steel tube of CFDST columns. Additionally, a remarkable improvement in the bond strength, the welded reinforcement bars would significantly improve the compressive strength of CFDST columns and eliminate the local buckling of the inner steel tube. On the other hand, the embedded shear studs (bolts) onto inner steel tubes can improve the bond strength with less shear resistance in comparison with the other interface types.

Ekmekyapar and Ghanim (2019) investigated an experimental study to explore the effect of the inner steel tube on the mechanical response of CFDST columns under axial compression. Two different D/t ratios and concrete classes (normal strength and high strength) were utilized, and sixteen specimens were tested for failure. The results show that the CFDST columns could attain greater performance over CFST columns when a proper configuration of the inner steel tube was used. Furthermore, the inner tube worked consistently with the shell concrete and played an important role in mitigating the failure mode of CFDST, even with high-strength concrete (HSC).

Shi *et al.,* 2020 conducted an experimental and numerical investigation on tapered concrete-filled double-skin steel tubular (CFDST) stub columns with a large void ratio under axial compression is presented in this paper. Twelve tapered CFDST specimens with different parameters, namely the void ratio and the outer steel tube diameter-to-thickness ratio, are tested. The load versus deformation curves, failure modes, and effects of different parameters are studied, respectively. It is found that tapered CFDST specimens with a large void ratio experience strength failure, and severe outward buckling occur near the column top. The diameter-to-thickness ratio of the outer steel tube and the void ratio significantly influence the ultimate capacity and ductility of tapered CFDST columns. A finite element (FE) model is developed to predict test results and further analyze tapered columns' working mechanisms. The result shows that changing the tapered angle and void ratio has distinct effects on the position of the failure section and distribution of the peak load of tapered columns. A method considering the influence of the failure section is finally proposed for calculating the ultimate capacity of tapered CFDST columns and a good, predicted result is presented.

Wang, Young and Gardner (2020) investigated finite element (FE) analysis of compressive behaviour on cross-sections with lean duplex and ferritic stainless steel outer tubes. FE models were initially developed and validated against available test results reported in the literature. A parametric study was undertaken to investigate the influence of key variables, including the local slendernesses of the outer and inner tubes, the concrete strength, and the adopted grade of stainless steel, on the ultimate response of the studied CFDST stub columns. Based on the generated FE data pool and the available test results, the applicability of the existing European, Australian and American design provisions for composite carbon steel members to the design of the studied CFDST cross-sections was evaluated. Modified design rules improved the accuracy and consistency of the design capacity predictions. Finally, statistical analyses were carried out to demonstrate the reliability of the modified design approaches.

Yan and Zhao (2020) investigated experimentally and numerically the compressive behavior of circular CFDST short columns in which only the sandwiched concrete is under axial compression. Totally 28 CFDST columns were loaded axially. Results suggest that the outer steel tube's wall thickness and yield stress significantly affect the failure modes, while the concrete strength shows an insignificant effect. The tested columns exhibited good ductility concerned. Likewise, finite element (FE) models were established and verified by comparing them with the test results.

Wang and Zhao (2020) investigated on experimental of circular specimens with furnace slag aggregate replacement ratio of 100%.with the different hollow ratios ranging from 0.5 to 0.75. A total of 8 specimens were tested to capture the behaviors of the creep, shrinkage, and ultimate strength before and after six months of sustained loading. The results indicated that the shrinkage strain of the sandwiched furnace slag aggregate concrete tended to stabilize after 30 days, and the creep constantly developed throughout the 180 days of

the test. The furnace slag aggregate CFDST specimens with stainless steel tubes have demonstrated well load carrying capacity and ductility under sustained loading.

An experimental investigation on the behavior of stiffened octagonal CFDST stub columns subjected to axial compression by Alqawzai *et al.,* (2020). A total of eight specimens were prepared and tested under axial compression. The specimens consist of two control specimens with and without stiffeners (unstiffened columns). Based on the test results, the ultimate load-carrying capacity, load-displacement curves, load-strain response, ductility, and failure modes were discussed and clarified. The test results indicated that the strength and ductility of the specimens were improved greatly by the presence of the stiffeners. The stiffeners significantly enhanced the confinement and prevented the occurrence of elastic-plastic local buckling of the outer tube.

Li *et al.,* (2021) investigated on Concrete-filled double-skin steel tubes (CFDSTs) are comprised of two concentrically placed steel tubes and a concrete core filled in the annulus between the two tubes. Several studies have demonstrated the excellent structural performance of CFDSTs as load-bearing columns under various loading conditions, attracting lots of interest from engineers and researchers. Despite the increasing popularity of using CFDSTs as load-bearing structural columns, there is limited knowledge on the blast-resistant performance of CFDST columns, particularly under close-in explosion. In this paper, an experimental study was conducted to investigate the residual axial load-carrying capacity of CFDST columns after being subjected to the close-in explosion. Field blast tests were first carried out on CFDST columns. Then, the blast-damaged columns were subjected to axial compression till failure under the quasi-static condition in the laboratory to examine their residual axial load-carrying capacities. Seven half-scale CFDST column specimens were constructed and tested. One column serves as a reference column that was directly tested under axial compression to check the

ultimate axial load-carrying capacity of CFDST columns without blast damage. The influences of design factors, including charge weight, stand-off distance, charge orientation, and section hollow ratio on blast-resistant performance of CFDST columns, were quantitatively assessed based on the residual axial capacity index. It was found that under close-in blast loading, CFDST columns showed localized cross-section denting with slight global deformation. The damaged columns can maintain up to 60% of their ultimate axial load-carrying capacity and exhibit good strength and ductility.

Yang et al., (2021) investigated the experimental and numerical study on the axial compressive behaviour of CFDST stub columns with a large void ratio. Nine specimens with various void ratios, the diameter-to-thickness ratio of the outer tube, and the compressive strength of concrete were tested under axial compression. The experimental results show that all specimens have good structural performance. The typical failure patterns of this new type of column include local buckling of outer or inner tubes and crushing of concrete infill at the primary buckling locations of both tubes. It is observed from the tests that there are three key stages in the load versus displacement (strain) relationship, namely: approximative elastic, elastoplastic, and non-linear post-peak, and with the augment of various void and diameter-to-thickness ratio and the reduction of Compressive strength, the ultimate capacity and elastic composite stiffness of the specimens decrease. A finite element (FE) model was developed and validated against the experimental results.

Yan *et al.,* (2021) investigated an experimental program consisting of 24 specimens to investigate the compressive behaviour of circular CFDST short columns with HSC and UHSC. The test results show that CFDST columns with higher-strength concrete generally achieve higher initial stiffness and axial strengths but lower ductility. Additionally, the axial strengths of CFDST columns are improved as the outer steel tubes' yield stress and wall thickness increase and as the hollow ratio decreases. A finite element (FE) model was

established and verified against the present test results, based on which the interaction of the steel tubes and concrete and the load distribution on components were analyzed. A parametric study using the verified FE model was conducted to further ascertain the influences of column variables on the compressive behavior of the studied CFDST columns.

Zhao et al., (2021) investigated experimental and numerical behaviors of circular concrete-filled double steel CFDST) slender columns in which the external tube employed stainless steel tube. Twelve slender columns were tested to obtain the failure patterns, load versus deflection relationships, and strain developments of stainless steel tubes. A finite element (FE) model was developed and verified by experimental results. The load distribution among the components and contact stress between the steel tube and sandwiched concrete were also analyzed. Finally, the design methods for CFDST, hollow CFST, and solid CFST members with carbon steel external tube, respectively suggested by Han et al. (2018), Chinese GB 50936-2014 (2014), and AISC 360-16 (2016) were employed to evaluate their applicability for the circular CFDST slender columns and beams with stainless steel outer tube.

Su *et al.,* (2021) investigated welded corrugated steel tube-concrete-flat steel tube column under the axial compressive behavior of 14 short column specimens. The test results indicated that the outer corrugated steel tube could provide good hoop confinement to the core concrete. The welded corrugated steel tube-concrete-flat steel tube composite structural columns failed with serious extrusion of the inner steel tubes' wave crests and inward buckling. The effects of the test parameters on the failure modes, strength, ductility, and strain responses were also discussed. Additionally, existing design models for concrete-filled double-skin tubular (CFDST) columns were assessed based on the test results in the literature. New models for CFDST columns and welded corrugated steel tube-concrete-flat steel tube columns were proposed.

Deng *et al.,* (2022) investigated tapered CFDST columns with large hollow ratios (LHR-CFDST) that have a good application potential in wind turbine towers, where they are commonly subjected to the combined action of compression, bending, shearing and torsion. The mechanism of columns and the effects of torsion-to-bending ratios, axial compression ratios, height-to-diameter ratios, tapered angles, hollow ratios, diameter-to-thickness ratios of steel tubes, and the material strength were shown. It is found that the failure mode of columns under compression-bending shear-torsion loads is related to the torsion-to-bending ratio. The columns behave in a ductile manner under moderate axial compression. The tapered angle has a slight effect on the bending capacity of the column, whereas the capacity declines with the increase of hollow ratio and torsion-to-bending ratio.

Shi *et al.,*(2022) investigated the experimental and numerical investigation on tapered CFDST stub columns with a large void ratio under axial compression. Twelve tapered CFDST specimens with different parameters, namely the void ratio and the outer steel tube diameter-to-thickness ratio, are tested. It is found that tapered CFDST specimens with a large void ratio experience strength failure, and severe outward buckling occur near the column top. The diameter-to-thickness ratio of the outer steel tube and the void ratio significantly influence the ultimate capacity and ductility of tapered CFDST columns. A finite element (FE) model is developed to predict test results and further analyze tapered columns' working mechanisms. The result shows that changing the tapered angle and void ratio has distinct effects on the position of the failure section and distribution of the peak load of tapered columns.

Summary

This chapter has presented the literature review on CFDST columns under uniaxial Existing experimental works, and nonlinear analysis of CFDST columns has been highlighted. The literature review shows that there are not

sufficient experimental and numerical studies on CFDST columns under axial load and uniaxial loads. Research on nonlinear analysis techniques for CFDST columns has been very limited. In addition, most of the nonlinear analyses did not consider the effect of the progressive local buckling of steel tubes and the ductility of thin-walled CFDST columns. Moreover, the effects of the nonlinear analysis and behavior of biaxially loaded thin-walled CFDST columns with local buckling have not been reported in the literature.

2.2. Gaps in the existing study

The use of CFDST is increasing day by day since it has several merits over conventional RC columns. Although the research on CFST columns started in the 1980s, however, significant research has been made in the last decade and is going on. A significant review of the literature has been made, and after the assessment of the existing literature, the following gaps were identified from the studies.

1. Most studies on CFDST have been made on columns subjected to concentric load. There is a need to understand the structural response of CFDST columns with different cross-sections subjected to axial and eccentric loads.

2. Previous studies on CFDST are limited to circular columns having outer skin shapes as circular and square. In the case of circular columns subjected to uni-axial bending, there is a need to investigate the behavior of CFDST columns with inner skin shapes as squares.

3. A few studies have been made to examine the influence of the aspect ratio of the inner steel tube on the bearing capacity of CFDST columns of different sections. So, to better understand the behavior of CFDST columns under axial and eccentric loading, it is essential to investigate the influence of the aspect ratio of the internal skin tube on the behavior of the CFDST column.

50

4. In the construction of conventional RC columns with bundled bars, it becomes difficult and time-consuming to place the bars and tie them during construction. To overcome this issue, there is a need to replace the bundled bars with the CFST and examine the behaviour of such double-skin columns.

2.3. Objectives of the present studies

The present research work primarily intends to study, explore, and compare the structural behavior of CFDST columns with different geometries, dimensions, and configurations. The major objectives of the study are:

- To generate a database of experimental results for the CFDST column of various cross-sections under axial and eccentric loads.

- To develop a nonlinear finite element numerical model to validate the experimentally tested specimen structural behavior, compressive strength, and deformed shapes of CFDST columns with different cross-sections under axial and eccentric loads.

- To study the variations of lateral confining effects provided by steel to concrete with different cross-sections of outer steel tube by various inner steel tube aspect ratios of the CFDST columns.

- To examine the structural behavior and enhanced compressive strength of the CFMST columns under axial and eccentric loading conditions.

Chapter -3
Material Characterization and Experimental
Operation

3.1. Overview

In order to attain the investigations on different cross-sections of CFDST and CFMST columns, it becomes necessary to assess the mechanical properties of the materials used in the present study. Moreover, an experimental set-up becomes essential to examine the structural behavior, load-carrying capacity, deformed shapes, and stress-strain rate of each loading phase under the axial and eccentric loading conditions. This chapter describes in detail the assessment of the material properties of the materials used in the specimens and the fabrication procedure used for preparing the CFDST and CFMST specimens. Furthermore, it provides the details of the experimental setup and the approaches used to process the raw data obtained from the LVDT to produce the results required to analyze the response of the columns and verify the numerical models, which have been discussed in chapter 4.

3.2. Material Characterization

The standard material testing machines were used to obtain the actual properties of steel and concrete used in the CFDST specimens. The following subsections describe the tests, geometry, dimensions of the tested specimens, testing apparatus, and measuring device.

3.2.1. Material Properties of Steel Tubes

The tensile coupon test was used to determine the mechanical properties of the outer and inner steel tubes of CFDST columns. The tensile test coupons

were prepared as per IS 1608 (IS 1608, 2005) for the inner and outer steel tubes of each cross-section used in the present study.

3.2.1.1. Test Samples (Coupon) Preparation

The steel coupon specimens for the tensile test were extracted parallel to the longitudinal axis of the steel tubes, as shown in Fig. 3.1. The gripped end of each test coupon was taken on the curved surface and flattened surface for the square to outfit the gripes of the testing machine. The shapes and sizes of specimens were in accordance with IS 1608 (IS 1608, 2005), as shown in Fig. 3.2. The gauge length of the coupons was set to be 50 mm for all the cross-section steel tubes. The specimen (coupons) thickness and width were measured at three points within the gauge length using a Vernier caliper. The average of these assessed measurements was used to determine the mechanical properties of the steel tubes.
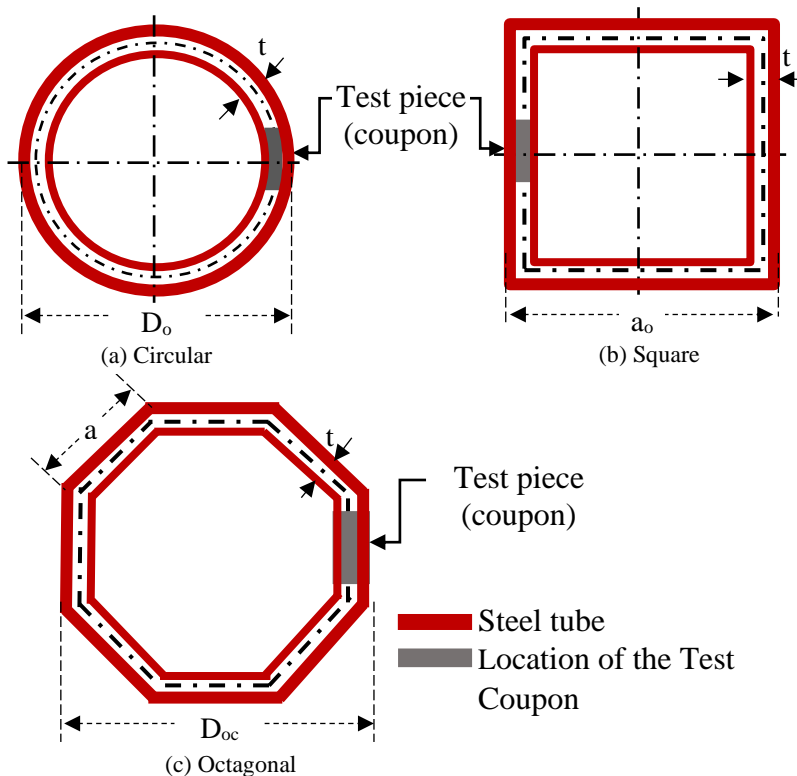
Fig. 3.1 Schematic view of the location of the test coupon for tensile testing of steel tubes.
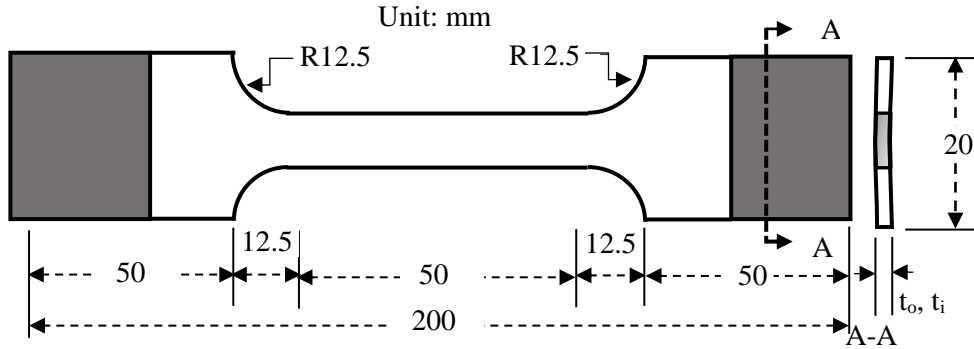
Fig. 3.2 Geometry and dimensions of test specimens (coupons)

3.2.1.2. Test Set-up and Procedure

The standard Biss dynamic UTM machine was used to perform the tensile coupon test with a capacity of 100 kN, as shown in Fig. 3.3. The displacement control method was employed to determine the properties of the steel coupons. The phase rate of loading was set to 1 mm/min. A crosshead-mounted load cell was used to measure the tensile axial load. The extensometer with a gauge length of 20 mm and travel distance of -2 mm to +2 mm was employed to measure the axial displacement of the central region of the test coupon before the yield point. The displacement transducer, integrated into the machine, was used to obtain the axial displacement after yielding the steel specimens.
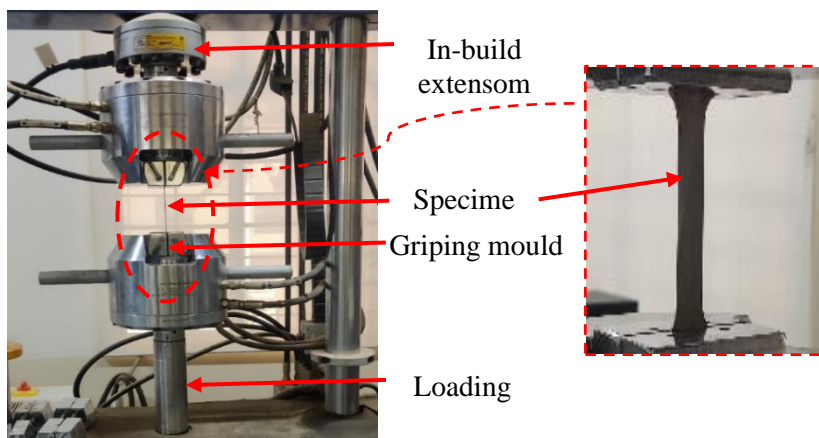
Fig. 3.3 Tensile coupon test set-up of Biss dynamic UTM machine

The results from the extensometer and the displacement transducer were then combined to obtain the complete displacement-time history of the samples. The load cell, extensometer, and displacement transducer measured the data at a frequency of 10 Hz, and the data were recorded using the software.

3.2.1.3. Test Result of Tensile Coupon Test

Fig 3.4 shows the tensile coupon test for a typical specimen before and after failure mode. The stress-strain curves obtained from the tensile tests conducted on the specimens (coupon) of external (o) -internal (i) steel tubes of circular ($diameters\ D_o\ and\ d_i$), octagonal ($largest\ diameter\ D_{oc}$) and square ($side\ lengths\ a_o\ and\ a_i$) section tubes are presented in Fig. 3.5. The mechanical properties of the steel tubes are shown in Table 3.1.

(a)	(b)
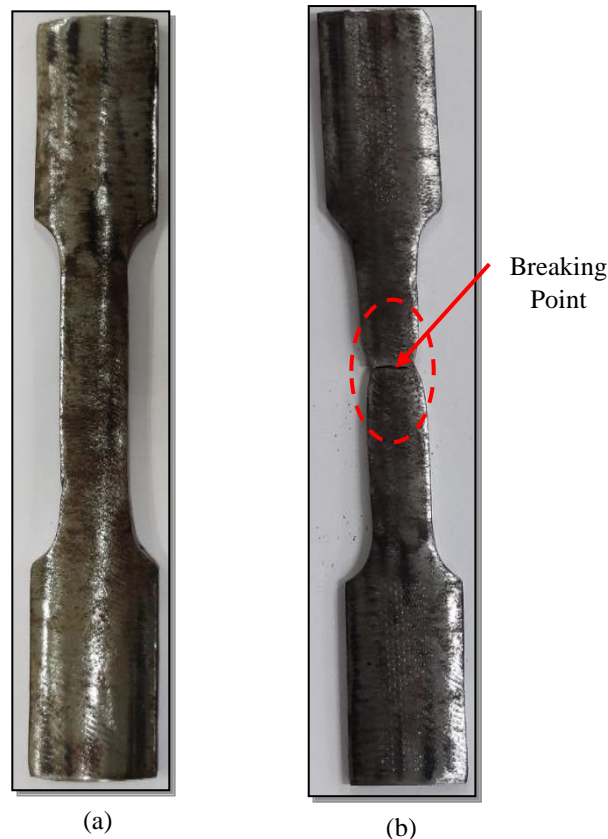
Fig. 3.4 Tensile coupon test specimen (a) Coupon test specimen before failure, (b) Coupon test specimen after failure
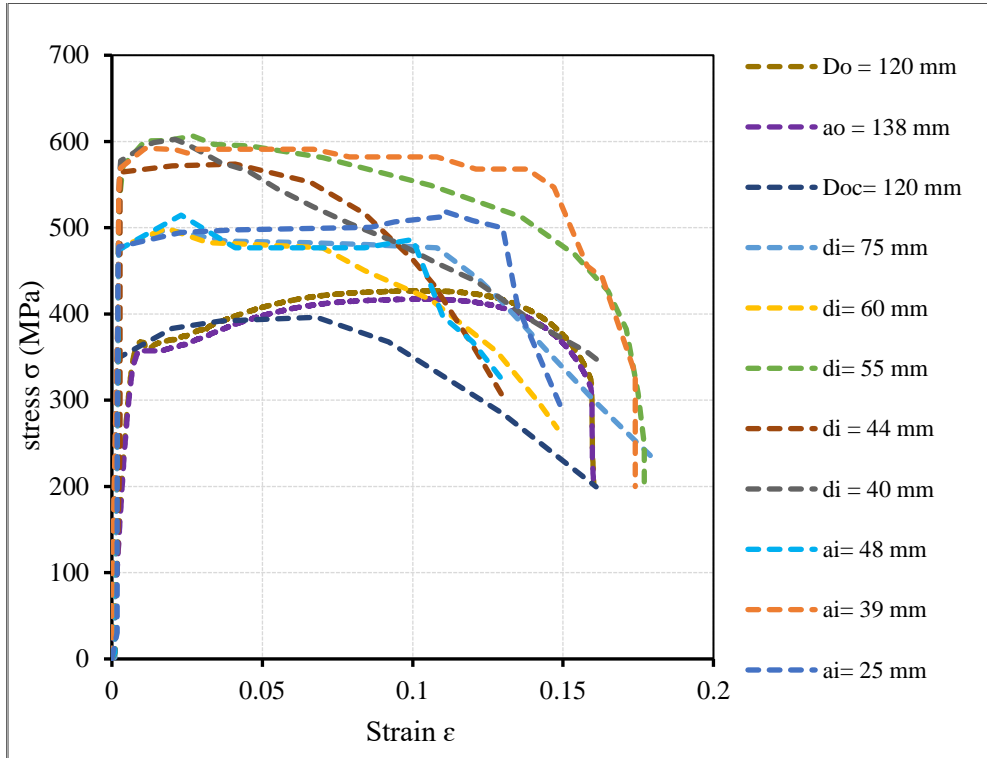
Fig. 3.5 Stress-strain curve of the steel tubes

Table. 3.1 Mechanical properties of steel tubes

Description	Diameter (mm)	Yield strength, $f_{syo,}$ f_{syi} (MPa)	Ultimate strength, $f_{syo,}$ f_{syi} (MPa)	Yield strain, ε_{sy}	Ultimate strain, ε_{su}	Elastic modulus, E_s (GPa)
Circular steel tube (D_o)	138	381	498	0.0018	0.021	212
Square steel tube (D_o)	140	383	500	0.0019	0.021	202
Octagonal steel tube (D_{oc})	120	348	396	0.0017	0.068	204
Circular steel tube (d_i)	75	474	497	0.0023	0.018	206
Circular steel tube (d_i)	60	476	499	0.0022	0.070	216
Circular steel tube (d_i)	55	531	606	0.0025	0.027	212
Circular steel tube (d_i)	44	564	574	0.0027	0.041	208
Circular steel tube (d_i)	40	571	599	0.0029	0.011	197
Square steel tube (a_i)	48	474	514	0.0023	0.023	206
Square steel tube (a_i)	39	569	591	0.0029	0.011	196
Square steel tube (a_i)	25	451	519	0.0021	0.011	215

56

3.2.2. Material Properties of Concrete

The Static concrete compression machine was used to determine the mechanical properties of unconfined concrete as per IS 456 (2000). These results were used for the numerical modeling of CFDST and CFMST columns under axial and eccentric loads.

3.2.2.1. Test Specimen Preparation

In this study, the concrete grade strength doesn't prominently impact the scale of the test (Chung *et al.,* 2013; Lai *et al.,* 2014; Le *et al.* 2017), so only a standard grade of concrete was used to fill the sandwich portion between the external and internal steel tubes. The raw material components of the infill concrete consist of 43 grades of conventional Ordinary Portland Cement (OPC), fine aggregate, coarse aggregate, and water. The mix proportion of sandwich concrete is shown in Table 3.2. The raw materials were mixed in two batches using a concrete mixer. For each batch, three standard concrete cubes (150 mm $\times$ 150 mm $\times$ 150 mm) and cylinders (150 $\times$ 300 mm) were cast along with the CFDST specimen and cured at the normal room temperature of 27°C. The compression tests on concrete cubes and cylinders were performed to decide their compressive concrete strengths after 28 days of the casting. The cubic (f_{cu}) and cylindrical (f_c) compressive strength tests were performed according to IS 456-2000 (IS 456, 2000) as, shown in Table 3.3.

Fig. 3.6 Casted Specimen of Cubes and Cylinders

Table. 3.2 Mix proportion of the sandwiched concrete

Material	Cement	Fine Aggregate	Coarse Aggregate	Water
Size / Grade	43	< 4.75 mm	20 mm	–
Quantity (kg / m^3)	499	718	968	192

3.2.2.2. Test set-up and procedure for compression test on unconfined concrete

The axial compressive load was applied using a hydraulic Advanced compression testing machine (ACTM) with a capacity of 2000 kN, as shown in Fig 3.7. The compressive load was increased continuously at a phase rate of 2kN /sec. The load and ultimate compressive strength were measured digitally using the automatic digital logger. No attempt has been made to measure the concrete strain because available laboratory equipment did not allow its measurements. Additionally, the numerical model described in Chapter 4 did not require input for concrete stress-strain characteristics.
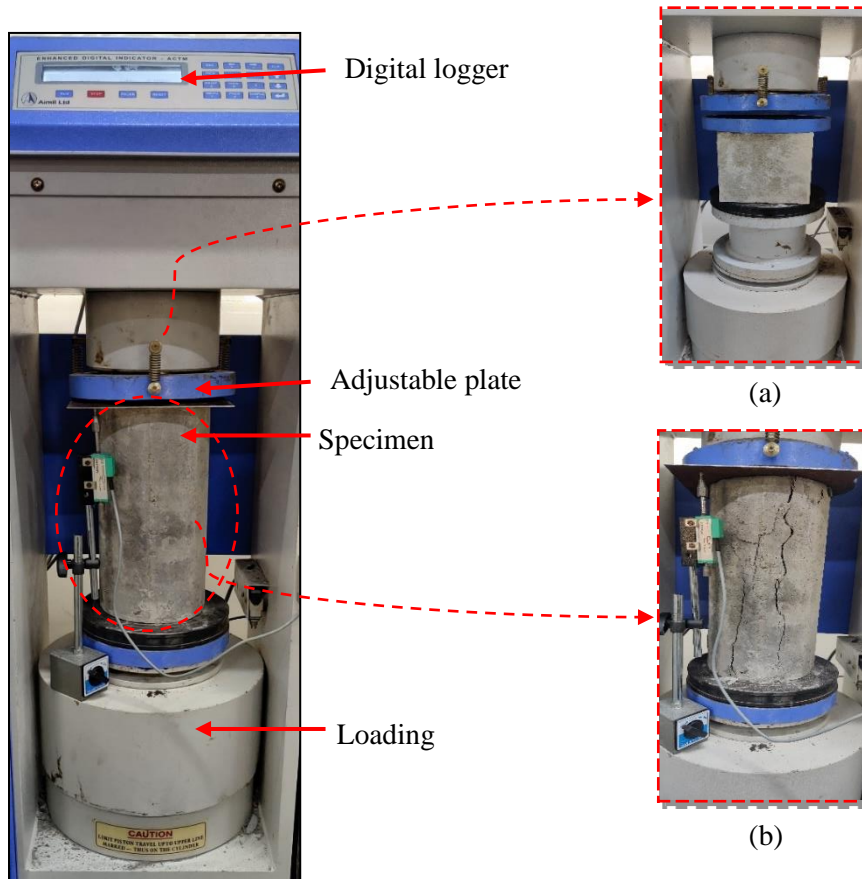
Fig. 3.7 Experimental Set-Up on Compression Testing Machine. (a) Cube testing, (b) cylinder testing

3.2.2.3. Test Result on Compression Test of Concrete

A summary of the compression test on unconfined from three cubes and three-cylinder is provided in Table 3.3.

Table. 3.3 Material properties of concrete

Description	Compressive Strength of Concrete (MPa)			
	Specimen 1	Specimen 2	Specimen 3	Average
Cube (f_{cu})	37.00	35.00	43.00	38.33
Cylinder (f_c)	33.00	31.00	32.00	32.00

3.3. Preparation of Specimens

In total, thirty-three CFDST, eight CFMST, and three CFST short columns with circular square and octagonal cross-sections were prepared. The hollow tubes of octagonal, circular, and square tubes of CFDST column

59

specimens were made of cold-formed steel. The design length of the column was 500 mm, which was cut from the prolonged steel tubes provided by the steel tube dealer, as shown in Fig. 3.8. The CFDST column samples were formed by concentrically aligning the external and internal hollow steel tubes. The markings were made on the bottom steel plate of the CFDST column, as shown in Fig. 3.9(a), to place a central line of the inner steel tube at the centroid of the outer steel tube. Fig. 3.9(b) shows the marking for the outer and inner tubes for the CFMST columns. The external and internal steel tubes were welded with a bottom plate of 5 mm thickness to maintain their concentrical position, as shown in Fig. 3.10. The top surface of the inner steel tube was locked using a tap to avoid the filling of concrete while concreting the sandwich portion of the column specimens, as shown in Fig. 3.11.

Fig. 3.8 Cutting of steel tubes as design length

(a) (b)
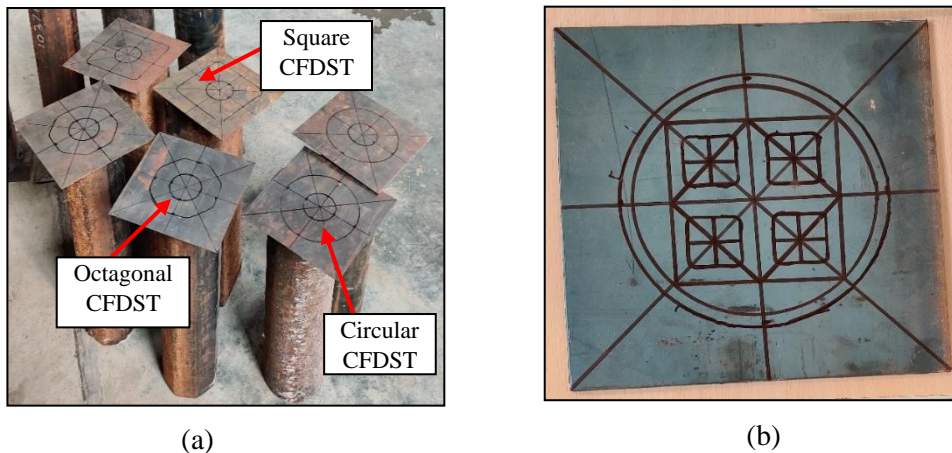
Fig. 3.9 Marking on bottom plate
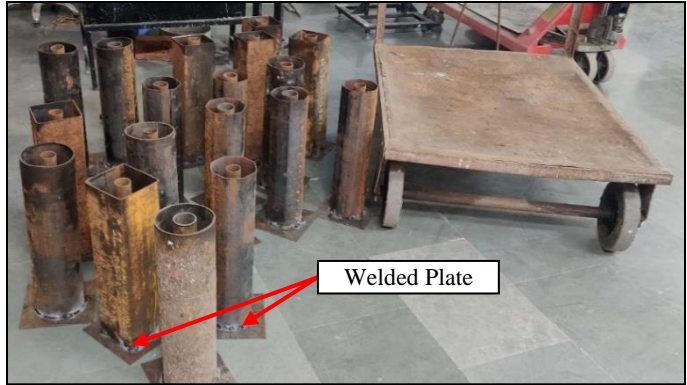
(a)
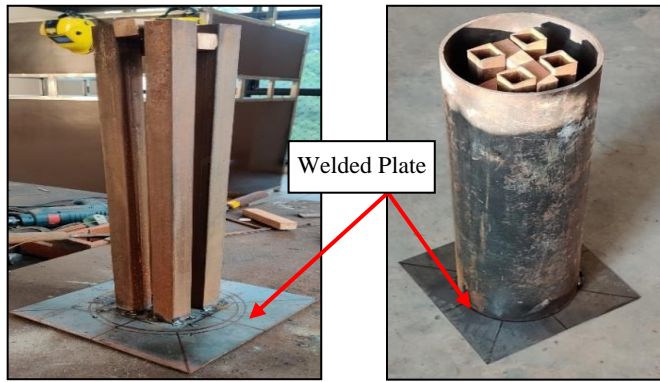
(b)

Fig. 3.10 Welding of bottom plate (a) different cross-section of CFDST column, (b) CFMST column

Fig. 3.11 Locking of Top surface on inner steel tube

Concrete was mixed using the drum mixer, as shown in Fig.3.12. The placing of concrete was done by a bucket from the top of the column specimen tube into five approximate equal layers of 100 mm each. A steel funnel was used to place the concrete between the two tubes in the case of CFMST columns. Each concrete layer was compacted by rodding and striking at the column's top surface from the outside. This process was carried out carefully to ensure no entrapped air pockets.

Fig. 3.12 Drum mixing of concrete

Fig. 3.13 CFDST specimen before placing of concrete

The column specimens were identified by OC-120-75, CC-120-39, and SC-120-25, where the first letter 'O', 'C' and 'S' indicates the shape of the external tube as octagonal, circular, and square, respectively, the second letter 'C' indicates the shape of the internal tube is circular. Moreover, the first and second numbers represent the diameter or width of the external and internal tubes, respectively. The geometrical specification of specimens and mechanical properties of the material are given in Tables 3.1 and 3.3.

Fig. 3.14 CFDST Specimen after Placing of Concrete

3.4. Experimental operation

The hydraulic CTM (Compression Testing Machine) with a capability of 3000 kN was used to employ the concentric and eccentric compressive load on the circular and octagonal CFDST short column. The CTM is fitted with an adjustable plate at the top and a flat bottom surface with a clear vertical distance of 1m. For CFDST specimens, the top and bottom facades are ground smooth and flat tires, using a hand grinding apparatus to safeguard uniform loading function as shown in Fig 3.15. The linear variable displacement transducers (LVDT) were placed using the standard magnetic to avoid the movement of the error to evaluate the axial deformation of circular and octagonal CFDST short columns, as shown in Fig 3.16 (a & b).
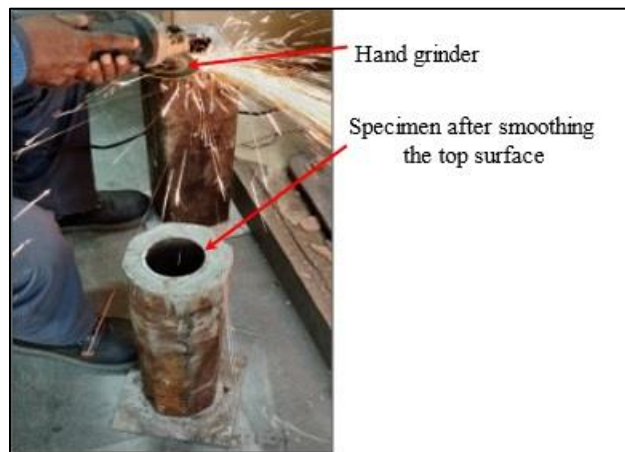
Fig. 3.15 Surfaces smoothing and flattening using a hand grinder

The specimens were gently squashed before testing to safeguard perfect vertical alignment over the machine using a right-angle triangle scale. The axial compressive load was promptly applied to the column's upper surface without restraining the column ends, as shown in Fig. 3.16 (b) schematic diagram. Due to the direct application of loading, the CFDST short column may undergo a higher capacity. Still, it may result in unconservative design suggestions. An end-warping mode occurs in actual buildings and bridges after terrible damage due to structural failure during Hanshin Earthquake in Kobe-Japan, in 1995

(Wardenier, 2001; Zhao and Han, 2006) and may occur in double-skin concrete-filled tubes (Uy, 2001; Ronagh, 2011).
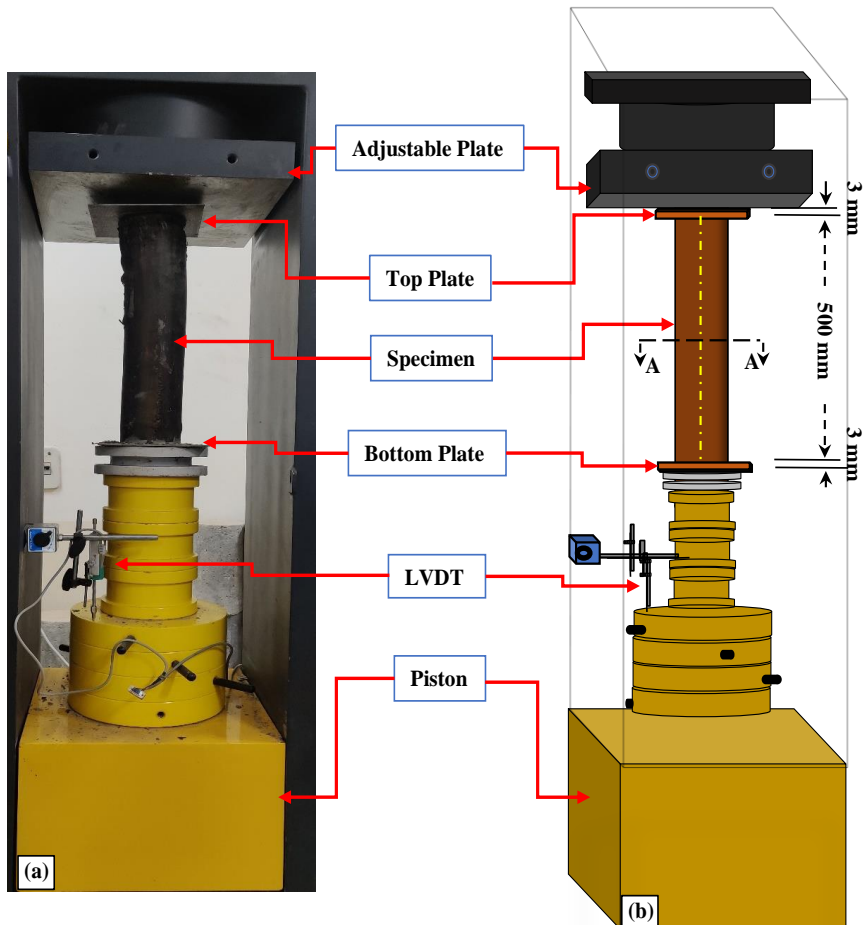
Fig. 3.16 Test set-up of CFDST column under concentric loading (a) Experimental test, (b) Schematic view

The load was employed at a 1.0 kN/sec rate at the elastic stage, whereas displacement-load control at a 1mm/min rate was employed following the slope of the load-displacement curve change. The applied load and LVDT data acquisition system readings were saved by computer control. The tests were ended till the axial deformation was reduced to about 30mm. The test set-up and assembly of dashboards are shown in Fig. 3.16.

Chapter – 4
Numerical Simulation

4.1. General

In general, experimental studies are the best method to study the structural behavior of a member or structure. However, experimental testing is generally very costly, requires more effort, and is time-consuming. The complication involved in such methods naturally rises with the increased number of parameters to be studied. Moreover, the application of experimental techniques also depends upon the viable availability and accessibility of materials, testing equipment, and machinery. In such situations, the numerical analysis provides an affordable alternative and solution to practical problems for a researcher to explore the behavior of a structural element in detail. This chapter presents the development of a full-scale Finite Element (FE) model to replicate the actual behavior of the CFST, CFDST, and CFMST.

4.2. Modelling of Concrete Core

In the CFST/CFDST/CFMST columns, concrete is confined by steel tubes; as a result, it is subjected to a tri-axial stress state. In the non-linear finite element analysis CFST/CFDST/CFMST members, the modeling of the concrete core plays a vital role. There are several constitutive models of concrete for capturing the non-linear response. However, due to the complex behavior of concrete core, there is no standard constitutive model for modeling a concrete core in CFST/CFDST/CFMST members. A model selection primarily depends on the nature of the problem to be analyzed. In the ABAQUS, the concrete core can be molded using the Drucker Prager (DP) model or the Concrete Damage Plasticity (CDP) approach. The DP and CDP models are widely used in the analysis of concrete-filled tubes, and their suitability has been verified with various experimental data by several researchers (Ahmed *et al.,* 2020; Alqawzai *et al.,* 2020; Han *et al.,* 2011; Hassanein *et al.,* 2018; İpek

et al., 2021; Wang *et al.,* 2019). In this study, the DP model is used for modeling the CFST column, and the CDP model is used to model CFDST and CFMST. The DP and CDP models are briefly described in the following sub-sections.

4.2.1. Drucker Prager (DP) Model

The Drucker-Prager (DP) model is a three-dimensional hydrostatic-pressure-dependent yield criterion, and it is suitable for modeling materials subjected to substantially high compressive stresses. The DP model has a circular yield locus in the deviatoric plane, and it is based on the assumption that in a meridian plane, the equivalent Von-Mises stress linearly depends on hydrostatic pressure (Wai-Fah Chen, 1982; Bardet, 1990). ABAQUS (2014) incorporates the Extended Druker-Pager (ED-P) model in three different forms, namely Linear, Hyperbolic and Exponential; however, the linear ED-P model has been used in this study. The detailed formulation of the ED-P model is given in Appendix-A.

4.2.1.1. Stress-strain Model for Confined Concrete

Based on the series of tests conducted by numerous researchers (Richart *et al.,* 1928; Mander *et al.,* 1988; Cusson and Paultre,1995; Attard and Setunge, 1996), it is well understood that the uniaxial compressive strength and the corresponding strain of confined concrete become much higher than those for unconfined concrete. According to Richart *et al.,* (1928), the enhanced peak uniaxial compressive strength of confined concrete (f'_{cc}) due to lateral confining pressure (f_l) and the uniaxial strain associated with peak strength (ε'_{cc}) may be estimated using the following equations

$$f'_{cc} = f'_c + k_1 f_l \tag{4.1}$$

$$\varepsilon'_{cc} = \varepsilon'_c \left[1 + k_2 \frac{f_l}{f'_c} \right] \tag{4.2}$$

where, f'_c is the unconfined cylindrical compressive strength of concrete, ε'_c the

is uniaxial strain corresponding to stress f_c' which is usually considered 0.002, as specified by ACI (2014). In Eq. (4.1 and 2), k_1 and k_2 are the constants usually taken as 4.1 and 20.5, respectively, as suggested by Richart *et al.,* (1928). In the CFST columns, the magnitude of f_l Significantly depends on the column's cross-sectional shape and the lateral dimension to steel tube thickness ratio. The magnitude of lateral confining pressure f_l for Circular, Square, Octagonal, and Elliptical CFST columns may be determined using the following equations (Hu *et al.,* 2003).

For Circular, octagonal, and elliptical CFST Columns

$$\frac{f_l}{f_y} = 0.043646 - 0.000832\left(\frac{D_0}{t}\right) \quad for \ 21.7 \le \frac{D_0}{t} \le 47 \tag{4.3}$$

$$\frac{f_l}{f_y} = 0.006241 - 0.0000357\left(\frac{D_0}{t}\right) \quad for \ 47 \le \frac{D_0}{t} \le 150$$

For Square CFST Columns

$$\frac{f_l}{f_y} = 0.055048 - 0.001885\left(\frac{a_0}{t}\right) \quad for \ 17 \le \frac{a_0}{t} \le 29.2 \tag{4.4}$$

$$\frac{f_l}{f_y} = 0 \quad\quad\quad\quad\quad\quad\quad\quad for \ 29.2 \le \frac{a_0}{t} \le 150$$

where, f_y = yield strength of the steel used in the tube, D_0 = external diameter of Circular, octagonal, and elliptical CFST column sections, a_0= external side length of Square CFST column section, and t = thickness of steel tube. Various researchers have proposed different uniaxial stress-strain models for confined concrete (Saenz, 1964; Mansur *et al.,* 1995; Susantha *et al.,* 2001; Karthik and Mander, 2011; Lai and Ho, 2016; Ahmed and Guneyisi, 2019). The uniaxial stress-strain model proposed by Saenz (1964) has been proved to satisfactorily predict the behavior of concrete confined in steel tube(s) in the ascending portion of the stress-strain curve when the strain in concrete, $\varepsilon \le \varepsilon_{cc}'$ as shown

in Fig. 4.6 (Hu *et al.,* 2003; Laio *et al.,* 2013; Han *et al.,* 2007). The ascending portion between points A and B in Fig. 4.1 ($\varepsilon \leq \varepsilon'_{cc}$) the relation between the stress (f) and strain (ε) is defined according to Saenz's stress-strain model, as

$$f = \frac{E_{cc}\varepsilon}{1 + (R + R_E - 2)\left[\frac{\varepsilon'_c}{\varepsilon'_{cc}}\right] - (2R - 1)\left[\frac{\varepsilon'_c}{\varepsilon'_{cc}}\right]^2 + R\left[\frac{\varepsilon'_c}{\varepsilon'_{cc}}\right]^3} \tag{4.5}$$

where, ε'_c is the peak strain in unconfined concrete and E_{cc} is the modulus of elasticity of confined concrete, and its value is calculated using the recommendations of ACI (2014) as

$$E_{cc} = 4700\sqrt{f'_{cc}} \tag{4.6}$$

In eq. 4.5, R_E and R are the model parameters which are defined as (Saenz, 1964)

$$R_E = \frac{E_{cc}\,\varepsilon'_{cc}}{f'_{cc}} \; ; \qquad R = \frac{R_E(R_\sigma - 1)}{(R_\varepsilon - 1)^2} - \frac{1}{R_E} \tag{4.7}$$

Where both the parameters R_ε and R_σ are taken equal to 4, as suggested by Hu and Schnobrich (1989).
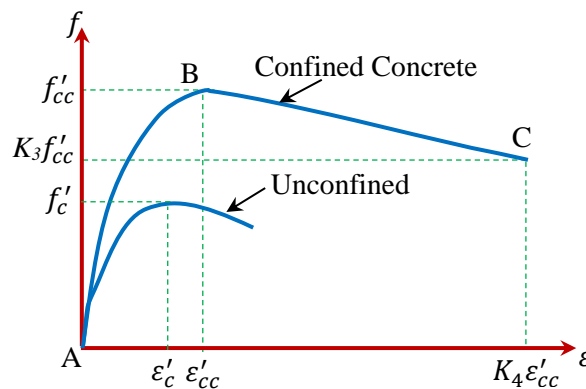

Fig. 4.1 Stress-Strain Curve of Confined Concrete (Mander et al., 1988)

When the strain in confined concrete exceeds ε'_{cc}. The stress in concrete is

assumed to decrease linearly up to strain level $K_4\varepsilon'_{cc}$ where the value of K_4 is normally considered equal to 11. In the descending segment of the stress-strain curve (between points B and C), the final stress point C is taken as $K_3 f'_{cc}$ where K_3 is a parameter, and its value depends on section geometry. The value of K_3 for different sections is calculated using the following empirical relations

For circular, octagonal, and elliptical CFST Columns

$$
\begin{aligned}
&K_3 = 1 && for\ 21.7 \leq \frac{D_0}{t} \leq 40 \\
&K_3 = 0.0000339 \left(\frac{D_0}{t}\right)^2 - 0.010085 \left(\frac{D_0}{t}\right) + 1.3491 && for\ 40 \leq \frac{D_0}{t} \leq 150
\end{aligned}
\tag{4.8}
$$

For Square CFST Columns

$$
\begin{aligned}
&K_3 = 0.000178 \left(\frac{a_0}{t}\right)^2 - 0.02492 \left(\frac{a_0}{t}\right) + 1.2722 && for\ 17 \leq \frac{a_0}{t} \leq 70 \\
&K_3 = 0.4 && for\ 70 \leq \frac{a_0}{t} \leq 150
\end{aligned}
\tag{4.9}
$$

Where, D_0 = external diameter of Circular, octagonal, and elliptical CFST column sections, a_0= external side length of Square CFST column section, and t is the thickness of the steel tube.

4.2.2. Concrete Damage Plasticity (CDP) Model

In order to model the strength of concrete infilled in the CFDST column, the uniaxial stress-strain model of confined concrete was proposed by various authors (Han *et al.,* 2007; Dong *et al.,* 2015; Kwan *et al.,* 2015, 2016; Lai and Ho 2016a, 2016b; Lai *et al.,* 2019a; Ho *et al.,* 2020; Lai *et al.* 2020a; Lai *et al.,* 2020a) has been examined. The uniaxial stress-strain behavior of confined concrete, the stress-strain model proposed by Han *et al*., (2007), has been adopted in this study since many authors have widely used it. According to Han Han *et al.,* (2007), the stress-strain curve of concrete confined in a hollow steel tube(s) may be expressed in terms of non-dimensional parameters. For normalizing the stress and strain at any stage of loading, the stress σ and strain ε are normalized by the peak stress in an unconfined state (σ_0) and the strain

corresponds to peak stress (ε_0) respectively. The normalized stress y $(= \sigma/\sigma_0)$ and normalized strain x $(= \varepsilon/\varepsilon_0)$ are defined as

$$y = \begin{cases} 2x - x^2 & (x \leq 1) \\ \dfrac{x}{\beta_0(x - 1)^2 + x} & (x > 1) \end{cases} \tag{4.10}$$

In Eq. (4.9), the parameter β_0 is the material factor defined as

For Circular, Octagonal, and Elliptical CFDST column

$$\beta_0 = (2.36 \times 10^{-5})^{[0.25+(\xi-0.5)^7]}(f_c)^{0.5} \times 0.5 \quad \geq 0.12 \tag{4.11a}$$

For the Square CFDST column

$$\beta_0 = \frac{f_c^{0.1}}{1.2\sqrt{1 + \xi}} \tag{4.11b}$$

In Han's model, the peak stress (σ_o) is taken as the unconfined cylindrical strength of concrete f_c (N/mm^2) and the peak strain (ε_o) is defined as

$$\varepsilon_o = \varepsilon_c + 800\xi^{0.2} \times 10^{-6} \tag{4.12}$$

where, $\varepsilon_c = (1300 + 12.5\,f_c') \times 10^{-6}$,

In Eq. (4.10 a & b) and (4.11), ξ is the confinement ratio, and it is calculated by Eq. (4.12).

$$\xi = \frac{A_{so}}{A_c} \cdot \frac{f_{yo}}{f_{ck}} = \alpha \frac{f_{yo}}{f_{ck}} \tag{4.13}$$

In the above expression, α is the ratio of the area of the cross-section of the outer hollow steel tube (A_{so}) and concrete core (A_c), f_y is the yield strength of steel tube material, and f_{ck} (= unconfined cylindrical compressive strength of concrete) as the characteristic strength of concrete. For standard-strength concrete, the characteristic strength f_{ck} is taken as 0.67 times the characteristic cube strength of concrete (f_{cu}) (Han *et al.,* 2005). The initial modulus of elasticity (Fig. 4.2) and Poisson's ratio of concrete are taken according to ACI

recommendations (ACI, 2014), given as $E_c = 4730\sqrt{f_c}$ and $\mu_c = 0.2$, respectively.
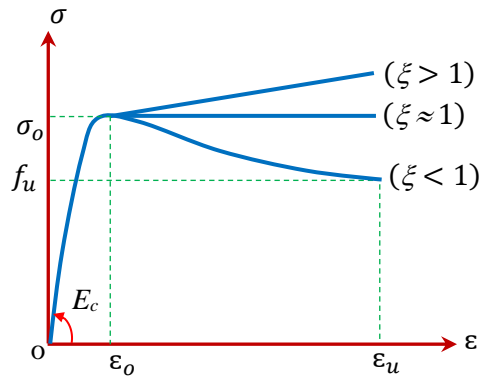

Fig. 4.2 Stress-strain curve for confined concrete

The uniaxial stress-strain curve for confined concrete is shown in Fig. 4.2, where f_u, and ε_u are the strength of concrete and strain at the ultimate (Failure) stage. The value of ε_u is taken as 0.05, and f_u is taken as 0.8 times the characteristic unconfined cylindrical strength of concrete (f_{ck}) i.e. $f_u = 0.8\, f_{ck} = 0.8 \times (0.67 f_{cu}) = 0.536 f_{cu}$. The tensile softening behavior of concrete needs to be set to analyze the CFDST column under axial compression in ABAQUS software. A kind of fracture energy model, which can be started by specifying the post-failure stress as a tabular function of cracking displacement proposed by Hillerborg (Hillerborg, Modéer and Petersson, 1976), was selected and used in the analysis.

4.2.2.1. Concrete Damage Plasticity

The concrete damage plasticity (CDP) model available in ABAQUS considers isotropic elastic damage in conjunction with isotropic tensile and compressive plasticity to incorporate the inelastic behavior of concrete (ABAQUS (2014). The CDP-based modelling of concrete includes a model representing the compressive behavior of concrete, a damage variable, a yield criterion, a hardening/softening rule, and a flow rule.

4.2.2.2. Dilation Angle

Dilation angle (ψ), which defines the direction of plastic flow, is one of the critical input parameters in Abaqus for carrying out the non-linear finite element analysis of structures. The dilation angle is defined as the ratio of plastic volume change to plastic shear strain. For concrete material, the magnitude of dilation ranges between $0°$ to $56°$ in ABAQUS, where a zero value of the dilation angle indicates that the volume of concrete is preserved during deformation. In the analysis of CFDST, as the value of ψ is increased, the dilation rate of concrete increases and results in stronger interaction between steel and concrete, which causes higher confining stresses in concrete at higher loads. Consequently, the computed ultimate strength of the CFST column increases with an increase of ψ.

Moreover, Tao (Tao, Wang and Yu, 2013) noticed that the initial portion of the axial-load vs. axial-strain curve is not significantly affected by the selection of ψ value, which infers that the adopted value of the dilation angle will predominantly affect the ultimate strength of the CFST column. Yu (Liao *et al.,* 2017) concluded that the selection of ψ value depends on the confining stress and plastic deformation of concrete. Since the plastic deformation of concrete is restrained by steel tubes, for circular sections, ψ is assumed to depend on confinement factor ξ only as (Tao, Wang and Yu, 2013).

$$\psi = \begin{cases} 56.3(1-\xi) & for\ \xi \leq 0.5 \\ 6.672e^{7.4/(4.64+\xi)} & for\ \xi > 0.5 \end{cases} \qquad (4.14)$$

The parameters associated with this model as input in ABAQUS are shown in Table 4.1. where the flow potential eccentricity (e) is 0.1, The (f_{b0}/f_c'), is the ratio of initial equiaxial compressive yield stress to initial uniaxial compressive yield, (K_C) is the shape factor of the yield surface and (k) is the viscosity parameter, where the time increment should be around 15% of step for the better solution.

Table. 4.1 Material parameters of the CDP model for concrete

Dilation angle (ψ)	Eccentricity ($\in$)	f_{b0} / f_{c0}	k_c	Viscosity parameter
31	0.1	1.16	0.67	0.002

$$\frac{f_{b0}}{f_c} = 1.5(f_c)^{-0.075} \tag{4.15}$$

$$K_c = \frac{5.5}{5 + 2(f_c)^{0.075}} \tag{4.16}$$

4.2.2.3. Concrete Damage Models

The non-linear behavior of concrete is attributed to damage and plasticity. The process of damage can be attributed to microcracking, coalescence, decohesion, etc. The plasticity behavior of concrete can be described by several phenomena, such as strain softening, progressive deterioration, volumetric expansion, etc., which reduces the strength and stiffness of concrete (Lubliner *et al.,* 1989; Grassl and Jirásek, 2006; Cicekli, Voyiadjis and Abu Al-Rub, 2007). Damage parameters usually characterize the degradation of stiffness. The isotropic scaled damage model from the continuum damage mechanics is introduced in ABAQUS to describe the stiffness degradation by Eq. (4.17) under uniaxial loading.

$$\sigma = (1 - d)E_0(\varepsilon - \varepsilon^{pl}) \tag{4.17}$$

where σ, ε, and ε^{pl} represent, respectively, the stress, total strain, and plastic strain; E_0 is initial (undamaged) elastic stiffness, and d is the damage factor, which characterizes the degradation of the elastic stiffness and has values in the range of 0-1 (zero is undamaged, and one is fully damaged) (Tao and Chen, 2015). The degraded stiffness E is defined as

$$E = (1 - d)E_0 \tag{4.18}$$

If no damage is considered in the concrete $(d = 0)$Eq. (4.16) is reduced to.

$$\sigma = E_0(\varepsilon - \varepsilon^{pl}) \tag{4.19}$$

in which the plastic stain (ε^{pl}) is the same as that without stiffness degradation (ε^p) as shown in Fig. 4.3(b). According to irreversible deformation/plastic strain, the stiffness degradation models can be classified into two types elastic degradation models and plastic degradation models (Lubliner *et al.,* 1989). The elastic degradation models are associated with the total strain (ε), indicating that no plastic strain exists ($\bar{\varepsilon}^p = \varepsilon^p = 0$, where $\bar{\varepsilon}^p$ = plastic strain with stiffness degradation), so the unloading branch passes through the origin as shown in Fig. 4.8. Then Eq. (4.17), in this case, can be rewritten as

$$\sigma = (1 - d)E_0\varepsilon \qquad\qquad (4.20)$$

Where ε is the total strain, Lubliner *et al.* (1989) highlighted that the concept of elastic degradation is correlated with the total deformation without a damage criterion. A plastic degradation, in which the stiffness degradation is associated with the plastic deformation instead of the total deformation, was established to overcome the elastic degradation model faults (Lubliner *et al.,* 1989). It means that irreversible deformation/plastic strain exists after the damage has occurred in which the plastic strain with stiffness degradation $\bar{\varepsilon}^p \neq 0$ as shown in Fig. 4.3(b) as a result, the Eq. (4.17) rewritten as

$$\sigma = (1 - d)E_0(\varepsilon - \bar{\varepsilon}^p) \qquad\qquad (4.21)$$

Lubliner *et al. (1989)* proposed a simple damage model in which plastic degradation occurs only in the softening range, and the stiffness is proportional to the cohesion (C) of the material

$$\frac{E}{E_0} = \frac{C}{C_{max}} = 1 - d \qquad\qquad (4.21)$$

$$d = 1 - \frac{C}{C_{max}} \qquad\qquad (4.22)$$

where C is cohesion in the yield criteria, which is proportional to stress (σ) and C_{max} is proportional to the strength of the concrete (Lubliner *et al.,* 1989). Under uniaxial tension or compression, Eq. (4.22) can be reduced to

$$d = 1 - \frac{\sigma}{f} \tag{4.23}$$

In which f is either the tensile or compressive stress in concrete. Based on the stress-strain curve shown in Fig. 4.3(b), $\bar{\varepsilon}^p$ can be related to the damage factor (d) is defined as

$$\bar{\varepsilon}^p = \varepsilon^p - \frac{d}{(1-d)}\frac{\sigma}{E_0} \tag{4.24}$$

Substituting Eq. (4.23) into Eq. (4.24) yields

$$\bar{\varepsilon}^p = \varepsilon - \frac{\sigma}{E_0} - \frac{f-\sigma}{E_0} = \varepsilon - \frac{f}{E_0} \tag{4.25}$$

in which (f/E_0) = elastic strain at the peak stress. Therefore, it is observed in this study that in the Lubliner *et al., (1989)* damage model, the elastic strain will remain constant (f / E_0) after the peak stress.
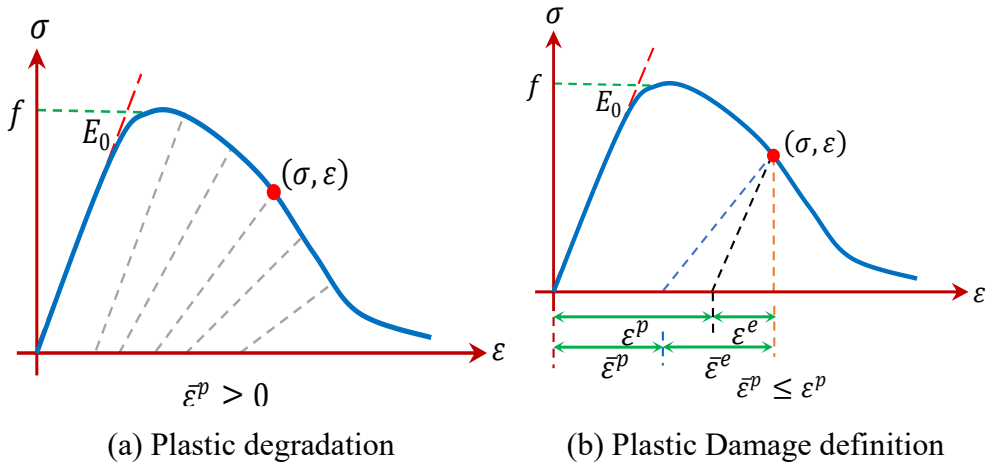

(a) Plastic degradation   (b) Plastic Damage definition

Fig. 4.3 Damage plasticity model of concrete

4.3. Modelling of Steel Tube

In order to capture the non-linear behavior of steel, a five-stage stress-strain curve has been used, where the stress-strain curve has been divided into five regions, namely, elastic $(O - A)$, elasto-plastic$(A - B)$, plastic$(B - C)$, strain-hardening $(C - D)$ and the secondary plastic $(D - E)$ regions as shown in Fig. 4.4 (Han, Zhao and Tao, 2001). For a steel having yield and ultimate strengths as f_{sy} and f_{su} respectively, the stress-strain relation is assumed linear up to the proportional limit $f_{sp}(= 0.8f_{sy})$ and its behavior is considered perfectly plastic when the stress in steel attains the ultimate stress f_{su} ($= 1.6f_{sy}$). The stress-strain relation for different regions are as follows:

$$\sigma = E_s\varepsilon \qquad\qquad for\ \varepsilon \le \varepsilon_1\left(= 0.8f_{sy}/E_s\right)$$

$$\sigma = -A\varepsilon^2 + B\varepsilon + C \qquad\qquad for\ \varepsilon_1 < \varepsilon \le \varepsilon_2(= 1.5\varepsilon_1)$$

$$\sigma = f_{sy} \qquad\qquad for\ \varepsilon_2 < \varepsilon \le \varepsilon_3(= 10\varepsilon_2)$$

$$\sigma = f_{sy}\left[1 + 0.6\frac{\varepsilon - \varepsilon_3}{\varepsilon_4 - \varepsilon_3}\right] \qquad\qquad for\ \varepsilon_3 < \varepsilon \le \varepsilon_4(= 100\varepsilon_2)$$

$$\sigma = 1.6f_{sy} \qquad\qquad for\ \varepsilon > \varepsilon_4$$

where A, B, and C are constants that are defined as

$$A = \frac{0.2f_{sy}}{(\varepsilon_2-\varepsilon_1)^2}, \qquad B = 2A\varepsilon_2, \qquad C = 0.8f_{sy} + A\varepsilon_1^2 - B\varepsilon_1 \qquad\qquad (4.26)$$

where, $\varepsilon_1 = 0.8f_{sy}/E_s$ and $\varepsilon_2 = 1.5\ \varepsilon_1$
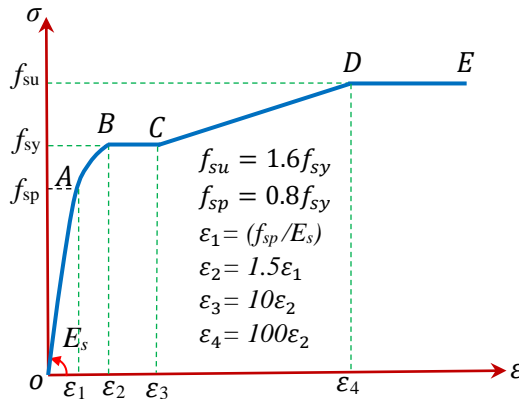

Fig. 4.4 Stress-strain curve for steel

4.4. Modelling of Steel tube – concrete interface

In order to simulate the interaction between the steel and concrete in the CFDST column in the ABAQUS, the contact interaction was used. The contact interaction is defined by the geometric and mechanical properties of the contact interface. The geometric property of contact surfaces is defined by selecting appropriate contact discretization, tracking approach, and defining the steel surface as the master surface and concrete as the slave surface. During the FE analysis, there remains a possibility that some individual nodes in the master surface (steel tube) may penetrate the slave surface (concrete). However, largely undetected, there is a low probability that penetrations of master surface nodes into the slave surface do not occur with this discretization. Such penetrations can be further eliminated by carefully selecting the master surface and discretizing contact surfaces with finite elements (Huang *et al.,* 2010). A small sliding tracking approach is selected for the contact since the actual sliding between steel and concrete surfaces in the CFDST column would be relatively minimal. To model the mechanical properties of normal behavior, "hard contact" is used. The Coulomb friction model is adopted in the tangential directions, and the friction coefficient is 0.6.

4.5. Finite Element Modelling of Concrete Filled Steel Tubular Members

ABAQUS FE software was adopted in this study to simulate the behavior of different cross-sectional geometries of the CFST, CFDST, and CFMST short columns under axial and eccentric compressive loading. The full-scale FE model is developed to replicate the actual composite behavior of the CFDST columns.

4.5.1. Selection of Elements Type

In the CFDST column, the concrete, inner and outer steel tubes are discretized using the 8-node brick elements with reduced integration (C3D8R).

The reason for using the C3D8R element to discretize the concrete core is attributed to the fact that the infilled concrete in a CFDST column under concentric axial compression mainly experiences compression as the dominant deformation, and there is no trace of rotation. Hence, the element C3D8R can effectively reflect the deformation features of the infilled concrete. The numerical studies carried out by Dai and his colleagues (Dai and Lam, 2010; Dai *et al.,* 2014) on elliptical CFST columns and by Durate (Duarte *et al.,* 2016) on the circular CFST stub column revealed that there was no significant difference between the predicted results obtained using elements S4R shell element and the C3D8R solid element. However, they pointed out that using shell elements may affect the steel tube contacting the curved surface and the infilled concrete because the wall thickness (shell thickness) is much smaller than the element size. This issue can be rectified by simulating the interaction surface between the concrete core and steel tube. Therefore, the concrete core and steel tubes were modeled using the C3D8R element, as shown in Fig 4.5
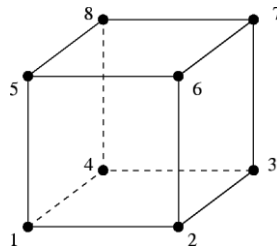

Fig. 4.5 Eight-node brick elements with reduced integration (C3D8R)

The outer and inner steel tubes are modeled using the solid C3D8R element. Each member (outer steel tube, inner steel tube, and concrete core) is modeled as a unit member using the assembly command, and the unit members are assembled as CFDST members, as shown in Fig 4.6.
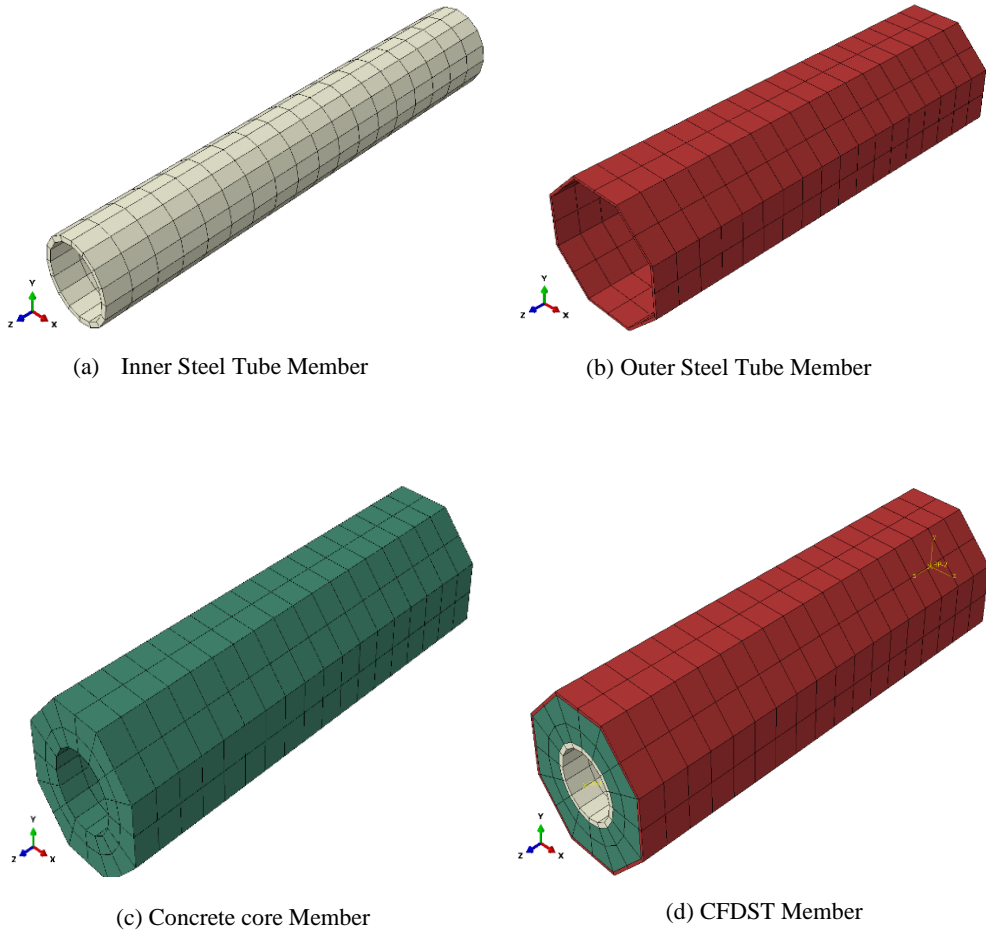
(a) Inner Steel Tube Member

(b) Outer Steel Tube Member

(c) Concrete core Member

(d) CFDST Member

Fig. 4.6 Modelling of Members

4.5.2. Boundary Conditions

For applying boundary conditions on axial and eccentric load on CFST, CFDST, and CFMST columns in ABAQUS, the reference points RP1 and RP2 are considered at the top and bottom face of the column. All the concrete core and steel tube nodes located at the top face of the column were connected to RP1 via rigid ties, and similarly, all the nodes of the concrete core and steel tube located at the bottom face were connected to RP2. While determining the column's axial compressive strength via experiments, rigid steel plates are usually provided at the top and bottom face of the column. These plates restrain the rotations at the ends of the column. In order to replicate the boundary

80

conditions analogous to those experienced by CFDST during the experiment, the RP2 was fully restrained $\left(i.e.\, U_x = U_y = U_z = UR_x = UR_y = UR_z = 0\right)$ while the point RP1 was allowed to displace along the axial loading direction only $\left(i.e.\; U_x = U_y = UR_x = UR_y = UR_z = 0;\; U_z \neq 0\right)$ as shown in Fig. 4.8. The axial load was applied at RP1 concentrically in the form of displacement control. The CDP model was used to simulate plastic deformation in the concrete core. The parameters associated with this model were given as input in ABAQUS.

4.5.3. Selection of Optimum Mesh Sizes

The optimum size of the mesh was determined by using mesh sensitivity analysis to reach the reliability of the FE simulations. In this study, thirty-two FE analysis trials were carried out on CFDST specimens tested by various researchers in the past. The CFDST specimens considered for mesh sensitivity analysis were C1-1 $(D_o \times B_o \times t_o = 220 \times 220 \times 3.62\text{mm},\; d_i \times b_i \times t_i = 159 \times 159 \times 3.72$ mm) (Han, Ren and Li, 2011b), scc2-1 $(a_o \times a_o \times t_o = 120 \times 120 \times 3.0\text{mm},\; d_i \times b_i \times t_i = 32 \times 32 \times 3.0$ mm) (Han *et al.,* 2004), O1S00 $(D_o \times a \times t_o = 300 \times 124.27 \times 2.73\text{mm},\qquad d_i \times b_i \times t_i = 114 \times 114 \times 4.0$ mm) (Alqawzai *et al.,* 2020), and E1-1 $(D_o \times B_o \times t_o = 240 \times 160 \times 3.62$ mm, $d_i \times b_i \times t_i = 186 \times 106 \times 3.72$ mm) (Han, Ren and Li, 2011b). All the above CFDST columns were modelled in ABAQUS with the different nominal approximate global mesh sizes ranging from 20 mm to 150 mm. Trials analyses indicated that if the adopted mesh sizes in the concrete core and steel tubes were smaller than 30 mm, the ultimate axial strengths errors were less than 1%. This issue is shown in Fig. 4.3, in which $N_{u,FEM,}$ is the predicted ultimate axial strength with the applied mesh size of p $(20mm \leq p \leq 150mm)$ and $N_{u,,Exp}$ represents the ultimate axial load obtained by the experiment. The variation of $(N_{u,FEM}/N_{u,Exp})$ with mesh size for different cross-sectional shapes is shown in Fig. 4.7. The figure shows that when the

applied mesh size is 30 mm, the $(N_{u,FEM}/N_{u,Exp})$ approaches near the base line drawn at unity. Therefore, a mesh size of 30×30 mm is adopted for the concrete core. A refined approximate global mesh sizes of 30×30 is also taken for the steel tube to predict the possible local instabilities of thin-walled steel tubes. A typical meshing scheme of specimens is shown in Fig. 4.8.
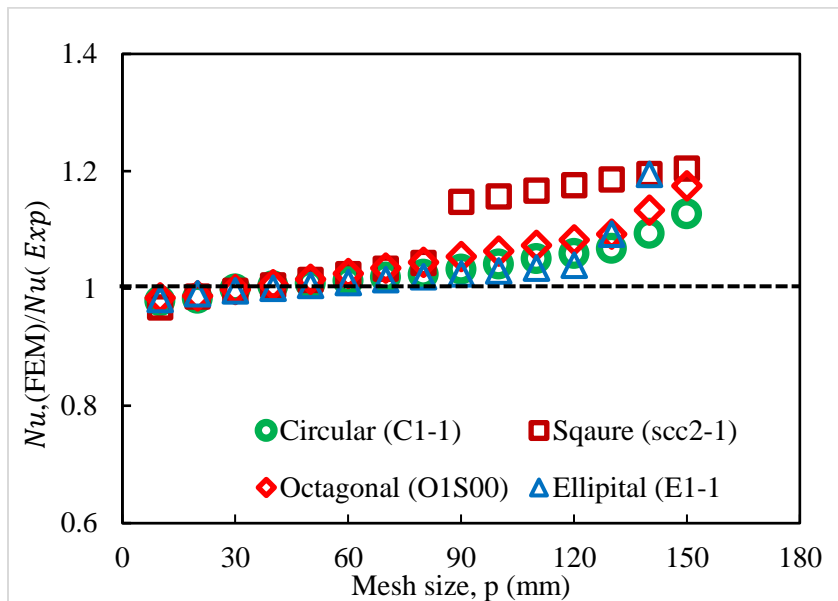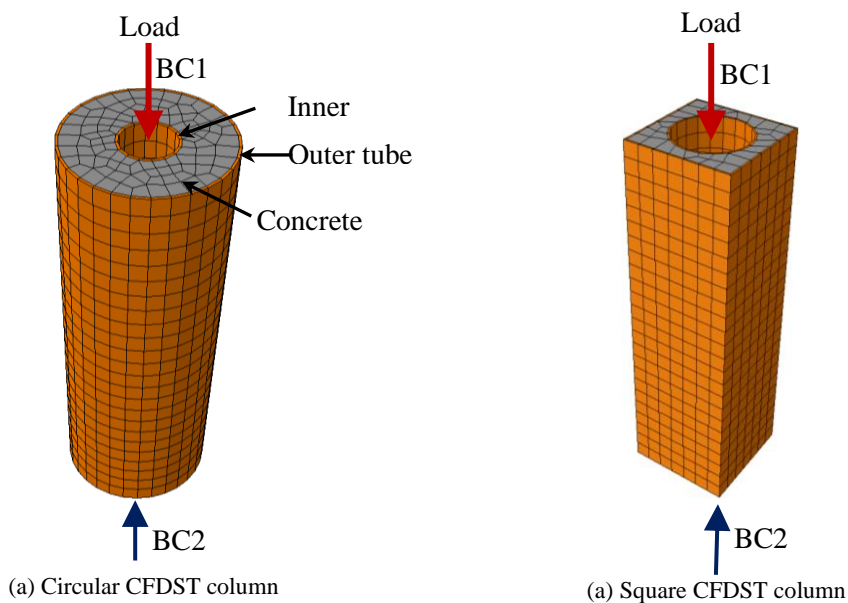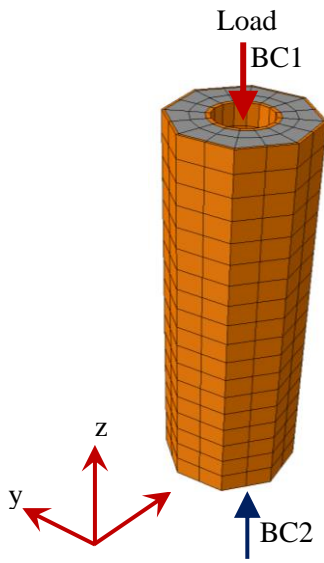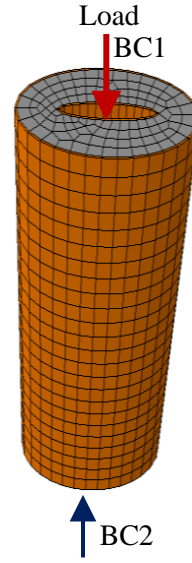

Fig. 4.7 Mesh sensitivity analysis

(a) Circular CFDST column

(a) Square CFDST column

(b) Octagonal CFDST column

(b) Elliptical CFDST column

BC1(RP-1): Clamped boundary condition $\left(U_x = U_y = UR_x = UR_y = UR_z = 0; \ U_z \neq 0\right)$

BC2 (RP-2): Fixed boundary condition $\left(U_x = U_y = U_z = UR_x = UR_y = UR_z = 0\right)$

**Fig. 4.8** Schematic view of mesh configurations and boundary conditions

Chapter – 5
Investigations on Axially Loaded CFDST Columns

5.1. General

To study the behavior of CFDST columns under the axial load, the outer shape of the column was selected as circular, square, octagonal, and elliptical; for each outer tube shape, the internal concentric tube shape was considered circular and square. The experimental and numerical responses of circular, square, octagonal, and elliptical CFDST columns with circular and square internal tubes placed concentrically are discussed in the following sub-sections.

5.2. Structural response circular CFDST Column

In total, eight circular CFDST columns were considered, out of which five had a circular internal tube, and three had square tubes prepared and tested. The circular column specimens with circular internal tubes are referred to as CC-120-75, CC-120-60, CC-120-55, CC-120-44, CC-120-40, and the circular column specimens with square internal tubes are denoted as CS-120-48, CS-120-39, CS-120-25. For a circular column with a circular inner tube CC-DDD-dd, and a circular column with a square inner tube CC-DDD-aa' 'DDD' indicates the diameter of the outer tube, 'dd' and 'aa' indicate the diameter and side length of the inner tube respectively. The geometrical properties and material properties of all the Circular section CFDST columns with circular and square internal tubes are shown in Table. 5.1. The schematic views for a typical section circular CFDST column specimen with circular and square internal tubes are shown in Fig. 5.1.
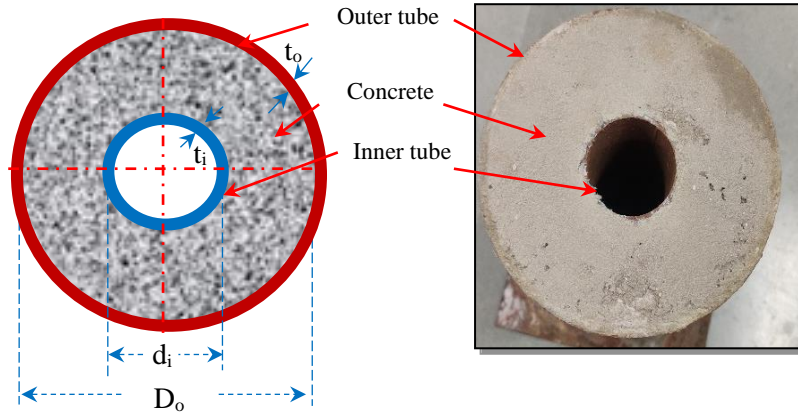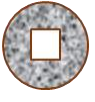
(a) CFDST column (CHS outer and CHS inner)
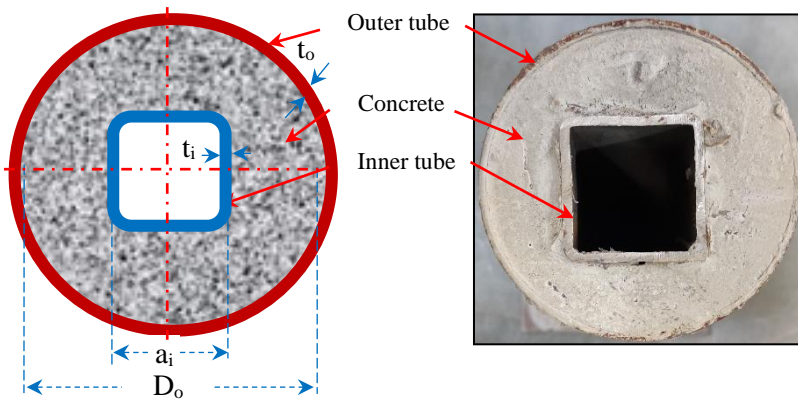
(b) CFDST column (CHS outer and SHS inner)

Fig. 5.1 Schematic view of circular CDFST columns

Table. 5.1 Geometrical and material properties of circular CFDST columns

Section	Specimen label	External tube			Internal tube			L (mm)	f_{cu} (MPa)
		D_o (mm)	t_o (mm)	f_{syo} (MPa)	d_i, a_i (mm)	t_i (mm)	f_{syi} (MPa)		
	CC-120-75	120	2.2	381	75	3.3	474	500	38.33
	CC-120-60	120	2.2	381	60	3.1	476	500	38.33
	CC-120-55	120	2.2	381	55	3.8	531	500	38.33
	CC-120-44	120	2.2	381	44	3.0	564	500	38.33
	CC-120-40	120	2.2	381	40	3.7	571	500	38.33
	CS-120-48	120	2.2	381	48	3.8	474	500	38.33
	CS-120-39	120	2.2	381	39	3.9	569	500	38.33
	CS-120-25	120	2.2	381	25	3.1	451	500	38.33

5.2.1. Experimental response of axially loaded circular CFDST columns

The experimentally observed failure mode of circular CFDST columns with circular and square internal tubes under the concentric loading is shown in Fig.5.2 and 5.4, respectively. It was observed that all the CFDST columns with circular internal tubes failed due combined failure mechanism, which includes local buckling of the external steel tube, inward buckling of the internal steel tube, and the crushing of concrete at the locations of local bucking of the external tube, as shown in Fig 5.2. The local buckling of external steel was observed once the column had reached its ultimate strength. The inward buckling of the internal tube occurred due to the fact that the internal tube is subjected to lateral pressure due to the expansion of sandwiched concrete. Since the sandwiched concrete is subjected to lateral forces from external and internal tubes and axial compressive stress due to applied load, concrete experiences tri-axial compressive stresses and causes crushing of concrete near ultimate loads. Fig.5.3(b) shows the column CC-120-75 at the failure stage. It can be observed from Fig.5.3 that the sandwiched concrete was squeezed out in the compression region, whereas the outer steel tube wall experienced outward local buckling. It was observed during the experiment that the failure of circular CFDST columns was initiated due to the external tube's local buckling, and the column loading beyond this stage did not exhibit sudden failure (collapse) of the column since after the buckling of outer and inner steel tubes the core concrete continued to bear the load until it was crushed.
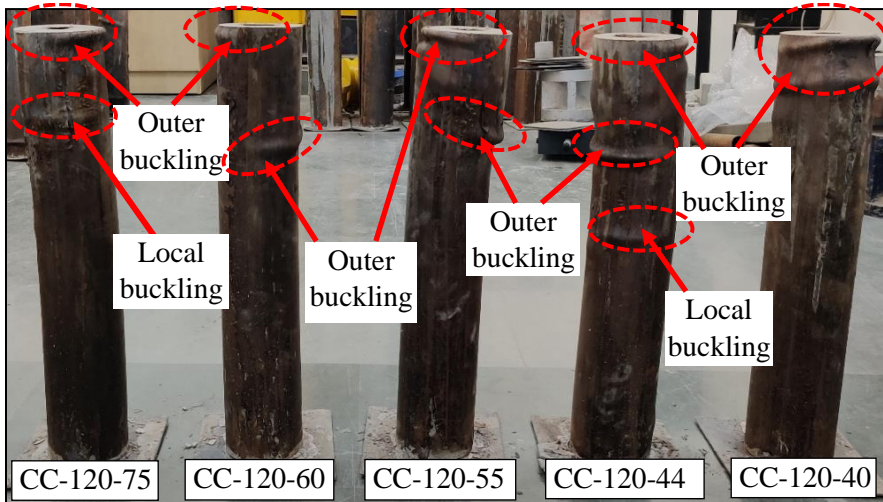
Fig. 5.2 Failure mode of circular CFDST column with internal circular tube under concentric loading
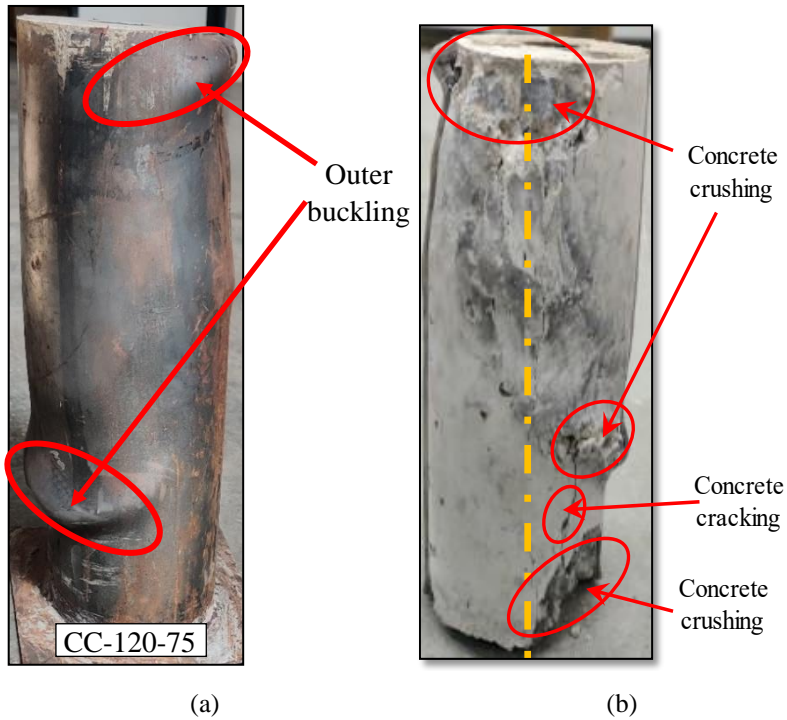

(a)

(b)

Fig. 5.3 Failure mode of circular CFDST column with internal circular tube under concentric loading (CC-120-75) - (a) Outer tube buckling effect and (b) Concrete crushing
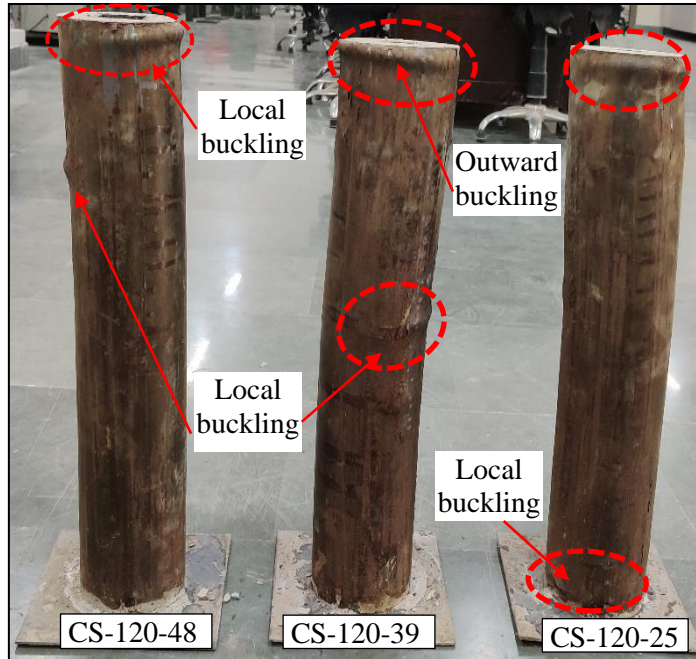
Fig. 5.4 Failure mode of square CFDST column with internal square tube under concentric loading
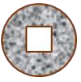
5.2.2. Numerical simulation of axially loaded circular CFDST columns

The finite element modeling of circular CFDST columns with circular and square internal tubes was carried out in ABAQUS, and the numerically obtained response was compared with that obtained experimentally. Table 5.2 shows the geometrical details of all the circular CFDSTs considered in this study. A comparison of experimentally obtained and numerically predicted ultimate load-carrying capacity of the circular CFDST columns is also shown in Table 5.2. Table 5.2 indicates that columns numerically obtained ultimate load-carrying capacity is in good agreement with the experimentally determined strengths, and the strength variation is not more than 4%. Moreover, the Table shows that in most cases, the experimentally obtained ultimate compressive strength of circular CFDST columns is lower than that predicted numerically. The probable cause for this discrepancy may be a minor error in applying the concentric load. Moreover, the experimentally observed deformed shape of a typical (CC-120-75) column at the ultimate load stage is compared

with the numerically predicted deformed shape in Fig.5.5. The figure clearly shows that the numerical modeling of the CFDST column can predict the failure mode of the Circular CFDST column.

For all the circular CFDST columns considered in this study, the numerically predicted axial load versus axial deformation curves are compared with the experimentally obtained curves, as shown in Fig. 5.6. From Fig. 5.6, it may be noticed that, generally, there is no significant variation between the numerically predicted axial-load versus axial-deformation curves. Therefore, the numerical simulation may be considered a reliable tool to predict the axial load versus deformation response of circular CFDST columns up to the failure stage. The peak and post-peak contract curves between experimental results and numerical predictions are generally good.

Table. 5.2 Comparison of FEM result with Experimental on circular CFDST columns under concentric loads

| Section	Specimen label	External tube (mm)		Internal tube (mm)		$\dfrac{d_i, a_i}{t_i}$	ψ	ξ	Ultimate strength (kN)		Error
		D_o	t_o	d_i	t_i				$N_{u(Exp)}$	$N_{u(FEM)}$	
	CC-120-75	120	2.2	75	3.3	23	0.59	1.96	1037	1024	0.99
	CC-120-60	120	2.2	60	3.1	19	0.46	1.55	980	1015	1.04
	CC-120-55	120	2.2	55	3.8	15	0.28	1.47	982	987	1.01
	CC-120-44	120	2.2	44	3.0	15	0.14	1.32	901	910	1.01
	CC-120-40	120	2.2	40	3.7	11	0.10	1.29	977	986	1.01
	CS-120-48	120	2.2	48	3.8	13	0.19	1.21	1187	1200	1.01
	CS-120-39	120	2.2	39	3.9	10	0.09	1.20	1200	1645	0.97
	CS-120-25	120	2.2	25	3.1	8	0.03	1.16	984	1002	1.02
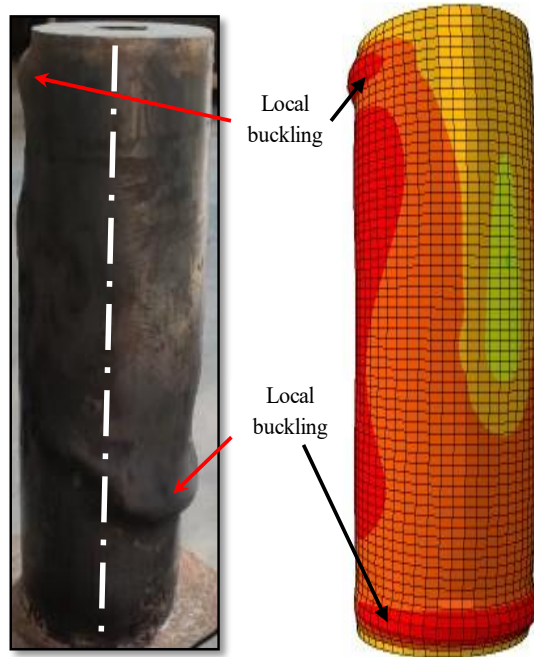
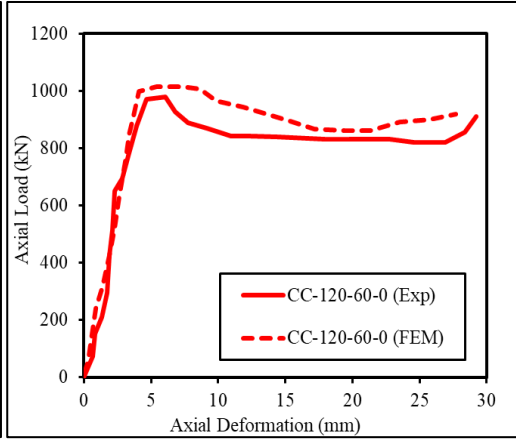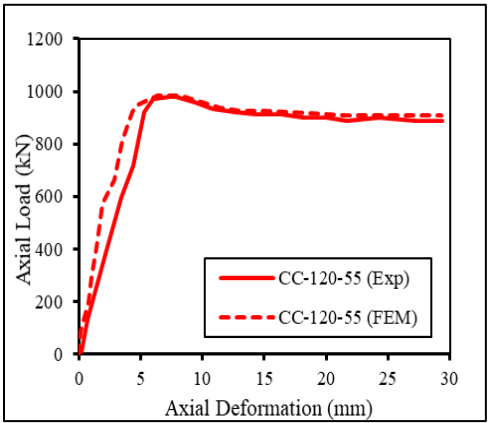(a) Outer tube buckling effect
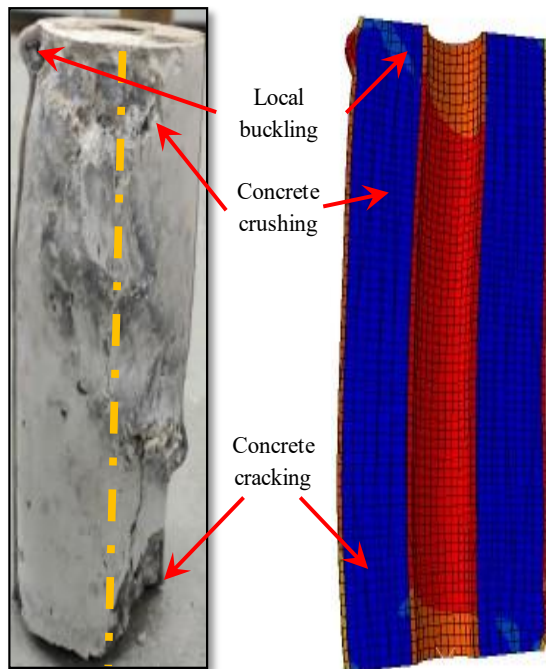
(b) Concrete crushing

Fig. 5.5 Comparison of test and FE failure modes of a specimen under concentric loading (CC-120-75) - (a) Outer tube buckling effect and (b) Concrete crushing
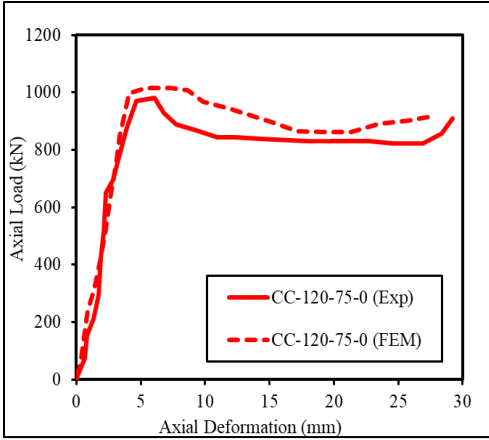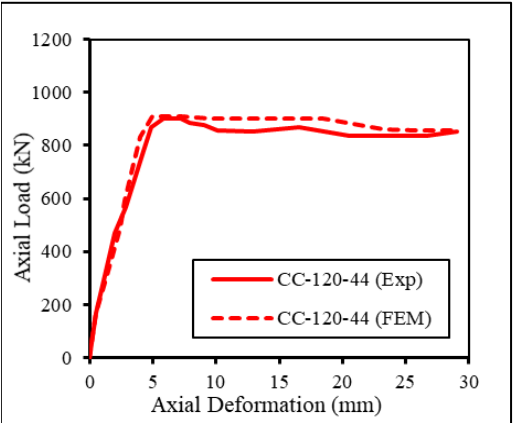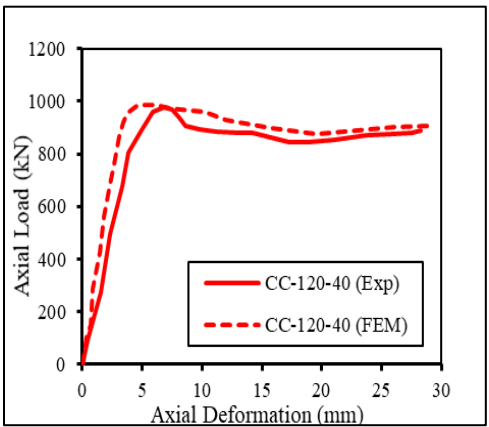
(a) CC-120-75

(b) CC-120-60

(c) CC-120-55

(d) CC-120-44

(e) CC-120-40

(f) CS-120-48

(g) CS-120-39   (h) CS-120-25
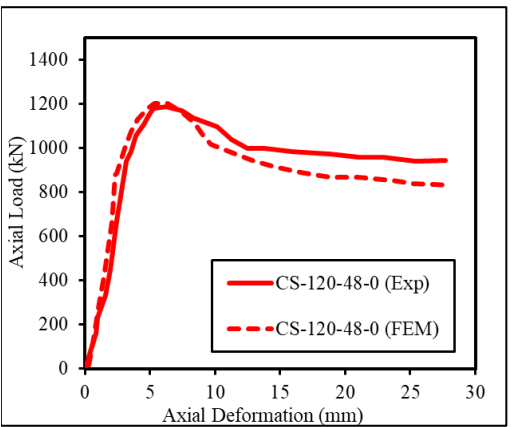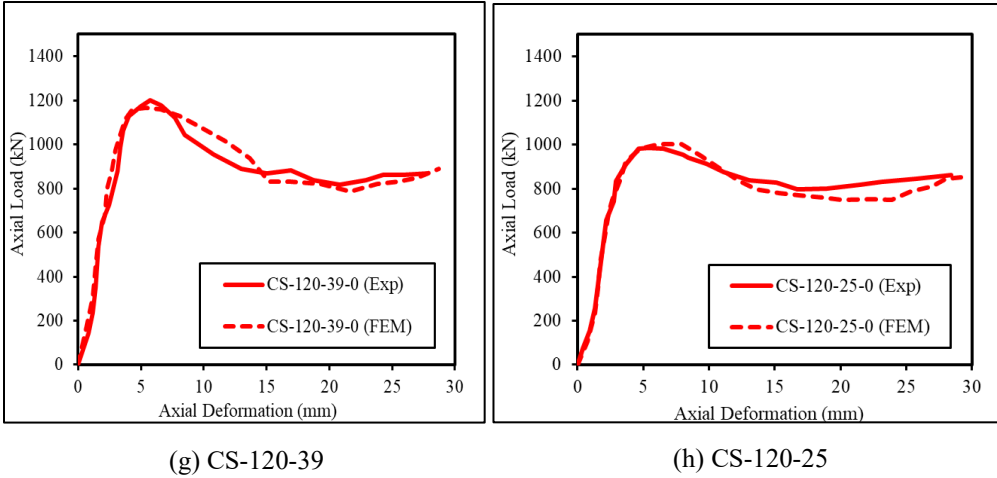
Fig. 5.6 Axial load versus axial deformation relations of circular CFDST columns under concentric loads

5.3. Structural response of square CFDST Column

In total, eight square CFDST columns were taken, out of which five were circular, and three had square tubes prepared and tested. The square column specimens with circular internal tubes are indicated as SC-138-75, SC-138-60, SC-138-55, SC-138-44, SC-138-40, and the square column specimens with square internal tubes are referred to as SS-138-48, SS-138-39, SS-138-25. For a square column with a circular inner tube CC-DDD-dd, and a square column with a square inner tube CC-DDD-aa' 'DDD' indicates the diameter of the outer tube, 'dd' and 'aa' indicate the diameter and side length of the inner tube respectively. The geometrical properties and material properties of all the square section CFDST columns with circular and square internal tubes are shown in Table. 5.3. The schematic views for a typical section square CFDST column specimen with circular and square internal tubes are shown in Fig. 5.7.
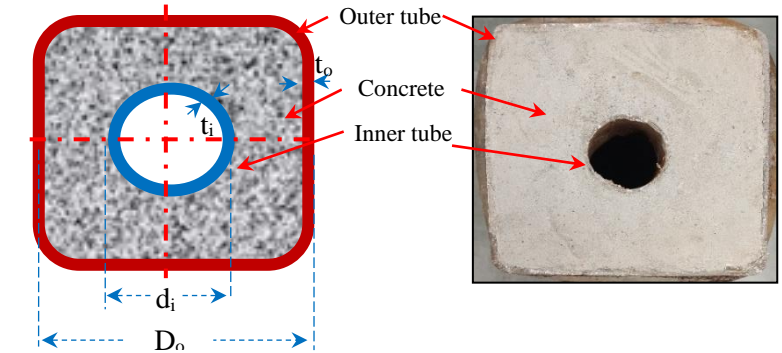
(a) CFDST column (SHS outer and CHS inner)
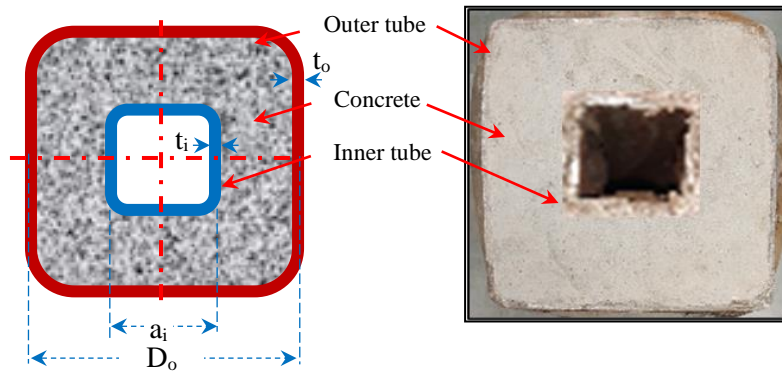
(b) CFDST column (SHS outer and SHS inner)

Fig. 5.7 Schematic view of Square CDFST columns

Table. 5.3 Geometrical and material properties of square CFDST columns

Section	Specimen label	External tube			Internal tube			L (mm)	f_{cu} (MPa)
		D_o (mm)	t_o (mm)	f_{syo} (MPa)	d_i, a_i (mm)	t_i (mm)	f_{syi} (MPa)		
	SC-138-75	138	3.2	383	75	3.3	474	500	38.33
	SC-138-60	138	3.2	383	60	3.1	476	500	38.33
	SC-138-55	138	3.2	383	55	3.8	531	500	38.33
	SC-138-44	138	3.2	383	44	3.0	564	500	38.33
	SC-138-40	138	3.2	383	40	3.7	571	500	38.33
	SS-138-48	138	3.2	383	48	3.8	474	500	38.33
	SS-138-39	138	3.2	383	39	3.9	569	500	38.33
	SS-138-25	138	3.2	383	25	3.1	451	500	38.33

5.3.1. Experimental response of axially loaded square CFDST columns

The failure mode of square CFDST columns with circular and square internal tubes under the concentric loading is shown in Fig.5.8 and 5.10, respectively. It was observed that the square CFDST columns with circular

internal tubes failed due combined failure mechanism of local buckling of the external steel tube, inward buckling of the inner steel tube, and the crushing of concrete at the spots of local buckling of the outer tube, as shown in Fig 5.9. The local buckling of external steel was observed once the column had reached its ultimate strength. The inward buckling of the internal tube appeared because the internal tube was subjected to lateral pressure due to the expansion of sandwiched concrete. Since the sandwiched concrete is subjected to lateral forces from external and internal tubes and axial compressive stress due to applied load, concrete experiences larger compressive stresses at the corner due to uneven distribution, and causes crushing concrete at the corner. Fig.5.9 shows the column CC-138-60 at the failure stage. It was observed during the experiment that the failure of square CFDST columns was initiated due to the external tube's local buckling only at the corners, and the column loading beyond this stage did not exhibit sudden failure (collapse) of the column since after the buckling of outer and inner steel tubes the core concrete continued to bear the load until it was crushed. It can be observed from Fig.5.9 that the sandwiched concrete was squeezed out in the compression region, whereas the outer steel tube wall experienced outward local buckling.
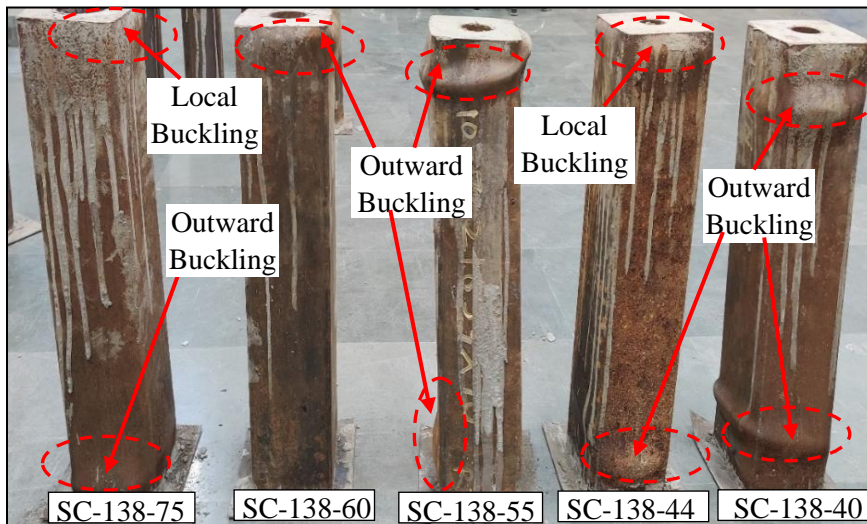

Fig. 5.8 Failure mode of square CFDST column with internal circular tube under concentric loading
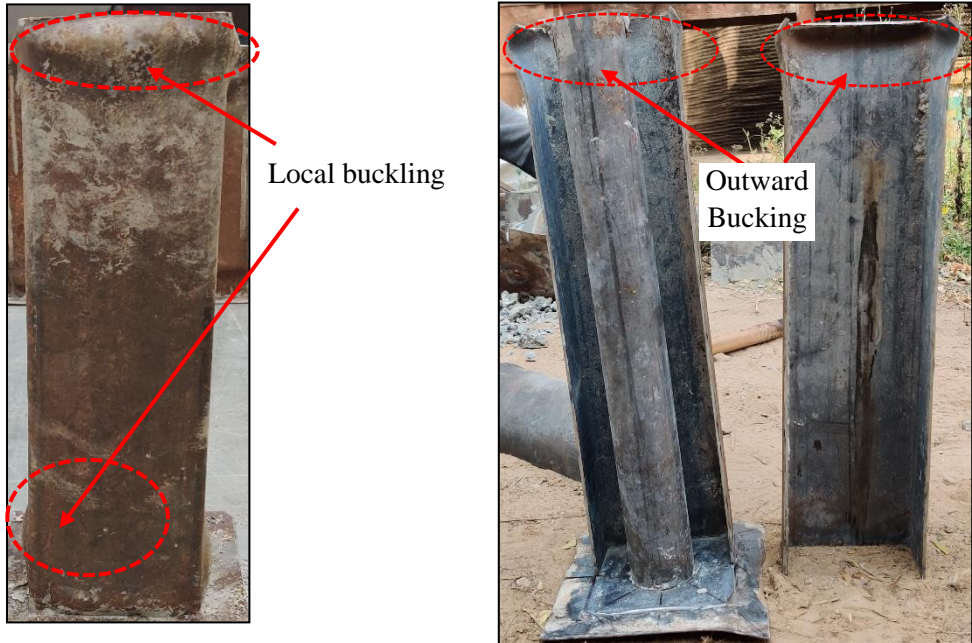
Fig. 5.9 Failure mode of square CFDST column with internal circular tube under concentric loading (SC-138-60)
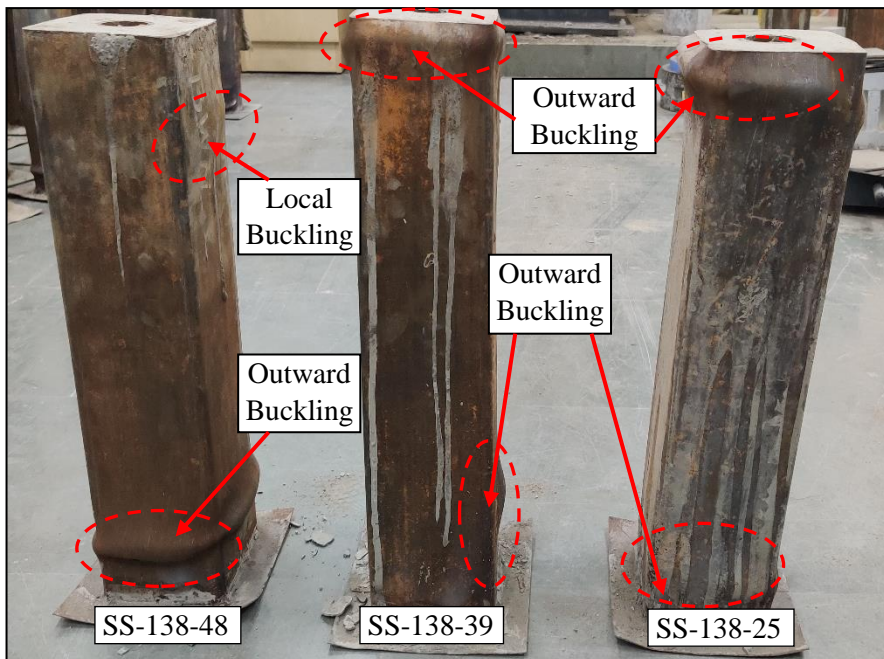

Fig. 5.10 Failure mode of square CFDST column with internal square tube under concentric loading

5.3.2. Numerical simulation of axially loaded square CFDST columns

The finite element modeling of a square CFDST column with circular and square internal tubes was carried out in ABAQUS, and the numerically obtained response was compared with that obtained experimentally. Table 5.3 shows the geometrical details of all the square CFDSTs considered in this study. A comparison of experimentally obtained and numerically predicted ultimate load-carrying capacity of the square CFDST columns is also shown in Table 5.4. Table 5.4 indicates that columns numerically obtained ultimate load-carrying capacity is in good agreement with the experimentally determined strengths. Moreover, the Table shows that in most cases, the experimentally obtained ultimate compressive strength of square CFDST columns is lower than that predicted numerically. The probable cause for this discrepancy may be a minor error in applying the concentric load. Moreover, the experimentally observed deformed shape of a typical (CC-138-44 and SS-138-39) column at the ultimate load stage is compared with the numerically predicted deformed shape in Fig.5.11. The figure clearly shows that the numerical modeling of the CFDST column can predict the failure mode of the square CFDST column.

For all the square CFDST columns considered in this study, the numerically predicted axial load versus axial deformation curves are compared with the experimentally obtained curves, as shown in Fig.5.12. From Fig.5.12, it may be noticed that, generally, there is no significant variation between the numerically predicted axial-load versus axial-deformation curves. Therefore, the numerical simulation may be considered a reliable tool to predict the axial load versus deformation response of square CFDST columns up to the failure stage. The peak and post-peak contract curves between experimental results and numerical predictions are generally good.

Table. 5.4 Comparison of FEM result with Experimental on square CFDST columns under concentric loads

Section	Specimen label	External tube (mm)		Internal tube (mm)		$\dfrac{d_{i,}a_i}{t_i}$	ψ	ξ	Ultimate strength (kN)		
		a_o	t_o	d_i	t_i				$N_{u(Exp)}$	$N_{u(FEM)}$	$\dfrac{N_{u(FEM)}}{N_{u(Exp)}}$
	SC-138-75	138	3.2	75	3.3	23	0.27	1.97	1832	1806	0.99
	SC-138-60	138	3.2	60	3.1	19	0.20	1.75	1597	1577	0.99
	SC-138-55	138	3.2	55	3.8	15	0.13	1.70	1695	1682	0.99
	SC-138-44	138	3.2	44	3.0	15	0.08	1.60	1649	1672	1.01
	SC-138-40	138	3.2	40	3.7	11	0.06	1.58	1551	1525	0.98
	SS-138-48	138	3.2	48	3.8	13	0.09	1.65	1728	1741	1.01
	SS-138-39	138	3.2	39	3.9	10	0.06	1.60	1728	1708	0.99
	SS-138-25	138	3.2	25	3.1	8	0.02	1.52	1554	1551	1.00

Local buckling

(a)

Outward
Buckling

(b)
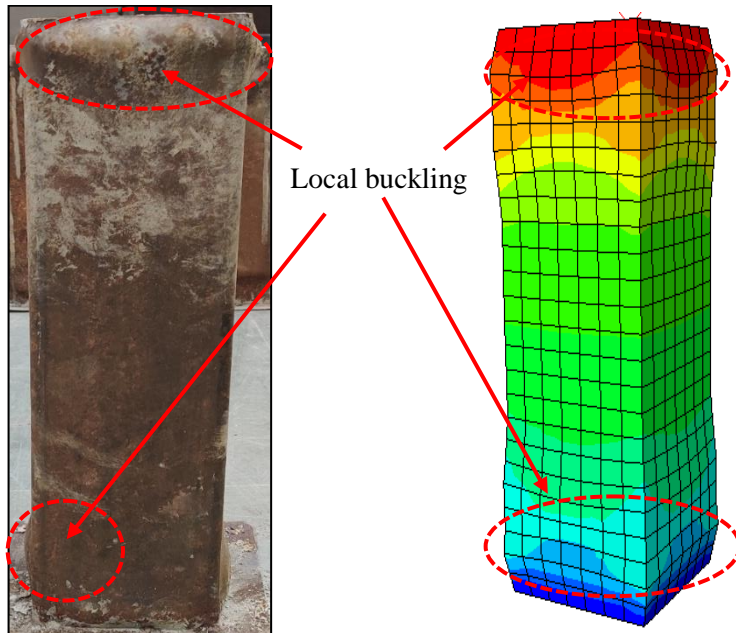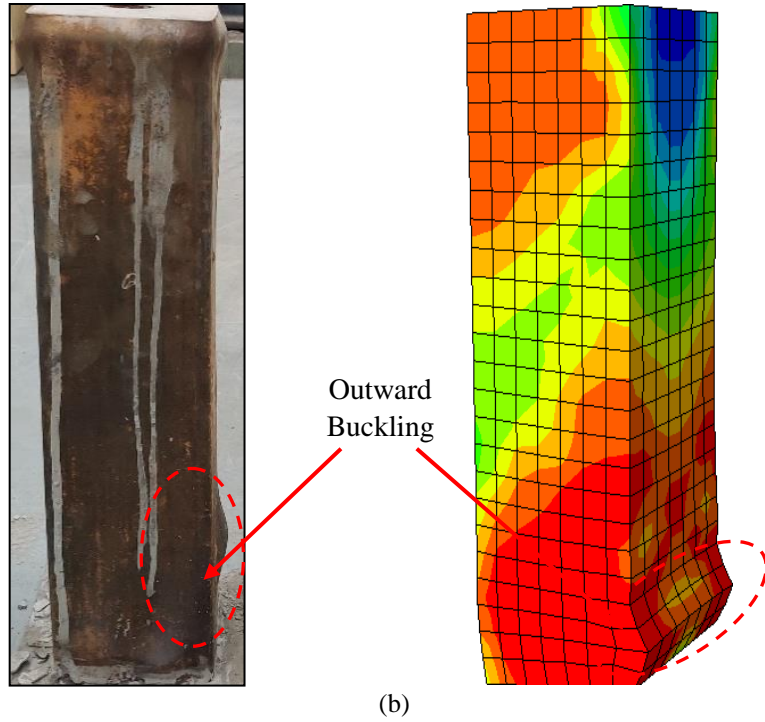
Fig. 5.11 Comparison of test and FE failure modes of square CFDST column (a) SC-138-44
and (b) SS-138-39

(a) SC-138-75

(b) SC-138-60

(c)   SC-138-55

(d)   SC-138-44

(e)   SC-138-40

(f)   SS-138-48

(g)   SS-138-39

(h)   SS-138-25
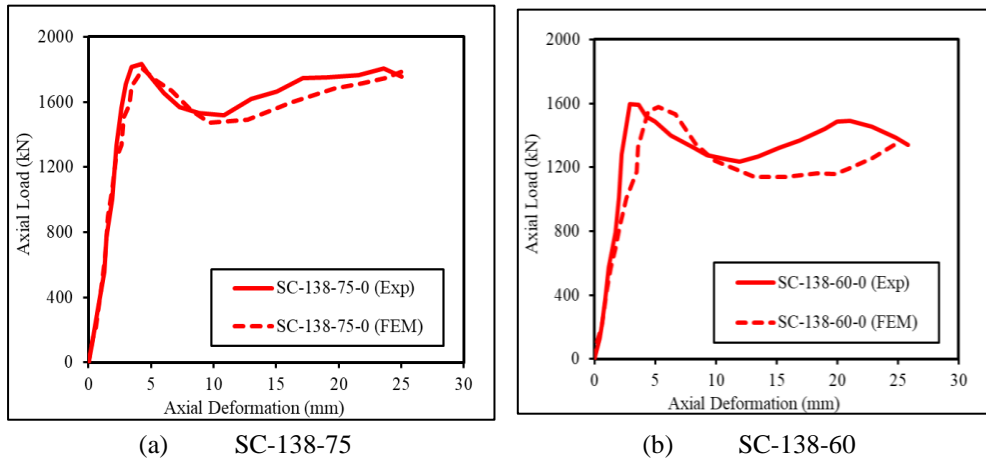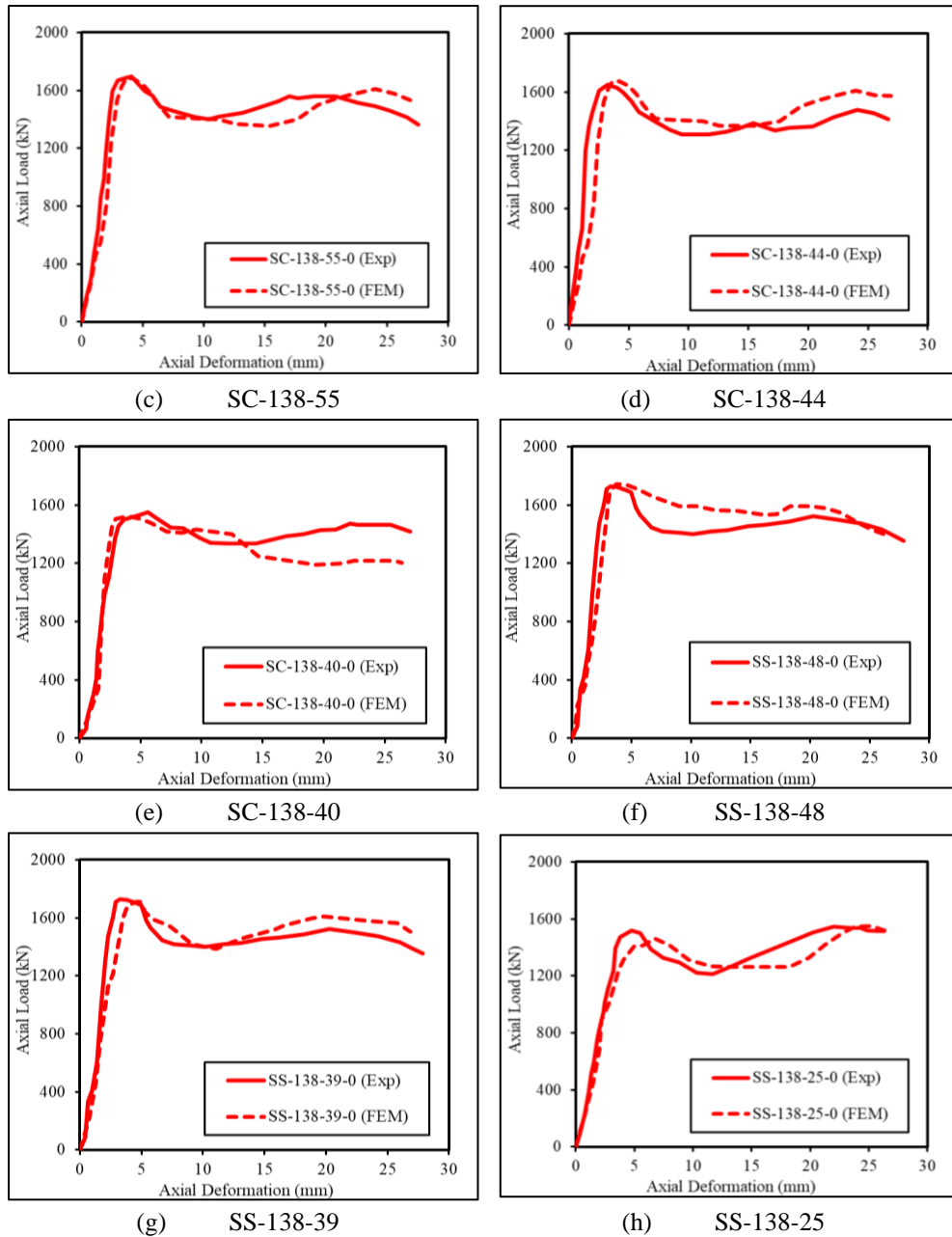
Fig. 5.12 Axial load versus axial deformation relations of square CFDST columns under concentric loads.

5.4. Structural response of octagonal CFDST column

A total of eleven octagonal CFDST columns were cast, out of which eight columns were tested under concentric axial loading and three under eccentric loading. Of the eight octagonal CFDST columns, five comprised a

circular section for the internal tube and three with a square section for the internal tube. The octagonal specimens were labeled as $OC-D_{oc}-d_i/a_i$, where OC indicates the octagonal shape of the outer tube, "D_{oc}" indicates the diameter of the outer tube and "d_i/a_i" indicates the diameter/side of the inner tube. The five specimens with a circular inner tube were labeled as OC-120-75, OC-120-60, OC-120-55, OC-120-44, and OC-120-40. The three specimens with square inner tubes were labeled as OC-120-48, OC-120-39, and OC-120-25. Table 5.5 highlights the geometric properties of octagonal test specimens. Fig 5.13 shows the sectional data of octagonal CFDST test specimens.
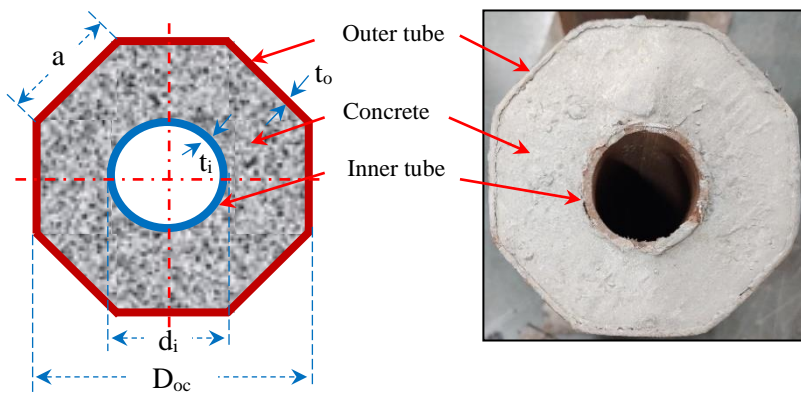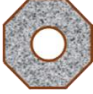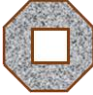
(a) CFDST column (OHS outer and CHS inner)
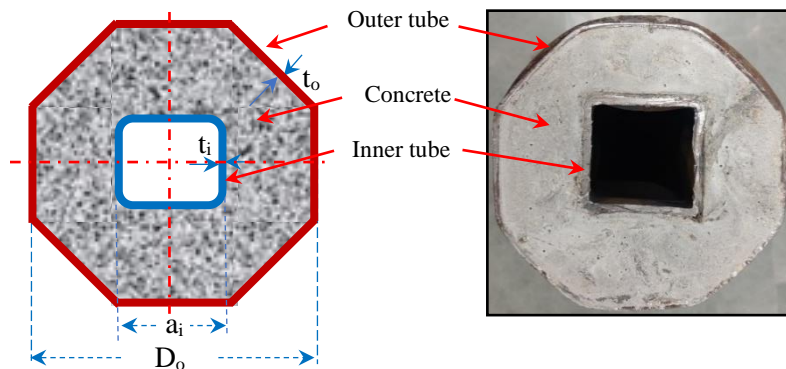
(b) CFDST column (OHS outer and SHS inner)

Fig. 5.13 Schematic view of octagonal CDFST columns

Table. 5.5 Geometrical and material properties of octagonal CFDST columns

Section	Specimen label	External tube			Internal tube			L (mm)	f_{cu} (MPa)
		D_{oc} (mm)	t_o (mm)	f_{syo} (MPa)	d_i, a_i (mm)	t_i (mm)	f_{syi} (MPa)		
	OC-120-75	120	2.1	348	75	3.3	474	500	38.33
	OC-120-60	120	2.1	348	60	3.1	476	500	38.33
	OC-120-55	120	2.1	348	55	3.8	531	500	38.33
	OC-120-44	120	2.1	348	44	3.0	564	500	38.33
	OC-120-40	120	2.1	348	40	3.7	571	500	38.33
	OS-120-48	120	2.1	348	48	3.8	474	500	38.33
	OS-120-39	120	2.1	348	39	3.9	569	500	38.33
	OS-120-25	120	2.1	348	25	3.1	451	500	38.33

5.4.1. Experimental response of axially loaded octagonal CFDST columns

Fig. 5.14 and 5.17 display the deformed shape captured at the end of testing. The observed failure pattern is of typical CFDST columns, where failure was from outward buckling of the outer tube, crushing of confined concrete, and inward bucking of the internal tube. Both types of octagonal CFDST specimens were observed to have similar failure patterns. Fig. 5.15 shows the failure of the OC-120-55 specimen, which depicts the post-testing response of the specimen. The post-peak response of octagonal CFDST specimens was investigated based on its mode of deformation and corresponding load-bearing capacity. The crushing of concrete was evident based on the deformed shape of the specimen, highlighting the significance of the confinement effect developed from the composite action of the CFDST specimen.
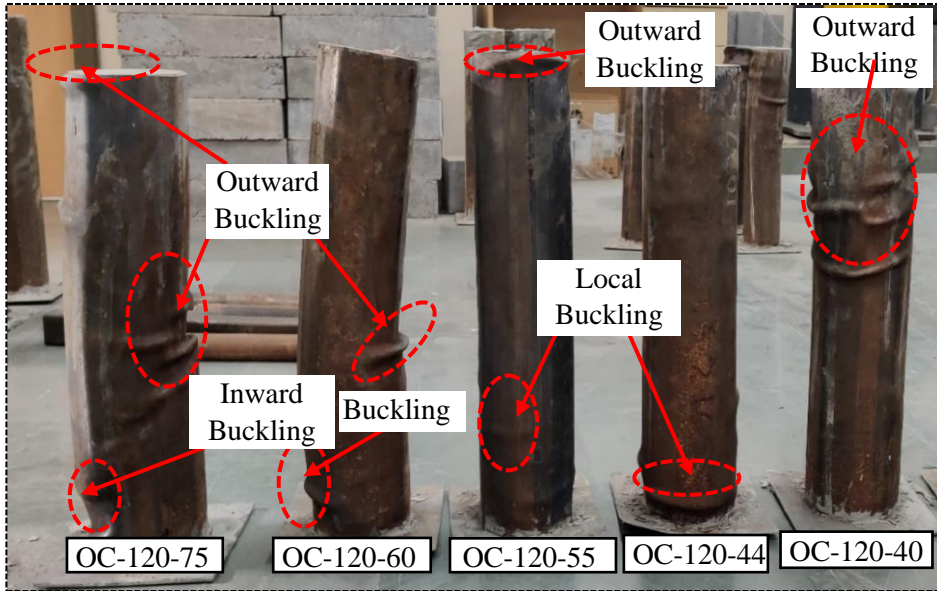
Fig. 5.14 Failure mode of octagonal CFDST column with internal circular tube under concentric loading
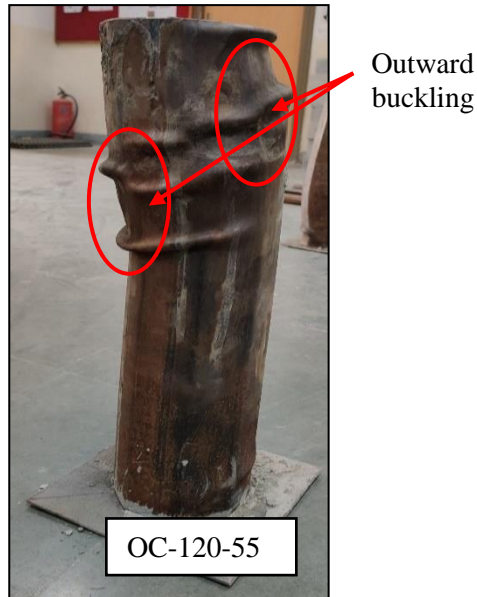
Fig. 5.15 Failure mode of octagonal CFDST column with internal circular tube under concentric loading (CC-120-55)
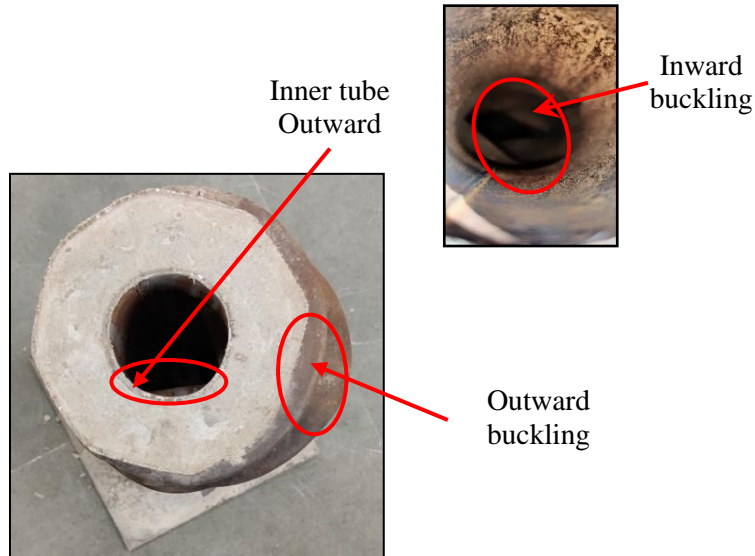
Fig. 5.16 Buckling effect of octagonal CFDST short column with internal
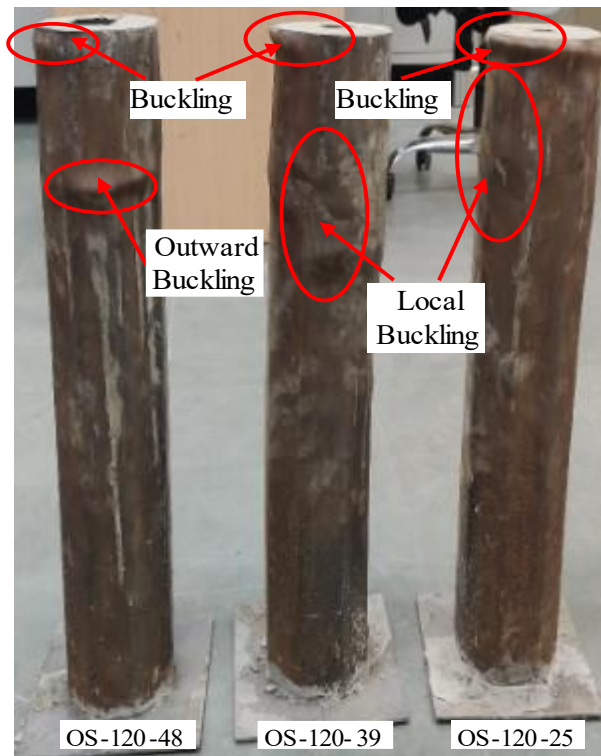
Fig. 5.17 Failure mode of square CFDST column with internal square tube under concentric loading
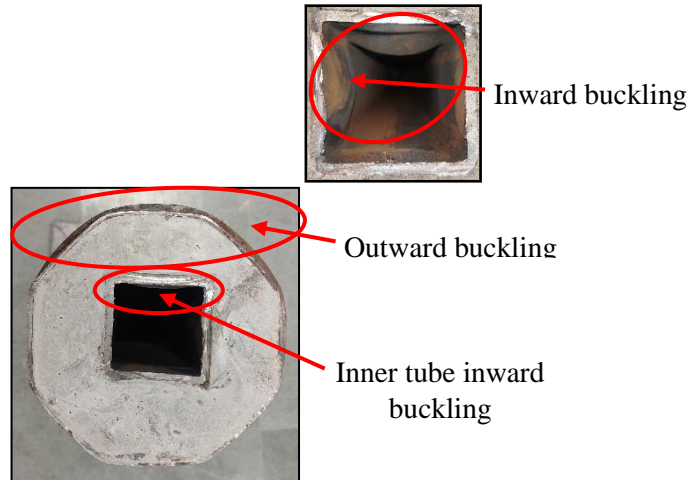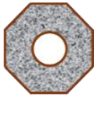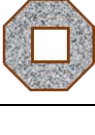
Fig. 5.18 Buckling effect of octagonal CFDST short column with internal square steel tube
(OS-120-48)

5.4.2. **Numerical simulation of axially loaded octagonal CFDST columns**

The numerical simulation of the octagonal CFDST column was carried out using ABAQUS. The response generated from ABAQUS was compared with the experimental data set to validate the input parameters of ABAQUS. Table 5.6 shows the axial load-bearing capacity developed by numerical specimens, which is also compared with experimental data to signify the accuracy of ABAQUS. The numerical response developed highlights that the numerical model successfully captured the realistic response of the octagonal CFDST specimen, marking that ABAQUS could simulate the confining effect for the octagonal outer tube section. Comparison based on the observed load-carrying capacity of experimentally tested octagonal CFDST column and its numerical counterpart is highlighted in Fig. 5.20. The comparison of deformed shape and load-carrying capacity developed from ABAQUS with its experimental counterpart marks the efficiency of the numerical modelling as the error observed between the two is less than 8.4%. Therefore, the numerical simulation may be considered a reliable tool for predicting the axial load-carrying capacity of octagonal CFDST columns up to the failure stage. The peak

and post-peak contract curves between experimental results and numerical predictions are generally good.

Table. 5.6 Comparison of experimental and FEM ultimate strengths of octagonal CFDST columns under concentric loading

Section	Specimen label	External tube (mm)		Internal tube (mm)		$\dfrac{d_i a_i}{t_i}$	ψ	ξ	Ultimate strength (kN)		
		D_o	t_o	d_i	t_i				$N_{u(Exp)}$	$N_{u(FEM)}$	Error
	OC-120-75	120	2.1	75	3.3	23	0.63	2.14	825	863	1.05
	OC-120-60	120	2.1	60	3.1	19	0.58	1.59	797	824	1.03
	OC-120-55	120	2.1	55	3.8	15	0.36	1.49	910	941	1.03
	OC-120-44	120	2.1	44	3.0	15	0.14	1.32	826	910	1.10
	OC-120-40	120	2.1	40	3.7	11	0.10	1.27	903	986	1.09
	OS-120-48	120	2.1	48	3.8	13	0.41	1.47	833	840	1.01
	OS-120-39	120	2.1	39	3.9	10	0.20	1.32	860	863	1.00
	OS-120-25	120	2.1	25	3.1	8	0.06	1.18	793	797	1.01
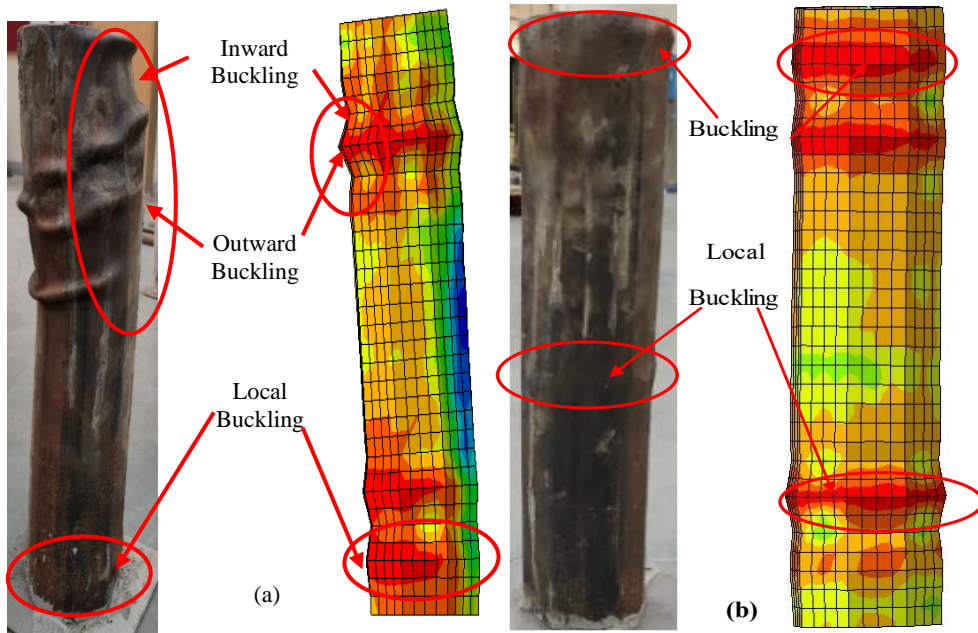
Fig. 5.19 Comparison of test and FE failure modes of octagonal CFDST column (a) OC-120-00 and (b) OS-120-39
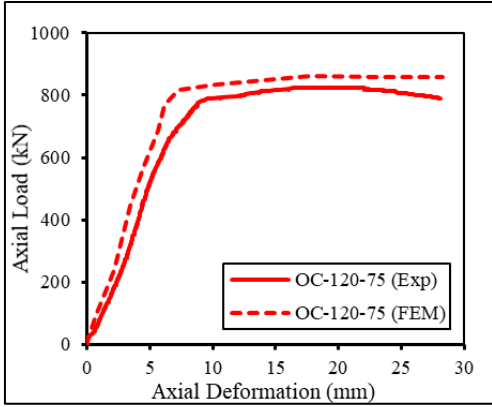
(a) OC-120-75
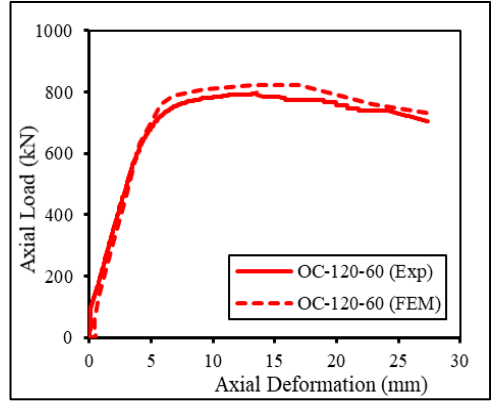
(b) OC-120-60
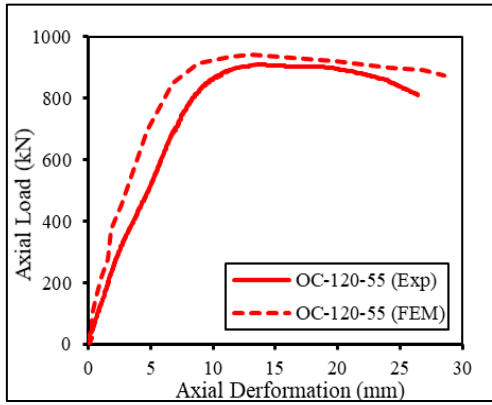
(c) OC-120-55
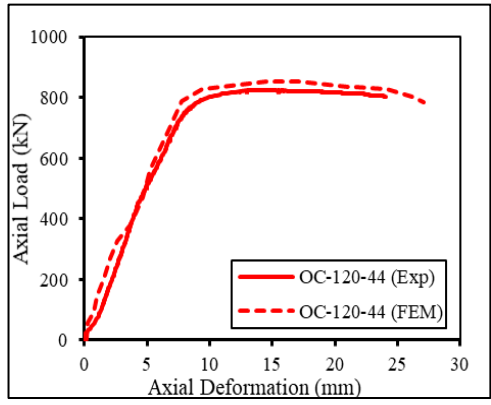
(d) OS-120-44
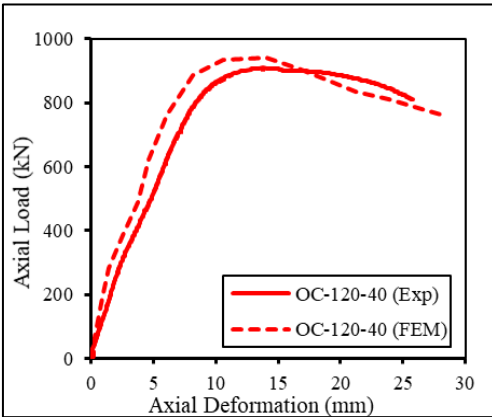
(e) OC-120-40

(f)OC-120-48

| (g) OS-120-39 | (h) OS-120-25 |
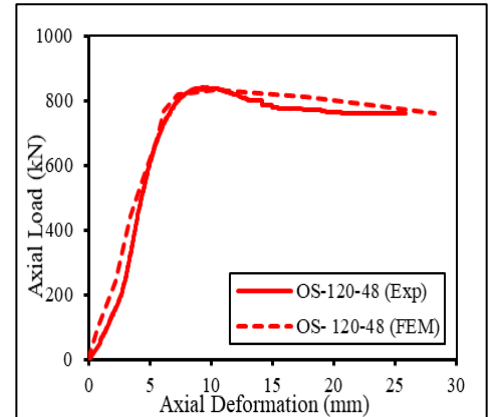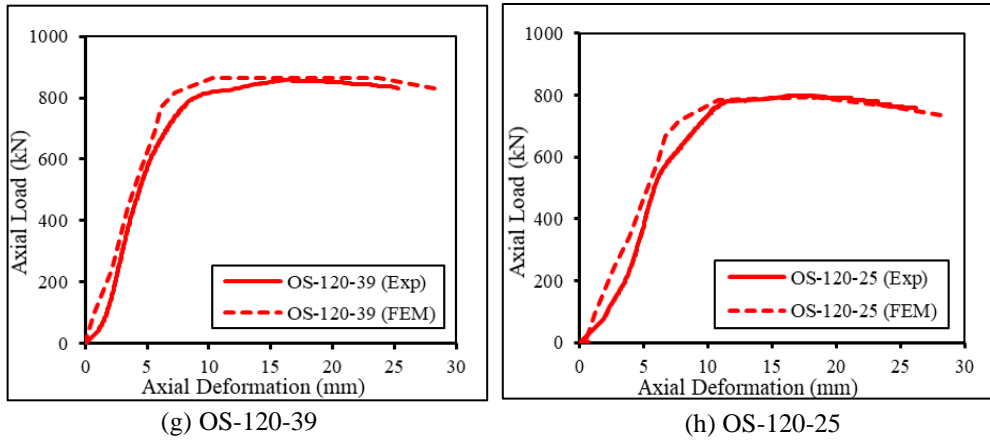
Fig. 5.20 Axial load versus axial deformation relations of octagonal CFDST short columns under axial loads

5.5. Structural response of elliptical CFDST column
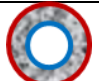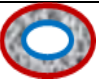
In the study, three-dimensional FE simulations of circular and elliptical CFDST columns under axial compression were developed and verified through the experimental test data from the perspectives of full load-displacement histories, ultimate axial strengths, and failure modes. The verified FE models were used to investigate and compare the structural performance of CFDST columns with circular and elliptical cross-section shapes by evaluating the overall load-deformation curves, interaction stress-deformation responses, and composite actions of the column.

5.5.1. Validation of the FE model on elliptical CFDST columns under concentric load

Validation of the current models involved comparing the previous experimental results of Han et al. (Han, Ren and Li, 2011a) with the corresponding ABAQUS model considering both concrete and steel models. Han *et al.* (2011) tested four specimens of circular and elliptical CFDST columns, from which each two replicates, to ensure the accuracy of the test procedure. The experimental and FE modeling comparisons are made by considering the ultimate loads, the load-axial displacement curve, and the observed failure mechanism. Table 5.1 provides the comparison between the

ultimate experimental loads ($N_{u,Exp}$) and the FE models $\left(N_{u,FEM}\right)$ considering the concrete and steel models of Han *et al.* model (Han, Zhao and Tao, 2001; Han, Yao and Tao, 2007). However, Table 5.7 shows that constitutive concrete and steel models adequately capture the CFDST column's ultimate load. On the other hand, Fig. 5.21. shows the load-axial deformation relationships for the columns considering the experimental and FE responses comparison between the experiments and those models considering Han's concrete and steel constitutive model (Han, Zhao and Tao, 2001; Han, Yao and Tao, 2007). Overall, the concrete and steel constitutive models (Han, Zhao and Tao, 2001; Han, Yao and Tao, 2007) give accuracy to the experimental recorded. Using concrete and steel constitutive models (Han, Zhao and Tao, 2001; Han, Yao and Tao, 2007) provides the typical experimental behavior of the CFDST columns. Hence, Han's model (Han, Zhao and Tao, 2001; Han, Yao and Tao, 2007) accurately fits the experimental results.

Table. 5.7 Comparison of ultimate axial strength of CFDST column obtained from test results with the FEM result

Section	Spec. Label	Outer tube (mm)	Inner tube (mm)	f_c (MPa)	f_{yo} (MPa)	f_{yi} (MPa)	Ultimate Load (kN)		$\dfrac{N_{u,FEM}}{N_{u,Exp}}$
		$D_o \times B_o \times t_o$	$d_i \times b_i \times t_i$				$N_{u,Exp}$	$N_{u,FEM}$	
	C1-1	220×220×3.62	159×159×3.72	43.95	319.6	380.6	2537	2567	1.01
	C2-1	220×220×3.62	106×106×3.72	43.95	319.6	380.6	3436	3458	1.01
	E1-1	240×160×3.62	186×106×3.72	43.95	319.6	380.6	2051	2090	1.02
	E2-1	240×160×3.62	142×62×3.72	43.95	319.6	380.6	2577	2580	1.00

Despite the insignificance of the post-ultimate stage in the design, Han's model (Han, Zhao and Tao, 2001; Han, Yao and Tao, 2007) was used for the parametric studies based on its accuracy along all behavioral loading stages. Fig. 5.21 displays the failure modes of the outer steel tubes observed from the ABAQUS models (ABAQUS (2014). The outer tube deformation shape was consistent across each of the four specimens tested, showing all faces of the tube bulging outwards as seen in the corresponding experimental tests.
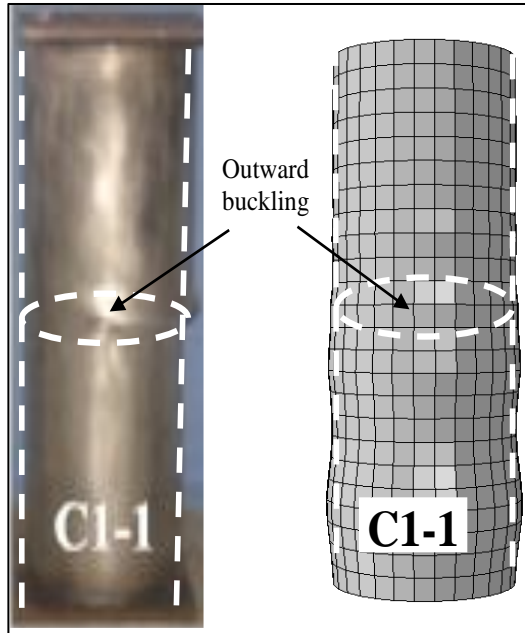
(a)
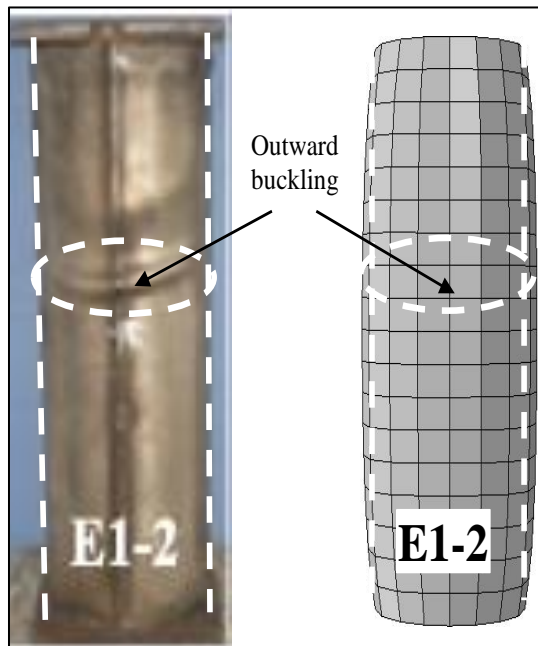
(b)

Fig. 5.21 Comparison of the experimental and analyzed failure modes of the specimen (a) C1-1 (Circular CFDST) and (b) E1-2 (Elliptical CFDST) (Han et al. 2011b).

| (a) C1 – 1 | (b) C2 – 1 |
| (c) E1 – 1 | (d) E2 – 1 |
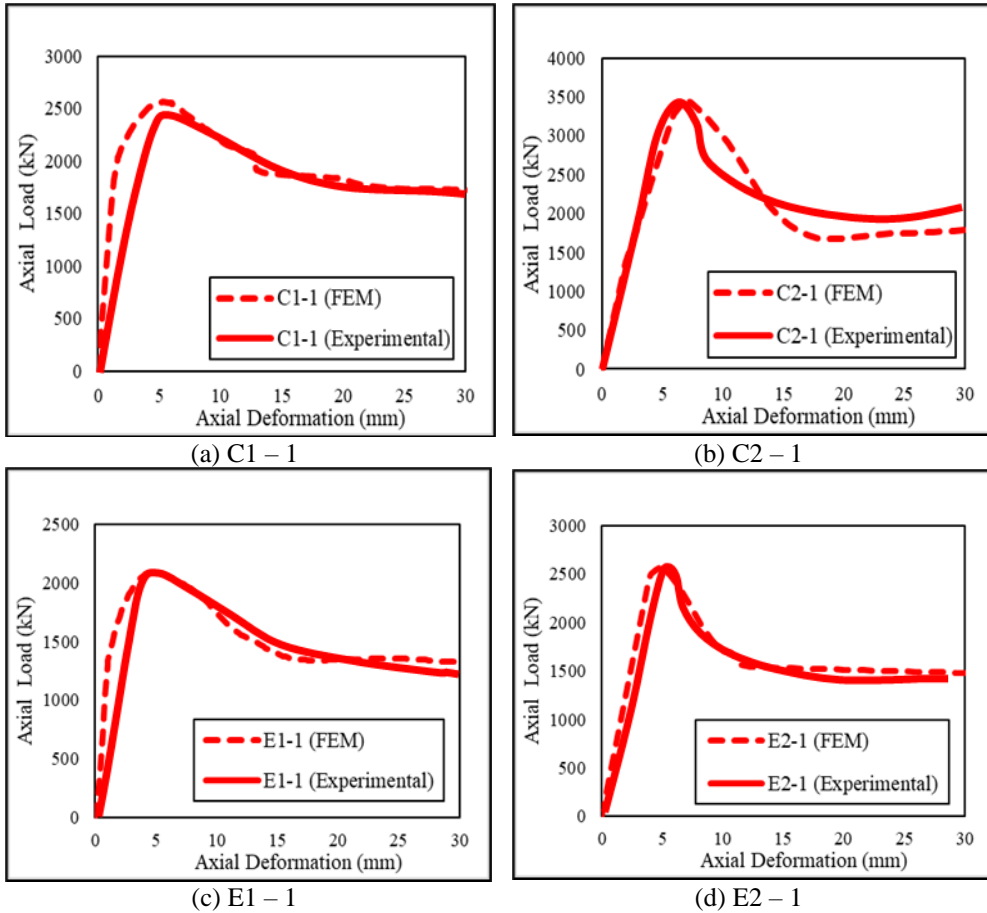
Fig. 5.22 Axial load vs. axial deformation for the verified models

5.5.2. Parametric study

This study examines the shape effect of the circular and elliptical CFDST column on its overall behavior under axial compressive load. In order to achieve this, finite-element models were generated in ABAQUS, paying particular attention to identifying appropriate stress-strain relationships for the materials. Past experimental tests on CFDST columns conducted by Han *et al.* (Han, Ren and Li, 2011a) were used to verify the methodology. A study was carried out by equaling the cross-sectional area of the steel tube of inner (A_{si}) and outer steel tube (A_{so}) and concrete core (A_c) of circular and elliptical CFDST columns with an equal wall thickness (t_o and t_i). Dimensions and material properties of CFDST specimens for the study are given in Table 5.8.

110

Table. 5.8 Dimensions and material properties of CFDST specimens for the study

Specimen Label	Outer tube (mm) $D_o \times B_o \times t_o$	Inner tube (mm) $d_i \times b_i \times t_i$	L (mm)	f_c (MPa)	f_{yo}, f_{yi} (MPa)	A_{so} (mm²)	A_{si} (mm²)	A_c (mm²)
C1	220×220×3.62	80×80×3.72	720	50	320			
E1	240×200×3.62	100×60×3.72	720	50	320	2460.8	891.5	30525.9
C2	240×240×3.62	100×100×3.72	720	50	320			
E2	280×200×3.62	140×60×3.72	720	50	320	2688.3	1125.2	34696.7
C3	260×260×3.62	120×120×3.72	720	50	320			
E3	320×200×3.62	180×60×3.72	720	50	320	2915.7	1358.9	38867.5
C4	280×280×3.62	120×120×3.72	720	50	320			
E4	360×200×3.62	200×40×3.72	720	50	320	3143.2	1358.9	47122.3

5.5.2.1. Behaviour of elliptical CFDST columns under concentric loads

(i) Strength

The strength of the infilled concrete had the highest impact on the ultimate axial strength of the CFDST column, and the circular and elliptical columns showed almost a similar sensitivity to concrete strength. It might be due to the equality of concrete cross-sectional area in both column shapes. The ultimate resistance of the CFDST obtained from ABAQUS was one of the main results of interest. Table 5.9 shows the strengths obtained after the finite element analysis on the columns under investigation. The parameter under investigation was the cross-sectional shape of an equal area of the steel tube and concrete; it became obvious that the column strength was also steadily enhanced for a constantly increasing outer diameter of the CFDST column. It was concluded that, as opposed to the enlargement of the outer diameter, a column with wide inner diameter tubes demonstrated a reduction in their maximum capacities. By maintaining the same outer steel tube diameter, the increase in the internal steel tube diameter decreases the concrete area, contributing to resisting the compressive loads acting on the CFDST column. The failure mechanism of the CFDST column can predict through the post-peak axial load-deflection responses. It is shown in Fig. 5.24 that the post-peak behavior of composite columns filled with strength concrete had a slow strength drop-off due to the

111

ductile behavior of CFDST columns. As shown in Fig. 5.24, the ductility indices of CFDST columns increase with both the external shape diameter. These observations may be due to the difference in the intensity of the steel tube confinement effect. As mentioned above, the elliptical steel tube provided the largest confinement effect on the concrete core, and the confinement effect supplied by circular steel tubes was slightly less. The residual strengths could also reflect this effect. The concrete core compressive strength in composite columns with the steel tube shape and the equal cross-sectional area did not significantly differ in the residual strength.

Table. 5.9 Result of a comparative study of circular and elliptical CFDST columns with equal steel and concrete area

Specimen Label	Outer tube (mm)	Inner tube (mm)	$\dfrac{D_o}{t_0}$	$\dfrac{d_i}{t_i}$	ψ	Ultimate load (kN)
	$D_o \times B_o \times t_o$	$d_i \times b_i \times t_i$				$N_{u,FEM}$
C1	220×220×3.62	80×80×3.72	61	21	0.38	2546
E1	240×200×3.62	100×60×3.72	66	27	0.37	2612
C2	240×240×3.62	100×100×3.72	66	27	0.43	2746
E2	280×200×3.62	140×60×3.72	77	38	0.40	2861
C3	260×260×3.62	120×120×3.72	72	32	0.47	3043
E3	320×200×3.62	180×60×3.72	88	48	0.42	3114
C4	280×280×3.62	120×120×3.72	77	32	0.44	3594
E4	360×200×3.62	200×40×3.72	99	54	0.34	3602

(ii) Axial load-deformation curve

The axial load-deformation curves of the CFDST columns are plotted in Fig.5.24. The outer diameter gets wider, and the increment of the load-bearing capacity of the specimens appears to get greater. Moreover, it was observed that a larger size of CFDST cross-sections enhanced the ductility while causing a more noticeable decrease in the capacity of the specimens after the maximum strength was attained. As contrasting to the effect of wide outer steel cross-sections, wide inner steel cross-sections were shown to reduce the CFDST

column resistance. Specifically, it was noted that the smaller the inner steel tube diameter, result in the more significant the capacity achieved. The columns also maintained better ductility levels with small inner tube cross-sectional sizes. Nevertheless, these members demonstrated the most considerable decrease in their load-bearing capacity after attain the maximum load.

(iii) Failure mode

In the CFDST column, with an equal cross-section area, the outward buckling was found around at the mid-height section of the circular steel outer tube. The inner tubes behaved differently from those of the sandwich concrete. The inner tube failure mode may be described as the ''distorted diamond'' mode of circular and elliptical CFDST column. The infilled sandwich concrete was crushed where the outward buckling occurred; as shown in Fig.5.23, it can be found that the cross-sectional strength ($N_{u,FEM}$) and stiffness of the column decreased with the increasing hollow ratio (ψ) and increased obviously with the infilling of the sandwiched concrete. It can also be seen that, generally, the vertical load was approximately proportional to the vertical displacement during the initial loading stage, and all the curves rise to the peak load and tend to drop after the peak load. It can be seen from Fig. 5.24 that, before the steel tube yields, inner and outer tubes are generally proportional to the load. After the ultimate load ($N_{u,FEM}$) is reached, the outward local buckling is found on the outer tube, and the inward buckling is found on the inner tube. As a result, the longitudinal and transverse strains on the bulged section developed continuously, while the strains of the other section increased slowly and even decreased due to the buckling of both the outer and inner tubes. Among the four types of sections, the circular section strains were fully developed. The elliptical section experienced a large transverse strain response. It is recognized that the circular and elliptical outer tube could provide an almost equal confinement effect for the core concrete, which is the same as that in any other shape of CFDST columns.

(a) Circular CFDST column (C1)   (b) Elliptical CFDST column (E1)
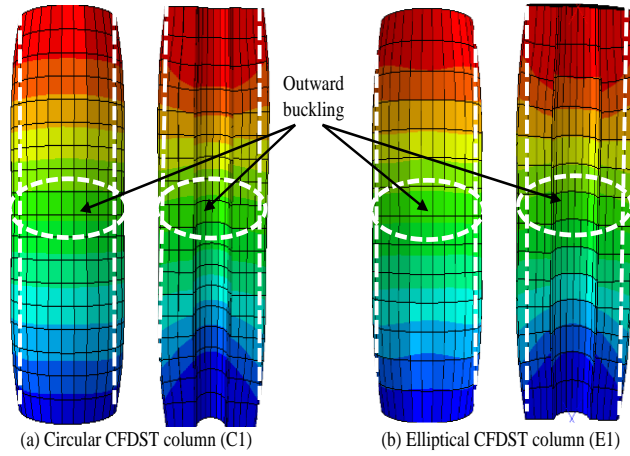
Fig. 5.23 Deformation shapes of CFDST column with an equal area of concrete core and steel tube

(a) C1 and E1

(b) C2 and E2

(c) C3 and E3

(d) C4 and E4
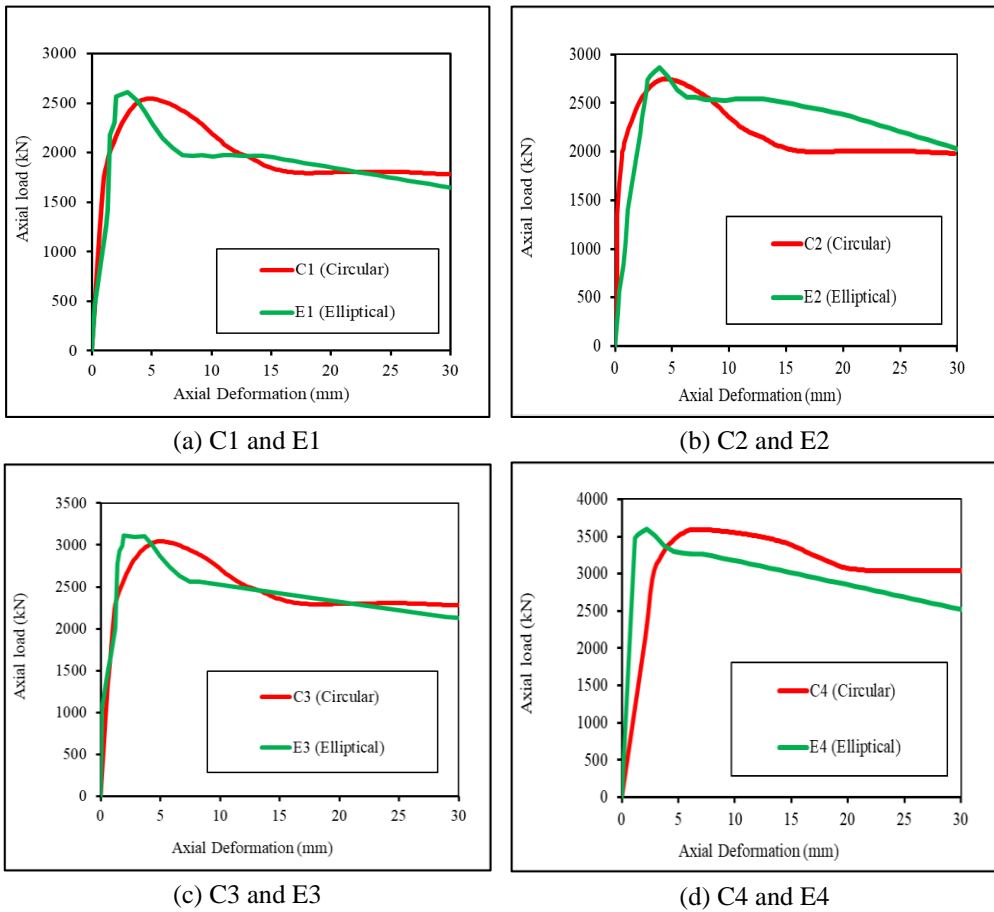
Fig. 5.24 Axial load versus axial deformation relations of elliptical CFDST columns

114

Investigation of Eccentrically loaded CFDST Columns

6.1. General

To study the behavior of CFDST columns under the eccentric load, the outer shape of the column was selected as circular, square, and octagonal. The internal concentric tube shape was circular and square for each outer tube shape. The experimental and numerical responses of circular, square, and octagonal CFDST columns with circular and square internal tubes placed concentrically are discussed in the following sub-sections.

6.2. Behaviour of circular CFDST columns under eccentric loads

Three cross-sections were considered to investigate the behavior of CFDST columns under eccentric loads. For all three sections, the shape of the outer as well as the internal tube was circular. Keeping the geometry of the outer tube constant, three different sizes of the tubes were taken as the internal tube, which was placed concentrically with the external tube. The schematic view for a typical section circular CFDST column specimen is shown in Fig. 6.1 All these column specimens were tested under the concentrated load applied at an eccentricity (e) of 20 mm with respect to the centroid of the section. These column specimens are designated as CC-120-55-20, CC-120-44-20, and CC-120-40-20, where CC indicates the circular shape of external and internal tubes, and the first and second numbers next to CC represent the diameters of external and internal tubes, respectively, and the last number indicates the magnitude of eccentricity. The geometrical details for all three CFDST sections are given in Table 6.1.
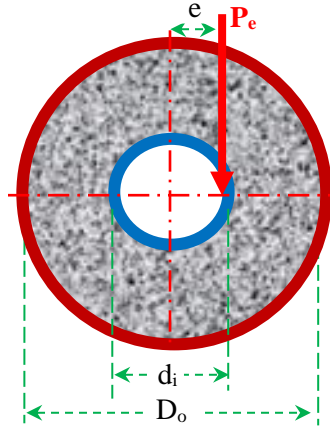
Fig. 6.1 Schematic view for a typical section of circular CFDST under eccentric loads.

6.2.1. Experimental response of eccentrically loaded circular CFDST columns

The experimentally determined ultimate load-carrying capacity of these columns under eccentric loading conditions ($N_{u,e(Exp)}$) are shown in Table 6.1. In order to investigate the effect of eccentricity on the ultimate load-carrying capacity of columns, the experimentally determined ultimate load-carrying capacity of these columns under eccentric loading conditions ($N_{u,e(Exp)}$), are compared with the experimentally determined ultimate load-carrying capacity under the axial load (e = 0) ($N_{u,0(Exp)}$) as shown in Table 6.1. As expected, the strength of the eccentricity-loaded column falls compared to the concentrically loaded column. To compare the performance of circular CFDST columns under the eccentric load, the strength of the eccentrically loaded column is normalized by its concentric strength. The table indicates that rather than internal tube thickness, the diameter of the internal tube more significantly affects the behavior of columns under an eccentric load case. This fact may be verified by comparing the performance of specimens CC-120-55-20 and CC-120-40-20, which has an almost similar thickness to the internal tube, since the variation of the inner tube diameter, the ($N_{u,e(Exp)}/N_{u,o(Exp)}$) ratio significantly differs. The table shows that as the diameter of the internal tube decreases, the ($N_{u,e(Exp)}/N_{u,o(Exp)}$) ratio decreases. Hence, it may be concluded that the

116

performance of a given circular CFDST column may be improved by using the larger diameter of the internal tube.

Table. 6.1 Experimental result on circular CFDST columns under eccentric loads

Section	Specimen label	External tube (mm)		Internal tube (mm)		e (mm)	Ultimate strength (kN)		
		D_o	t_o	d_i	t_i		$N_{u,0(Exp)}$	$N_{u,e(Exp)}$	$\dfrac{N_{u,e(Exp)}}{N_{u,o(Exp)}}$
	CC-120-55-20	120	2.2	55	3.8	20	982	901	0.918
	CC-120-44-20	120	2.2	44	3.0	20	901	797	0.885
	CC-120-40-20	120	2.2	40	3.7	20	977	813	0.832

During the tests on the circular CFDST columns under the eccentric load, it was observed that eccentrically loaded circular CFDST column specimens failed mainly due to the buckling of external and internal steel tubes and the crushing of concrete. For a typical eccentrically loaded circular CFDST column specimen CC-120-55-20, the failure mode is shown in Fig.6.3. Figs 6.2(a) and 6.2(b) show the bucking of the outer tube and inner tube, respectively. Fig. 6.2(b) and 6.2(c) show that the crushing of concrete occurs at the column's top face at the concrete core's periphery. Moreover, the inside view of the internal tube at the failure stage is also shown in Fig. 6.2(c). It can be observed from Fig 6.2 (a) that the column buckling of the outer steel tube occurs near the top portion of the column; however, the buckling of the internal tube occurs near the mid-height of the column as shown in Fig. 6.2(b). The outward buckling of the inner tube causes increases in lateral pressure in sandwiched concrete; however, the inward buckling of the inner tube results in the separation of the interior steel tube from the concrete core. With the increase in the magnitude of eccentric load, the initiation of outer tube buckling was observed near the ends of the columns before the crushing of concrete near mid-height, which resulted in the premature collapse of the column (compared to concentrically loaded). Consequently, the circular CDFST columns under the eccentric load exhibited lower load-carrying capacity than the concentrically loaded column.

117
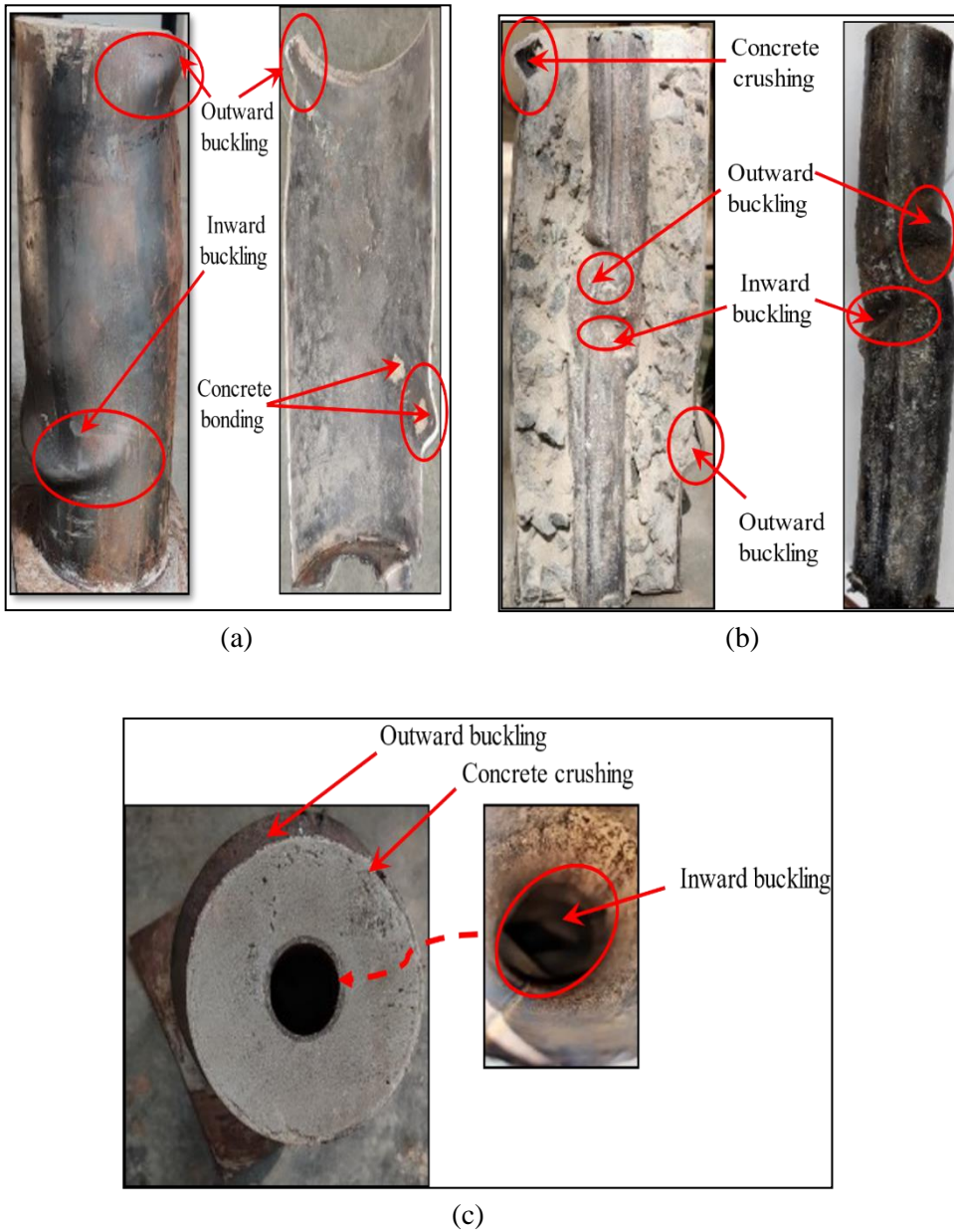
Fig. 6.2 Failure mode of circular CFDST column under eccentric loading (CC-120-55-20) (a) Outer tube buckling effect (b) Inner tube buckling effect and (c) Inward buckling effect of inner steel tube
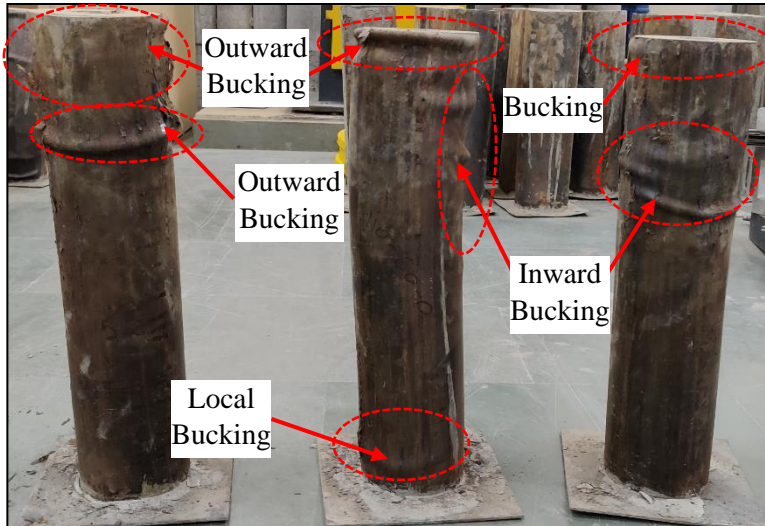
Fig. 6.3 Failure mode of circular CFDST column with internal circular tube under eccentric loading (CHS-CHS)

6.2.2. Numerical simulation of eccentric loaded circular CFDST columns

In addition to the experimental study described above, the finite element analysis was also carried out for all the circular CFDST columns under the eccentric concentrated load using the ABAQUS to reproduce the experimental results. The geometrical details of the circular CFDST column specimens modelled in ABAQUS are shown in Table 6.1. The details regarding the modeling of CFDST columns in ABAQUS were discussed earlier in Chapter 4. The numerically predicted ultimate load-carrying capacity of columns, along with the experimentally obtained strength, are shown in Table 6.2. For all the cases, the numerically predicted strength of columns was found to be lower than the experimental strengths; however, the deviation in strength is not more than 7%. The probable cause for getting lower strength via numerical simulation may be handling error. In the experiment, the load was applied as a line load at eccentricity 'e'; however, in the FE modeling, the load was applied as the concentrated load at the point located at eccentricity 'e' on the axis.

Table. 6.2 Comparison of experimental and FEM ultimate strengths of circular CFDST columns
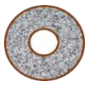
Section	Specimen label	External tube (mm)		Internal tube (mm)		e (mm)	Ultimate strength (kN)		
		D_o	t_o	d_i	t_i		$N_{ue(Exp)}$	$N_{ue(FEM)}$	$\dfrac{N_{ue(Exp)}}{N_{ue(FEM)}}$
	OC-120-55-20	120	2.2	55	3.8	20	901	852	1.06
	CC-120-44-20	120	2.2	44	3.0	20	797	752	1.06
	CC-120-40-20	120	2.2	40	3.7	20	813	763	1.07

Fig. 6.5 shows the numerically obtained failure modes of external and internal steel tubes for a typical column specimen CC-120-55-20. Moreover, Fig. 5.8 also includes the deformed shape of the same column specimen observed in a laboratory at the failure stage of the column. The numerical and experimental failure mode of external as well as internal steel tubes pretends to be similar, as shown in Fig. 6.5. It can be examined from Fig. 6.4 that the concentrically loaded column fails with outward buckling of the external steel tube at the upper and lower end of the column. In contrast, in the eccentrically loaded column, the specimen fails with buckling the external and internal steel tubes at the upper and lower end and the inward buckling of the inner steel tube, as shown in Fig.6.5 (a and b). The load-deformation curves for all three circular CFDST columns under the concentric loading and eccentric loading were plotted using the experimental data, and they are compared with the numerically obtained curves in Fig. 6.6. It can be noted from the curves plotted in Fig.6.6 that the contact between experimental results and numerical predictions are generally good.
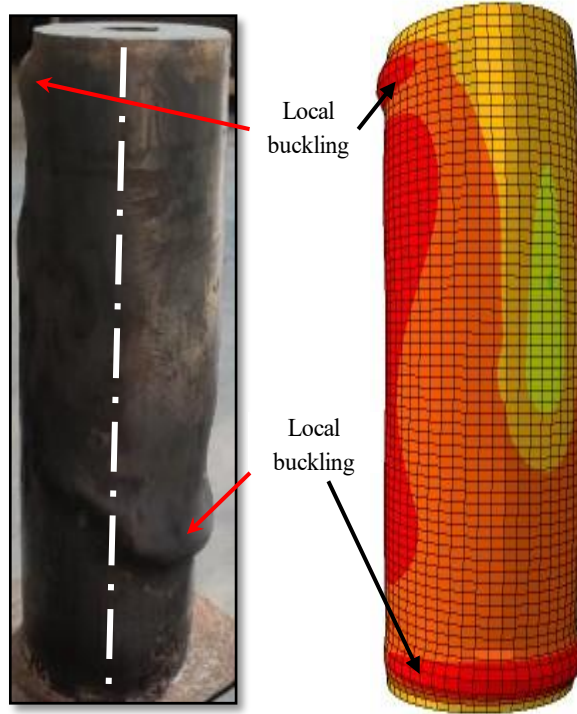
Fig. 6.4 Comparison of test and FE failure modes of specimen (CC-120-55-0) under concentric load

(a) Outer tube buckling effect   (b) Inner tube buckling effect
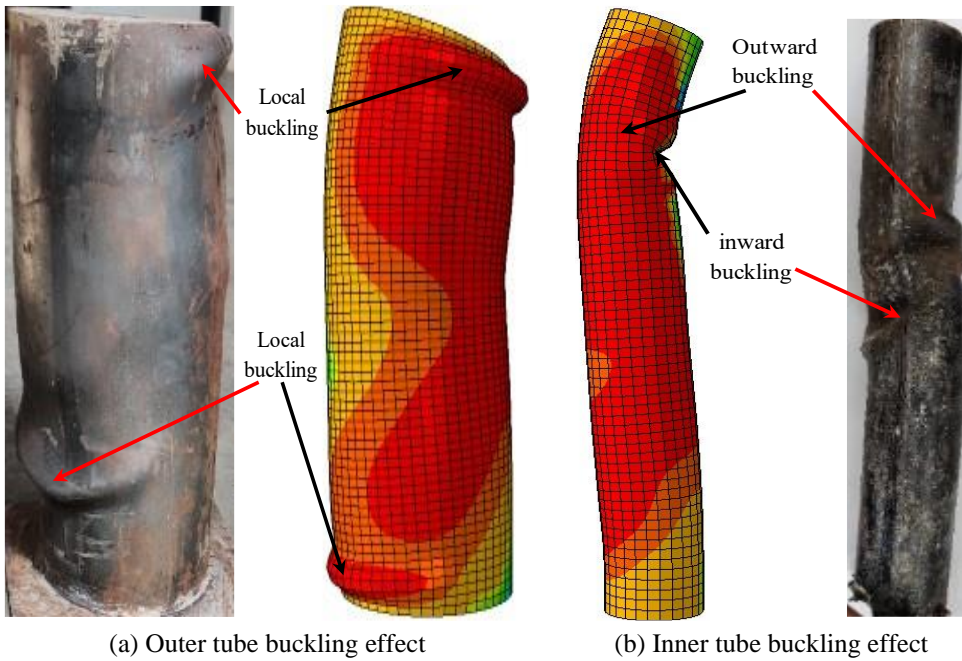
Fig. 6.5 Comparison of test and FE failure modes of specimen (CC-120-55-20) under eccentric load

(a) CC-120-22-20

(b) CC-120-44-20

(c) CC-120-40-20
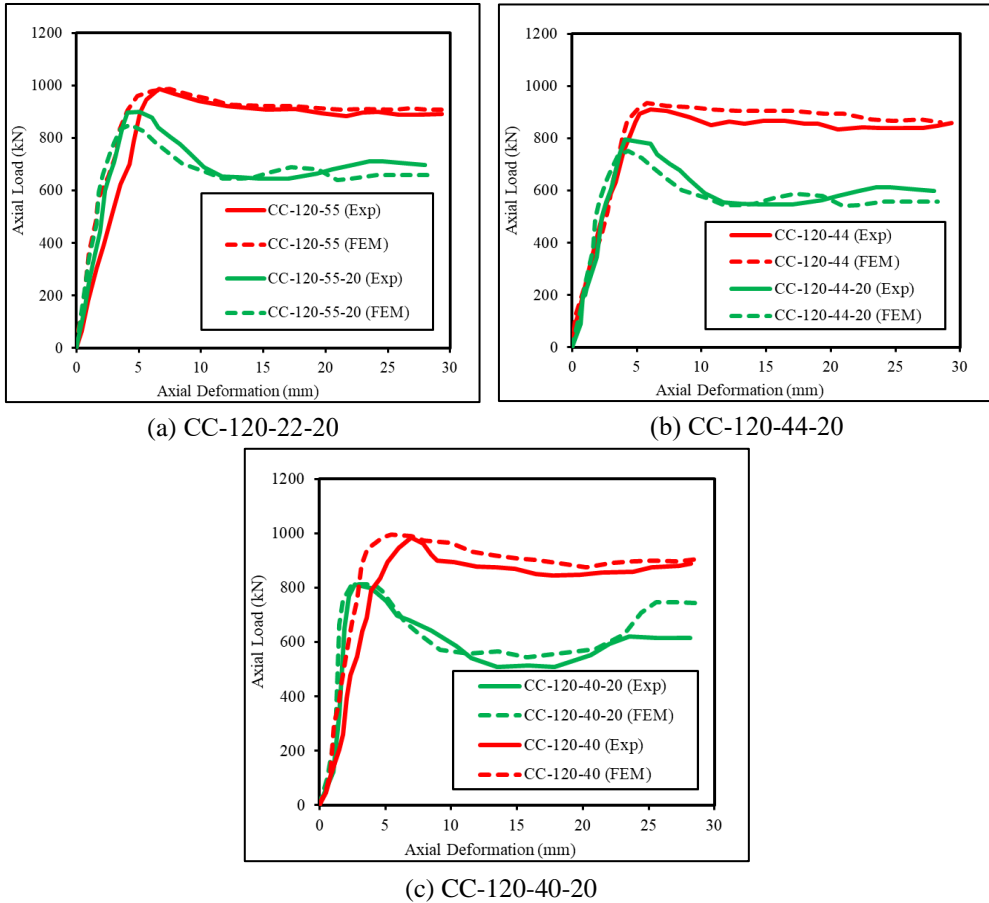
Fig. 6.6 Axial load versus axial deformation relations of circular CFDST columns under eccentric loads

6.3. Behaviour of square CFDST columns under eccentric loads

Three cross-sections were considered to investigate the behavior of CFDST columns under eccentric loads. For all three sections, the outer shape is square, and the internal tube is circular. Keeping the geometry of the outer tube constant, three different sizes of the tubes were taken as the internal tube, which was placed concentrically with the external tube. The schematic view for a typical section square CFDST column specimen is shown in Fig. 6.7 All these column specimens were tested under the concentrated load applied at an eccentricity (e) of 20 mm with respect to the centroid of the section. These column specimens are designated as SC-138-55-20, SC-138-44-20, and SC-

138-40-20, where 'S' indicates the square shape of the external and 'C' indicates the internal tubes, and the first and second numbers next to SC represent the diameters of external and internal tubes, respectively, and the last number indicates the magnitude of eccentricity.
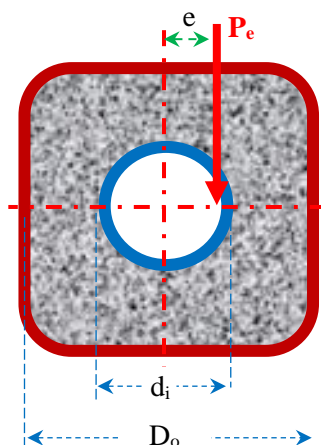
Fig. 6.7 Schematic view for a typical section of square CFDST under eccentric loads

6.3.1. Experimental response of eccentrically loaded square CFDST columns

The experimentally determined ultimate load-carrying capacity of these columns under eccentric loading conditions ($N_{u,e(Exp)}$) are shown in Table 6.3. In order to examine the effect of eccentricity on the ultimate compressive strength of columns, the experimentally defined ultimate compressive strength of these columns under eccentric loading conditions ($N_{u,e(Exp)}$), are compared with the experimentally defined ultimate compressive strength under the axial load (e = 0) ($N_{u,0(Exp)}$) as shown in Table 6.3. As usual, the strength of the eccentricity-loaded column falls compared to the concentrically loaded column. To compare the performance of square CFDST columns under the eccentric load, the strength of the eccentrically loaded column is standardized by its concentric strength. The table indicates that rather than internal tube thickness, the diameter of the internal tube more substantially affects the behavior of columns under eccentric load case. This piece of evidence may be verified by comparing the performance of specimens SC-138-55-20 and SC-138-40-20,

which has an almost similar thickness to the internal tube, since the variation of the inner tube diameter, the $(N_{u,e(Exp)}/N_{u,o(Exp)})$ ratio significantly varies. The table shows that as the diameter of the internal tube decreases, the $(N_{u,e(Exp)}/N_{u,o(Exp)})$ ratio decreases. Hence, it may be concluded that the performance of a given square CFDST column may be improved by using the larger diameter of the internal tube.

Table. 6.3 Experimental result on square CFDST columns under eccentric loads

Section	Specimen label	External tube (mm)		Internal tube (mm)		$\dfrac{e}{d_i}$	Ultimate strength (kN)		
		D_o	t_o	d_i	t_i		$N_{u,0(Exp)}$	$N_{ue(Exp)}$	$\dfrac{N_{ue(Exp)}}{N_{u,0(Exp)}}$
	SC-138-55-20	138	3.2	55	3.8	15	1695	1606	0.95
	SC-138-44-20	138	3.2	44	3.0	15	1649	1574	0.95
	SC-138-40-20	138	3.2	40	3.7	11	1551	1257	0.81

During the tests on the square CFDST columns under the eccentric load, it was observed that eccentrically loaded square CFDST column specimens failed mainly due to the buckling of external and internal steel tubes and the crushing of concrete. For typical eccentrically loaded square CFDST column specimens, the failure mode is shown in Fig.6.8. Fig 6.8 shows the bucking of the outer and inner tubes, respectively. It can be observed from Fig 6.8 that the column buckling of the outer steel tube occurs near the top portion of the column; however, the internal tube's buckling occurs near the column's mid-height, as shown in Fig. 6.8. The outward buckling of the inner tube causes increases in lateral pressure in sandwiched concrete; however, the inward buckling of the inner tube results in the separation of the interior steel tube from the concrete core. With the increase in the magnitude of eccentric load, the initiation of outer tube buckling was observed near the ends of the columns before the crushing of concrete near mid-height, which resulted in the premature collapse of the column (compared to concentrically loaded). Consequently, the square CDFST columns under the eccentric load exhibited lower load-carrying capacity than the concentrically loaded column.
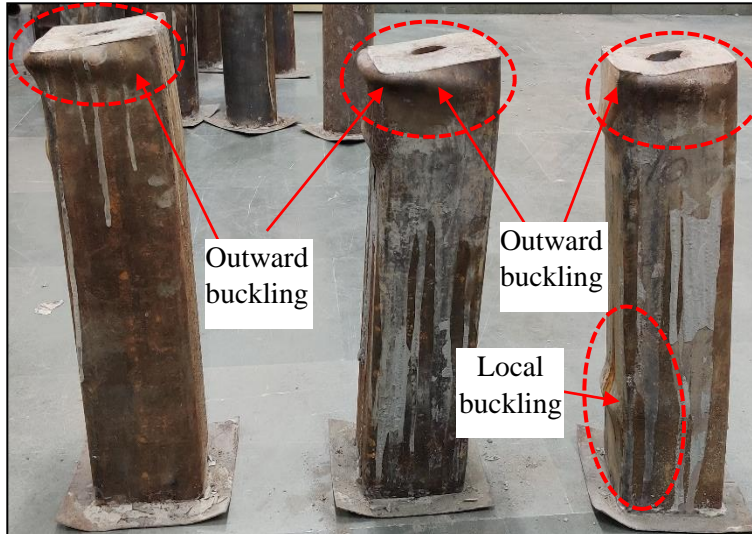
Fig. 6.8 Failure mode of square CFDST column with internal circular steel tube under eccentric load (SHS-CHS)

6.3.2. Numerical simulation of eccentric loaded square CFDST columns

The finite element analysis was carried out for all the square CFDST columns under the eccentric concentrated load using the ABAQUS to validate the experimental results. The numerically predicted ultimate compressive strength of columns, along with the experimentally achieved strength, are shown in Table 6.4. For all the cases, the numerically forecast strength of columns was found to be lower than the experimental strengths; however, the deviation in strength is not more than 5.9%. The probable cause for getting lower strength via numerical simulation may be handling error. In the experiment, the load was applied as a line load at eccentricity 'e'; however, in the FE modeling, the load was applied as the concentrated load at the point located at eccentricity 'e' on the axis.

Table. 6.4 Comparison of experimental and FEM ultimate strengths of square CFDST columns under eccentric loading

Section	Specimen label	External tube (mm)		Internal tube (mm)		Ultimate strength (kN)		
		D_o	t_o	d_i	t_i	$N_{ue(Exp)}$	$N_{ue(FEM)}$	$\dfrac{N_{ue(FEM)}}{N_{ue(Exp)}}$
	SC-138-55-20	138	3.2	55	3.8	1606	1573	1.021
	SC-138-44-20	138	3.2	44	3.0	1574	1481	1.063
	SC-138-40-20	138	3.2	40	3.7	1257	1270	0.990

Fig. 6.10 shows the numerically obtained failure modes of external and internal steel tubes for a typical column specimen SC-138-55-20. Moreover, Fig. 6.8 also includes the deformed shape of the same column specimen observed in a laboratory at the failure stage of the column. The numerical and experimental failure mode of external as well as internal steel tubes pretends to be similar, as shown in Fig. 6.10. It can be examined from Fig. 6.9 that the concentrically loaded column fails with outward buckling of the external steel tube at the upper and lower end of the column. In contrast, the specimen fails to buckle the external and internal steel tubes at the upper and lower end in the eccentrically loaded column. The inward buckling of the inner steel tube, as shown in Fig.6.10. The load-deformation curves for all the three square CFDST columns under the concentric loading and eccentric loading were plotted using the experimental data. They are compared with the numerically obtained curves in Fig. 6.11. It can be noted from the curves plotted in Fig.6.11 that the contract between experimental results and numerical predictions is generally good.
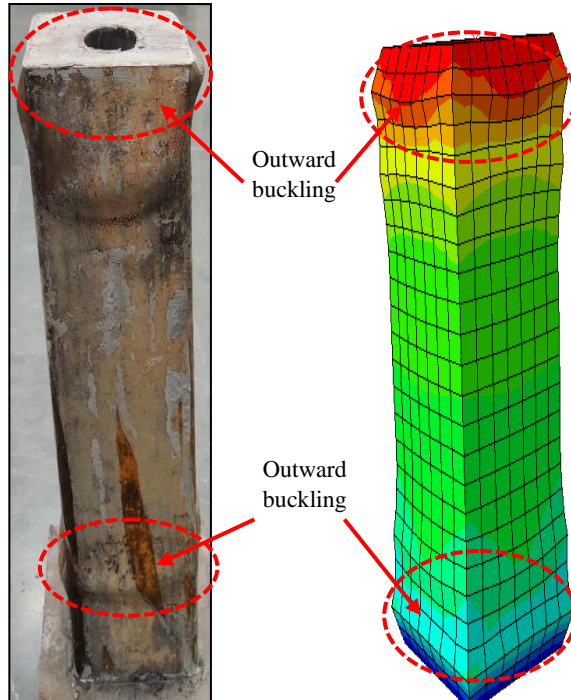
Fig. 6.9 Comparison of test and FE failure modes of square CFDST column under concentric load - (SC-138-39)
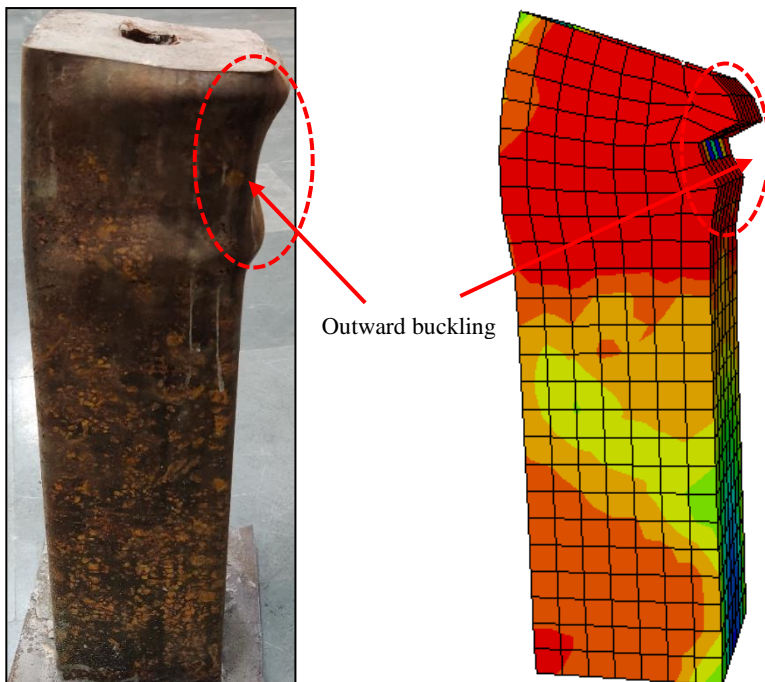
Fig. 6.10 Comparison of test and FE failure modes of square CFDST column under eccentric load - (SC-138-39-20)

(a) SC-138-55-20   (b) SC-138-44-20

(C) SC-138-40-20
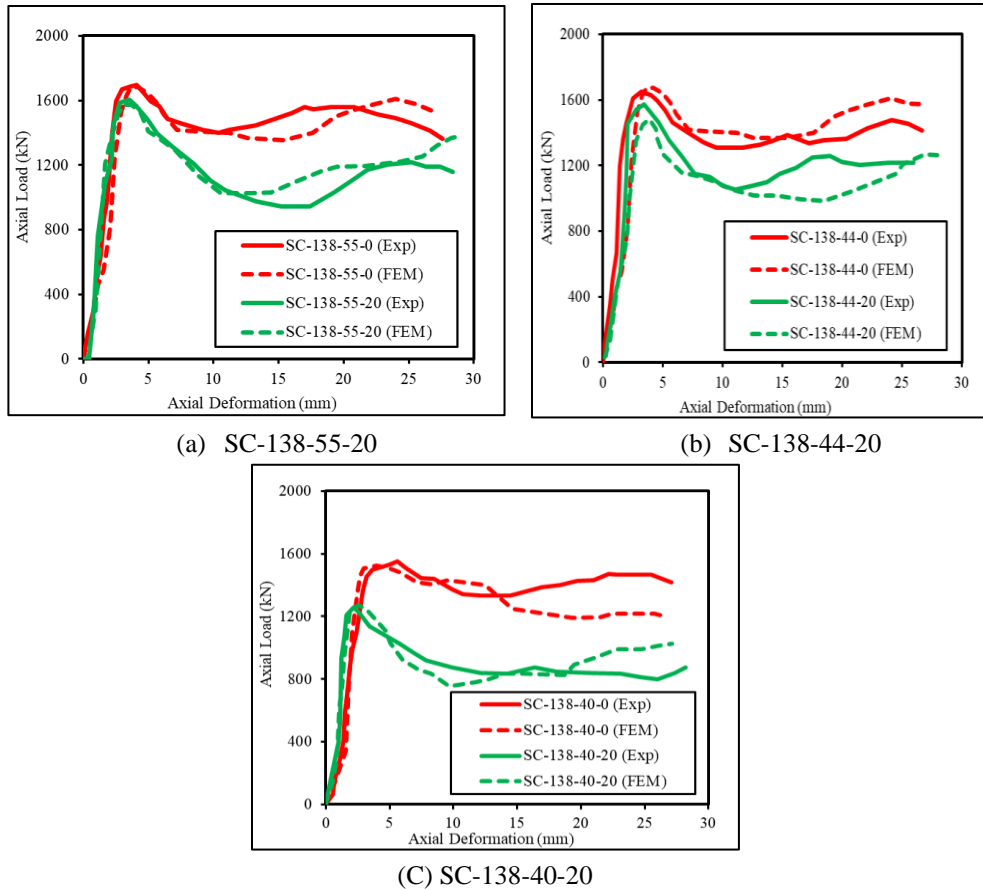
Fig. 6.11 Axial load versus axial deformation relations of square CFDST short columns under eccentric loads.

6.4. Behaviour of octagonal CFDST columns under eccentric loads

The study consisted of three specimens made from octagonal CFDST to investigate its repose under eccentric axial loading. The specimen geometry consisted of a constant cross-section of the outer and inner tubes. The outer tube for all specimens consisted of an octagonal cross-section, and the corresponding internal tubes were circular in cross-section. The axial load was applied with an eccentricity of 20mm for all three specimens. Fig.6.12 shows the schematic view of the cross-section of octagonal CFDST and the position of loading according to the experiment design. The column specimens are designated as OC-120-55-20, OC-120-44-20, and OC-120-40-20, where 'O' indicates the

(octagonal) shape of the external and 'C' indicates the internal tubes shapes (circular) and the first and second numbers next to OC represent the diameters of external and internal tubes respectively, and the last number indicates the magnitude of eccentricity.
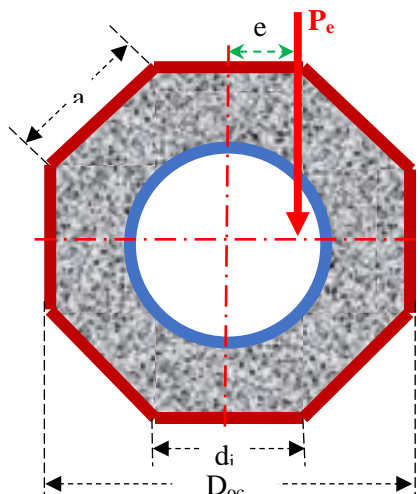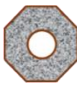
Fig. 6.12 Schematic view for a typical section of octagonal CFDST under eccentric loads

6.4.1. Experimental response of eccentrically loaded octagonal CFDST columns

The load-carrying capacity of eccentrically loaded specimens is mentioned under $N_{u,e(Exp)}$ designation and later is compared with concentrically loaded octagonal CFDST (e=0). The eccentrically loaded column showed strength degradation and higher curvature developed from outward buckling. The percentage fall in strength depicted in Table 6.5 in terms of the ratio of strengths observed makes it evident that the inner tube plays a significant role in governing the eccentrically loaded octagonal CFDST column response falls compared to the concentrically loaded column. To compare the performance of columns under the eccentric load, the strength of the eccentrically loaded column is normalized by its concentric strength. The table indicates that rather than internal tube thickness, the diameter of the internal tube more significantly affects the behavior of columns under an eccentric load case. This fact may be verified by comparing the performance of specimens

CC-120-55-20 and CC-120-40-20, which have an almost similar thickness to the internal tube, but because of variation in diameter of the internal tube, the $(N_{u,e(Exp)}/N_{u,o(Exp)})$ ratio significantly differs for these two specimens. The table shows that as the diameter of the internal tube decreases, the $(N_{u,e(Exp)}/N_{u,o(Exp)})$ ratio also decreases. Hence, it may be concluded that the performance of a given octagonal CFDST column may be improved by using the larger diameter of the internal tube.

Table. 6.5 Experimental result on octagonal CFDST columns under eccentric loads

Section	Specimen label	External tube (mm)		Internal tube (mm)		e (mm)	Ultimate strength (kN)		
		D_o	t_o	d_i	t_i		$N_{u,0(Exp)}$	$N_{ue(Exp)}$	$\dfrac{N_{ue(Exp)}}{N_{u,0(Exp)}}$
	OC-120-55-20	120	2.1	55	3.8	20	910	780	0.86
	OC-120-44-20	120	2.1	44	3.0	20	826	731	0.88
	OC-120-40-20	120	2.1	40	3.7	20	903	859	0.95

The experiment revealed that the failure of eccentrically loaded octagonal CFDST specimens was caused by the buckling of the external and internal tubes along with the crushing of concrete. The post-testing deformed shapes for the octagonal CFDST specimen are shown in Fig. 6.13. Fig. 6.14 makes it evident that the predominant effect of buckling is visible in the top and bottom portions of the specimen. With the increase in the magnitude of eccentric load, the initiation of outer tube buckling was observed near the ends of the columns before the crushing of concrete near mid-height, which resulted in the premature collapse of the column (compared to concentrically loaded). Consequently, the octagonal CDFST columns under the eccentric load exhibited lower load-carrying capacity than the concentrically loaded column.
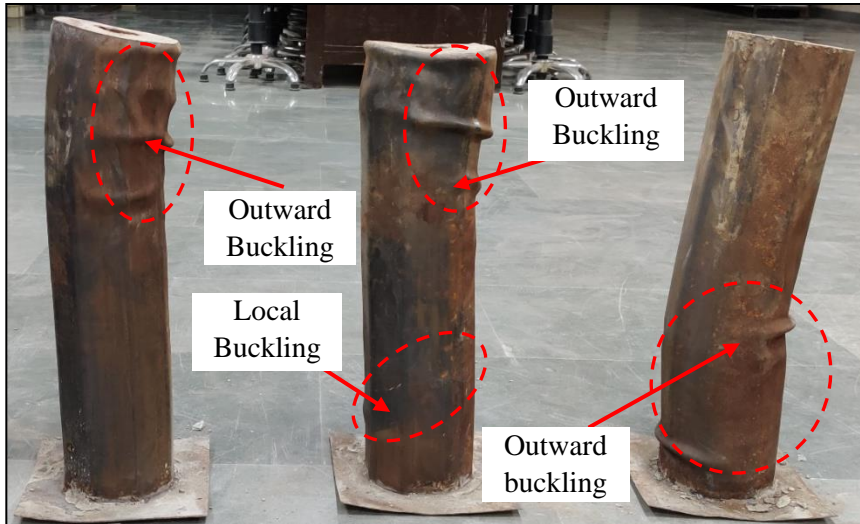
Fig. 6.13 Failure mode of octagonal CFDST column with internal circular steel tube under eccentric loads (OHS-CHS)
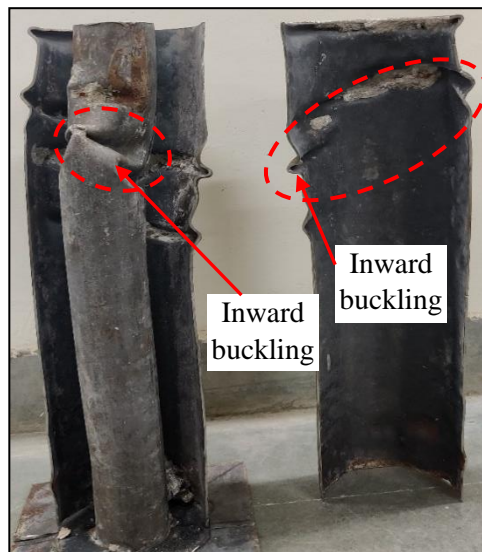
Fig. 6.14 Failure mode of octagonal CFDST column with internal circular steel tube under eccentric loads (OHS-CHS)

6.4.2. Numerical simulation of eccentric loaded octagonal CFDST columns

The finite element analysis was carried out for all the octagonal CFDST columns under the eccentric concentrated load using the ABAQUS to reproduce the experimental results. The geometrical details of the octagonal CFDST column specimens modelled in ABAQUS are shown in Table 6.5. The details regarding the modeling of CFDST columns in ABAQUS were discussed earlier

131

in Chapter 4. The numerically predicted ultimate load-carrying capacity of columns, along with the experimentally obtained strength, are shown in Table 6.6. For all the cases, the numerically predicted strength of columns was found to be lower than the experimental strengths; however, the deviation in strength is not more than 5.45%. The probable cause for getting lower strength via numerical simulation may be handling error. In the experiment, the load was applied as a line load at eccentricity 'e'; however, in the FE modeling, the load was applied as the concentrated load at the point located at eccentricity 'e' on the axis.

Table. 6.6 Comparison of experimental and FEM ultimate strengths of CFDST columns under eccentric loading
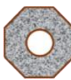
Section	Specimen label	External tube (mm)		Internal tube (mm)		e (mm)	Ultimate strength (kN)		
		D_o	t_o	d_i	t_i		$N_{ue,0(Exp)}$	$N_{ue(FEM)}$	$\dfrac{N_{ue,0(Exp)}}{N_{ue(FEM)}}$
	OC-120-55-20	120	2.1	55	3.8	20	825	780	1.06
	OC-120-44-20	120	2.1	44	3.0	20	746	731	1.02
	OC-120-40-20	120	2.1	40	3.7	20	847	859	0.99

Fig. 6.15(a) shows the numerically obtained failure modes of external and internal steel tubes for a typical column specimen OC-120-40-20. Moreover, Fig. 6.15 also includes the deformed shape of the same column specimen observed in a laboratory at the failure stage of the column. The numerical and experimental failure mode of external as well as internal steel tubes pretends to be similar, as shown in Fig. 6.15. It can be examined from Fig. 6.15(b) that the concentrically loaded column fails with outward buckling of the external steel tube at the upper and lower end of the column. In contrast, in the eccentrically loaded column, the specimen fails with buckling the external and internal steel tubes at the upper and lower end and the inward buckling of the inner steel tube, as shown in Fig.6.15 (a and b). The load-deformation curves for all three octagonal CFDST columns under the concentric and eccentric loading were plotted using the experimental data. They are compared with the numerically obtained curves in Fig. 6.16. It can be noted

from the curves plotted in Fig.6.16 that the contract between experimental results and numerical predictions is generally good.
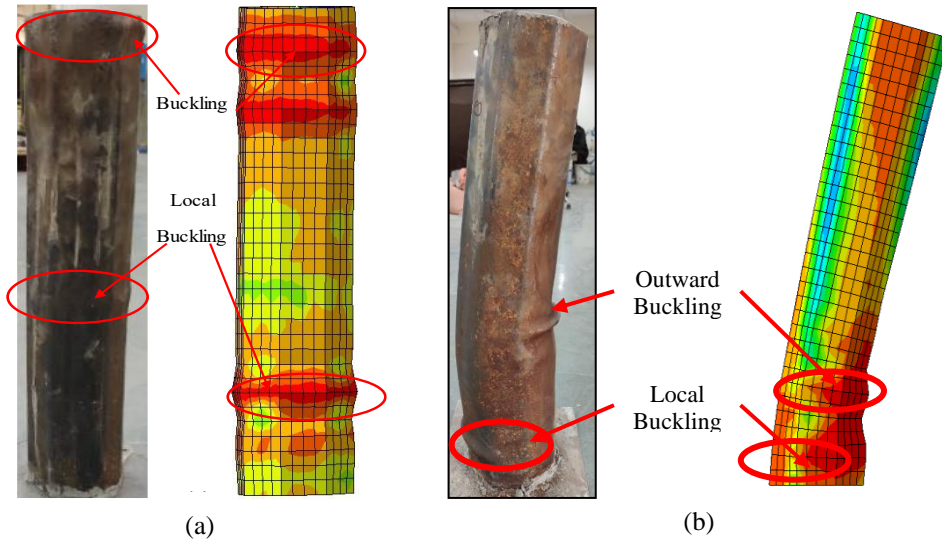
Fig. 6.15 Comparison of test and FE failure modes of CFDST column under concentric load (a) OC-120-40 and (b) OC-120-40-20
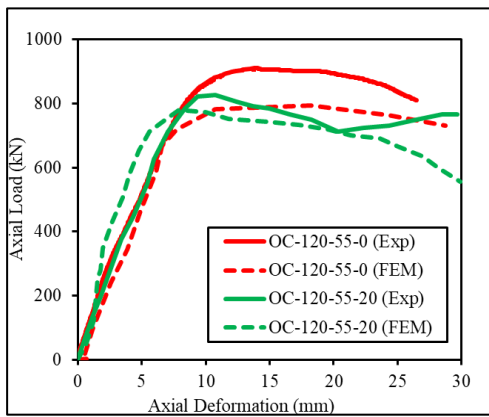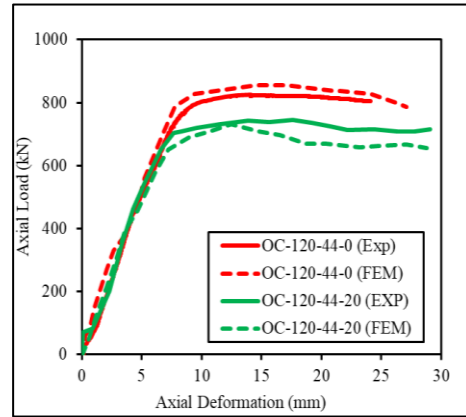
(a) OC-120-55-20   (b) OC-120-44-20
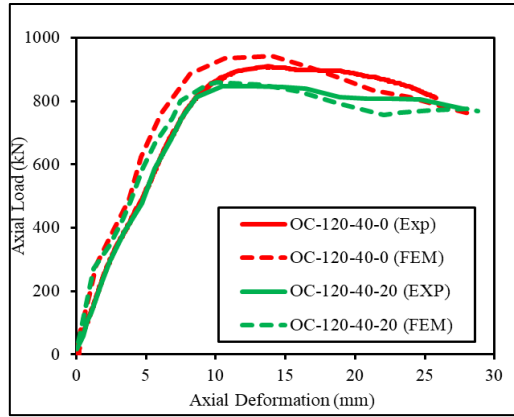
(c) OC-120-40-20

Fig. 6.16 Axial load versus axial deformation relations of octagonal CFDST short columns under eccentric loads

Chapter - 7
Investigation on Axially and Eccentrically loaded CFMST Columns

7.1. General

The experimental observations and numerical studies were carried out to u nderstand the structural behavior of Concrete-Filled Multi-skin Tubular steel (CF MST) columns with different cross-sections under the concentric and eccentric l oading been summarized in this chapter, and relevant conclusions have been d rawn.

7.2. Behaviour of Concrete-filled multi-skin steel tubular column (CFMST)

In total, eight CFMST columns with four circular and four-square cross-sections were prepared and tested. A characteristic of the circular and square CFMST column specimen is shown in Fig. 7.1. The column specimens were identified by CS-120-24(4)-0, CS-120-24(4)-20 CS-120-24(4)-30 CS-120-24(4)-40, SS-120-24(4)-0, SS-120-24(4)-20, SS-120-24(4)-30, and SS-120-24(4)-40 wherein C(S)-120-25(4)-20 "C" is the circular section CFDST column, "S" is the square section CFDST column "120" is the outer dimension of external octagonal steel tube, and "25" is the outer dimension of internal steel tube of CFDST short column, " (4)'' is the number of internal tubes and "20" is the eccentricity of the columns. Table 7.1 highlights the geometric properties of CFMST specimens.
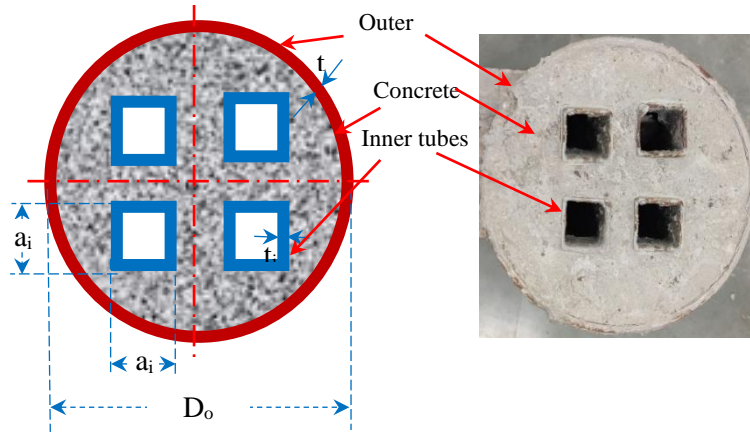
(a) CFMST column (CHS outer and SHS inner)
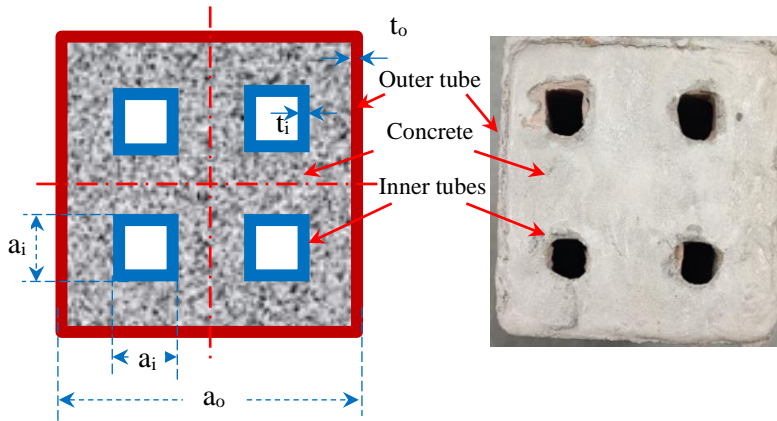
(b) CFMST column (SHS outer and SHS inner)

Fig. 7.1 Schematic view of circular and square CFMST columns

Table. 7.1 Geometrical and material properties of CFMST columns

Section	Specimen label	External tube			Internal tube			L (mm)	f_{cu} (MPa)
		D_o, a_o (mm)	t_o (mm)	f_{syo} (MPa)	a_i (mm)	t_i (mm)	f_{syi} (MPa)		
	CC-120-25(4)-0	120	2.2	381	25	3.0	564	500	38.33
	CC-120-25(4)-20	120	2.2	381	25	3.0	564	500	38.33
	CC-120-25(4)-30	120	2.2	381	25	3.0	564	500	38.33
	CC-120-25(4)-40	120	2.2	381	25	3.0	564	500	38.33
	SS-138-25(4)-0	138	3.2	383	25	3.0	564	500	38.33
	SS-138-25(4)-20	138	3.2	383	25	3.0	564	500	38.33
	SS-138-25(4)-30	138	3.2	383	25	3.0	564	500	38.33
	SS-138-25(4)-40	138	3.2	383	25	3.0	564	500	38.33

7.2.1. Circular CFMST column with four internal square steel tube

Table.7.2 indicates the effect of different eccentricity ratios on the axial deformation performance of CFMST columns with four internal square steel

tubes. As explained in Figs. 7.1(a), the load versus displacement curves of CFMST columns are basically in coincidence no matter what types of eccentricity ratios of four internal steel tubes possess. All load-displacement curves have almost the same peak loads, the same slope in the elastic stage, and the same axial deformation trends, which indicates that the eccentricity ratio exerts little influence on the ultimate strength, initial stiffness, and deformation capacity of CFMST short columns with double internal steel tubes. This is mainly owing to the fact that the bearing capacity and stiffness characteristics provided by the sandwiched concrete and steel tubes remain entirely unchanged, though the eccentricity ratio of four internal steel tubes presents an apparent variation. In terms of the ductility, the eccentricity exerts little effect on the ductility of CFMST columns, whatever kinds of embedded inner square steel tubes are embraced. This is because the ductility offered by the sandwiched concrete and steel tubes remains unchanged, although the eccentricity ratio of the four internal steel tubes varies.

Table. 7.2 Experimental result on circular CFMSTcolumns

Section	Specimen label	External tube (mm)		Internal tube (mm)		e (mm)	Ultimate strength (kN)		$\dfrac{N_{u(FEM)}}{N_{u(Exp)}}$
		a_o	t_o	d_i	t_i		$N_{u(Exp)}$	$N_{u(FEM)}$	
	CC-120-25(4)-0	120	2.2	25	3.0	0	1541	1541	1.00
	CC-120-25(4)-20	120	2.2	25	3.0	20	1481	1506	0.98
	CC-120-25(4)-30	120	2.2	25	3.0	30	1395	1388	1.01
	CC-120-25(4)-40	120	2.2	25	3.0	40	1309	1335	0.98

The columns generally have similar failure modes under axial and eccentric compressive loading. The columns mainly fail in the local buckling of steel tubes and the crushing of sandwiched concrete, as described by several researchers on CFDST columns. From Fig.7.3, the differences on the outside face of CFMST columns could be clearly noted, whereas the differences in internal steel tubes failed to be examined through the loading process. It has been observed that there were no obvious cracks and deformation on the outside face of the columns until the applied load approached 60% of the ultimate

compressive load. It is a known phenomenon that the internal steel tubes will begin to bugle inward gradually since there is no infilled concrete inside the inner steel tubes. In other words, the double internal steel tubes would achieve their yield strength. The failure modes of internal steel tubes after eccentric compression were demonstrated in Fig. 7.2. Subsequently, the outer square steel tube began to bulge outward gradually with the increase of the applied load. Owing to the existence of sandwiched concrete, the outward bulging of outer steel tubes was later than the inward bulging of internal steel tubes.

In this experiment, the specimens failed with the local buckling. As shown in Fig.7.2(a and b) (CS-138-25(4)-00), pronounced bulge rings were observed on the external square steel tubes of specimens, which was defined as the local buckling. Fig.7.2 (b) (CS-138-25(4)-40) showed the local buckling, which had a much more obvious bugle characteristic than the local buckling of other specimens. It can be found that the geometric shapes of the internal steel tube, section hollow ratio, and eccentricity ratio have no direct effects on the failure modes of specimens. In the overall trend, the failure modes of specimens gradually change because the enhancement of confinement concrete strength can effectively mitigate the local buckling of external steel tubes and the crushing of sandwiched concrete.
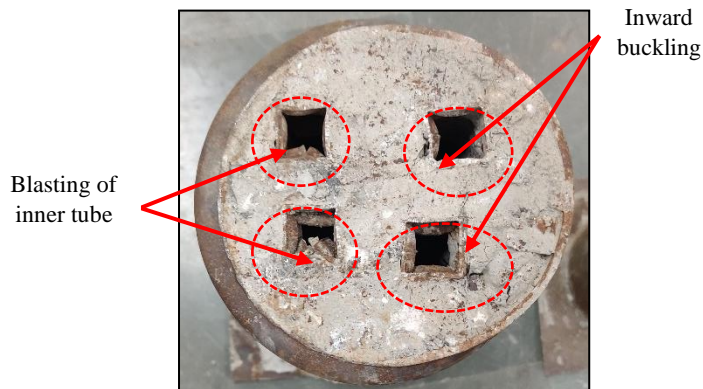
(a) Inward buckling effect in the top surface
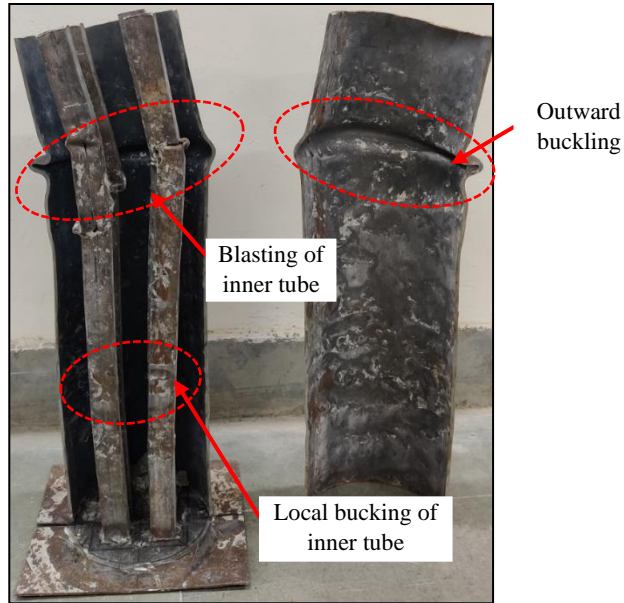
(b) Inner tube buckling effect in section view

Fig. 7.2 Failure mode of circular CFMST column under eccentric loading (CS-138-25(4)-40)

Fig. 7.3 Failure mode of circular CFMST column

(a) CS-120-25(4)-00 (Exp) (b) CS-120-25(4)-20 (Exp)

CS-120-25(4)-30 (Exp) CS-120-25(4)-40 (Exp)
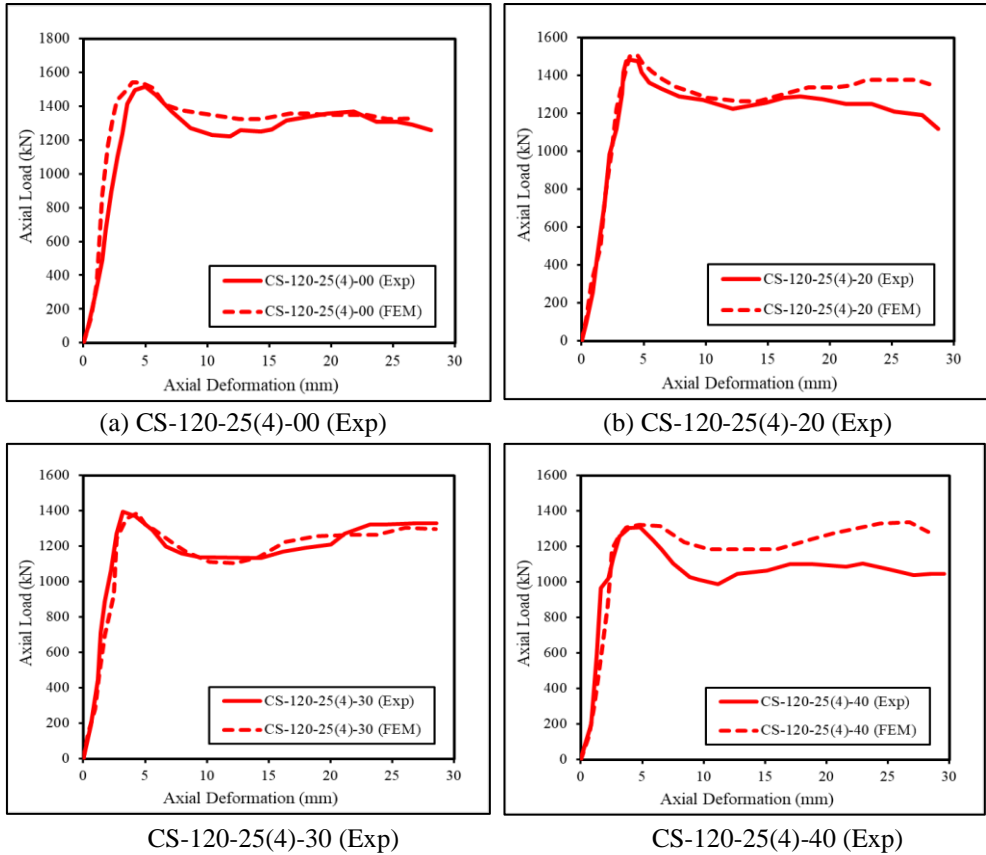
Fig. 7.4 Axial load versus axial deformation relations of circular CFMST short columns

7.2.2. Square CFMST column with four internal square steel tube

Table.7.3 indicates the effect of different eccentricity ratios on the axial deformation performance of CFMST columns with four internal square steel tubes. As explained in Fig.7.7, the load versus displacement curves of CFMST columns are basically in coincidence no matter what types of eccentricity ratios of four internal steel tubes possess. All load-displacement curves have almost the same peak loads, the same slope in the elastic stage, and the same axial deformation trends, which indicates that the eccentricity ratio exerts little influence on the ultimate strength, initial stiffness, and deformation capacity of CFMST columns with four internal steel tubes. This is mainly owing to the fact that the bearing capacity and stiffness characteristics provided by the

140

sandwiched concrete and four edges of steel tubes remain entirely unchanged. However, the eccentricity ratio of four internal steel tubes presents an apparent variation. In terms the ductility, the eccentricity exerts little effect on the ductility of CFMST columns; this is because the ductility offered by the sandwiched concrete and four edges of steel tubes remains unchanged, although the eccentricity ratio varies.

Table. 7.3 Experimental result on square CFMST columns

| Section	Specimen label	External tube (mm)		Internal tube (mm)		e (mm)	Ultimate strength (kN)		$\dfrac{N_{u,0(FEM)}}{N_{u(Exp)}}$
		a_o	t_o	d_i	t_i		$N_{u,0(Exp)}$	$N_{u(FEM)}$	
	SS-138-25(4)-00	138	3.2	25	3.0	0	2242	2249	1.00
	SS-138-25(4)-20	138	3.2	25	3.0	20	2130	2077	1.03
	SS-138-25(4)-30	138	3.2	25	3.0	30	2037	2044	1.00
	SS-138-25(4)-40	138	3.2	25	3.0	40	1871	1878	1.00

The columns generally have similar failure modes under axial and eccentric compressive loading. The columns mainly fail in the local buckling of steel tubes and the crushing of sandwiched concrete, as described by several researchers on CFDST columns. From Fig.7.4(b), the differences on the outside face of CFMST columns could be clearly noted, whereas the differences in internal steel tubes failed to be examined through the loading process. It has been observed that there were no obvious cracks and deformation on the outside face of the columns until the applied load approached 60% of the ultimate compressive load. It is a known phenomenon that the internal steel tubes will begin to bugle inward gradually since there is no infilled concrete inside the inner steel tubes. In other words, the four internal steel tubes would achieve their yield strength. The failure modes of internal steel tubes after eccentric compression were demonstrated in Fig. 7.4(a). Subsequently, the outer square steel tube began to bulge gradually at four corners with the increased applied load. Owing to the existence of sandwiched concrete, the outward bulging of outer steel tubes was less than the inward bulging of internal steel tubes.

In this experiment, the specimens failed with the local buckling. As shown in Fig. 7.4(a and b) (SS-138-25(4)-00), pronounced bulge rings were observed on the external square steel tubes of specimens, which was defined as the local buckling. Fig. 7.4(b) (SS-138-25(4)-40) showed the local buckling, which had a much more apparent bugle characteristic than the local buckling of other specimens. It can be found that the eccentricity ratio has no direct effects on the failure modes of specimens. In the overall trend, the failure modes of specimens gradually change because the enhancement of confinement concrete strength can effectively ease the local buckling of outer steel tubes and the crushing of sandwiched concrete.
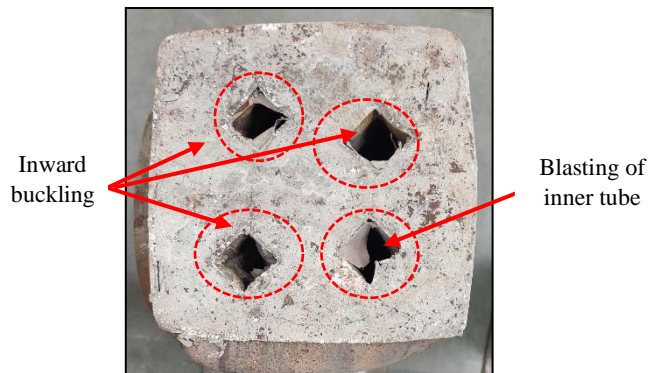
(a) Inward buckling effect in the top surface
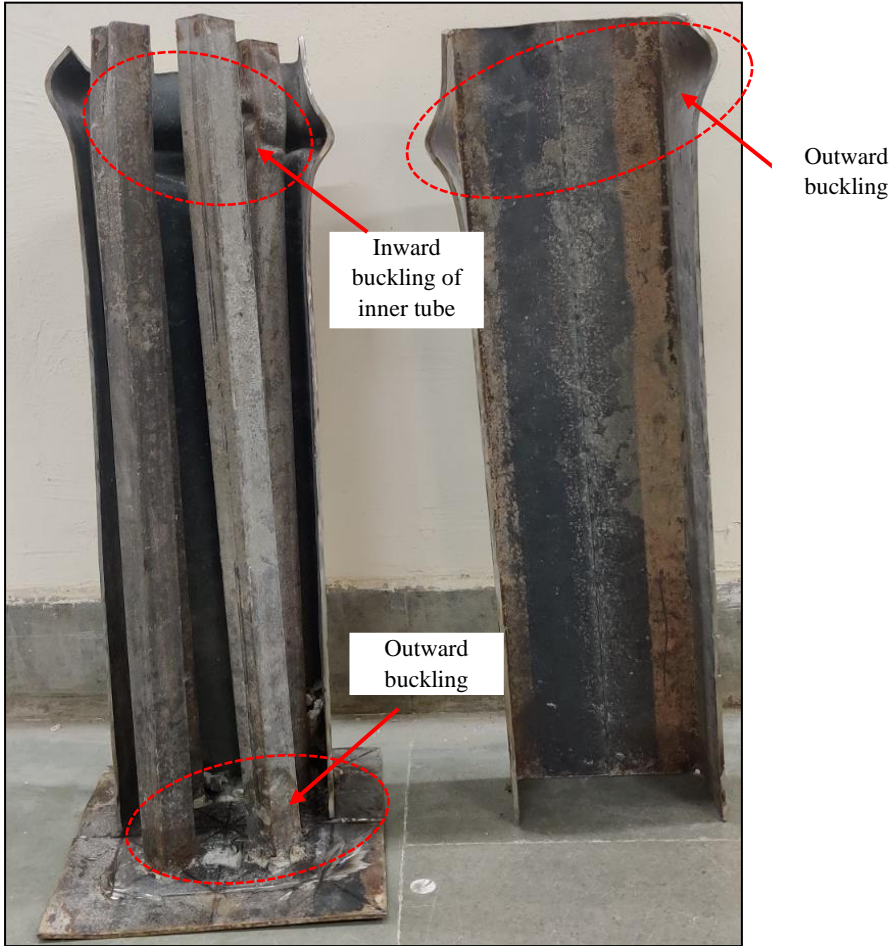
(b) Inner tube buckling effect in section view

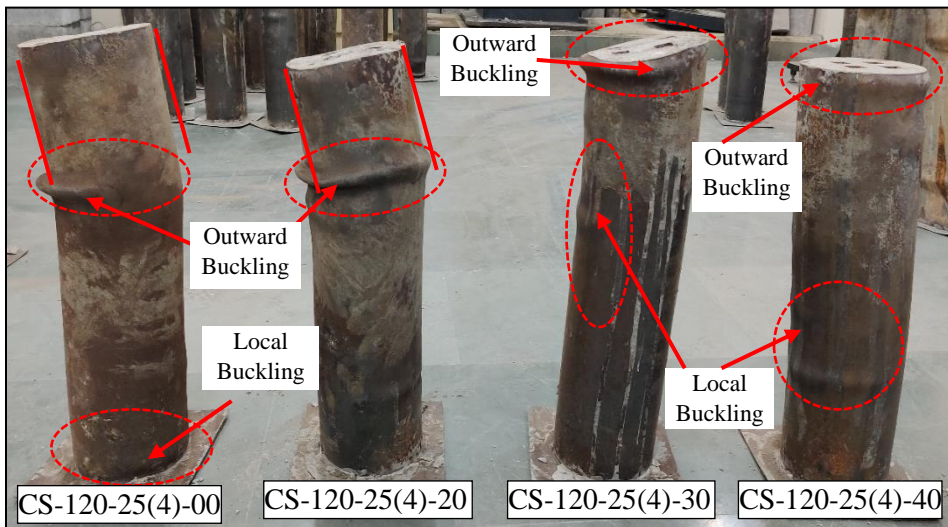**Fig. 7.5** Failure mode of square CFMST column under eccentric loading (SS-138-25(4)-40)

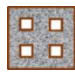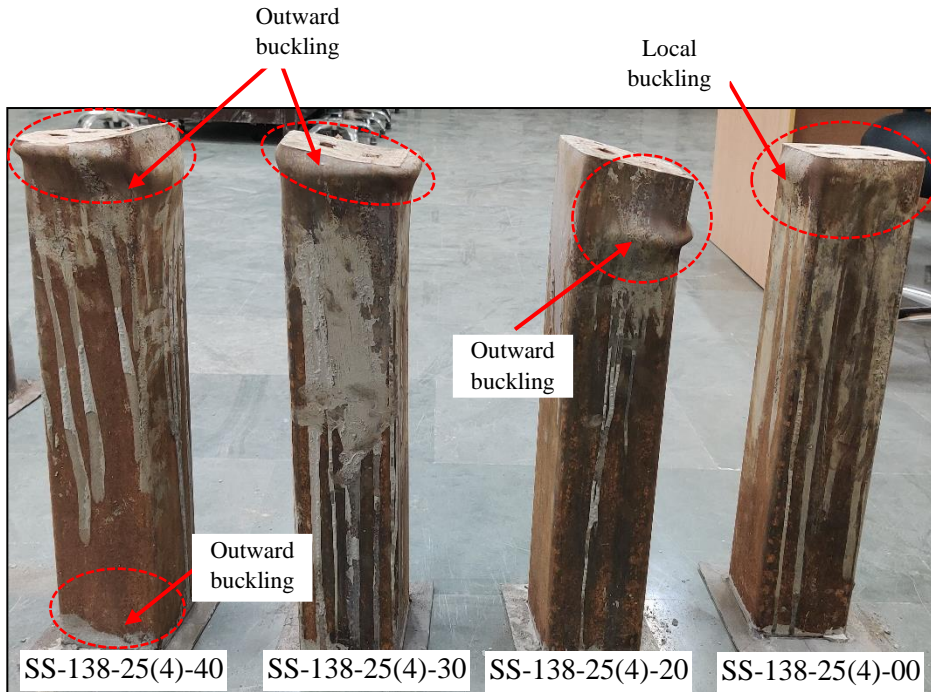**Fig. 7.6** Failure mode of square CFMST column

7.2.3. Numerical simulation of eccentric loaded circular CFDST columns

The finite element modeling of circular and square CFMST columns with four square internal tubes was carried out in ABAQUS, and the numerically obtained response was compared with that obtained experimentally. A comparison of experimentally obtained and numerically predicted ultimate load-carrying capacity of the circular and square CFMST columns is also shown in Tables 7.2 and 7.3. The table indicates that columns numerically obtained ultimate load-carrying capacity is in good agreement with the experimentally determined strengths. Moreover, the Table shows that in most cases, the experimentally obtained ultimate compressive strength of square CFMST columns is almost similar to the predicted numerical results.

Moreover, the experimentally observed deformed shape of a typical (CS-120-25(4)-20 and SS-138-25(4)-20) column at the ultimate load stage is compared with the numerically predicted deformed shape in Fig.7.6. The figure clearly shows that the numerical modeling of the CFMST column can predict the failure mode of the square CFMST column.

144

For all the circular and square CFMST columns considered in this study, the numerically predicted axial load versus axial deformation curves are compared with the experimentally obtained curves, as shown in Fig.7.7 and 7.8. From the figure, it may be noticed that, generally, there is no significant variation between the numerically predicted axial load versus axial-deformation curves. Therefore, the numerical simulation may be considered a reliable tool to predict the axial load versus deformation response of square CFDST columns up to the failure stage. The peak and post-peak contract curves between experimental results and numerical predictions are generally good.

Bucking
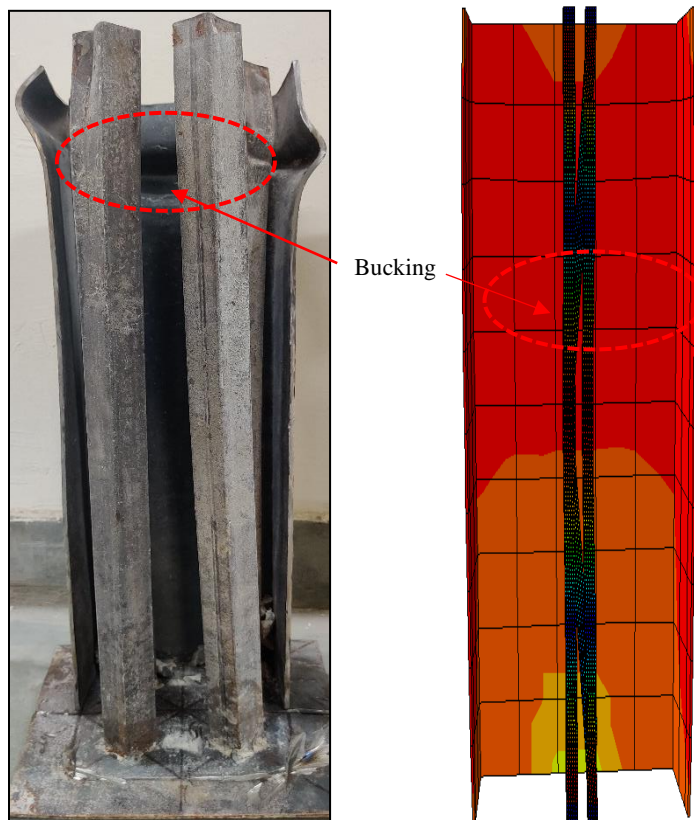
Fig. 7.7 Comparison of test and FE failure modes of specimen (CC-120-55-0) under eccentric load

(a) SC-120-25(4)-00   (b) SC-120-25(4)-20

(c) SC-120-25(4)-30   (d) SC-120-25(4)-40
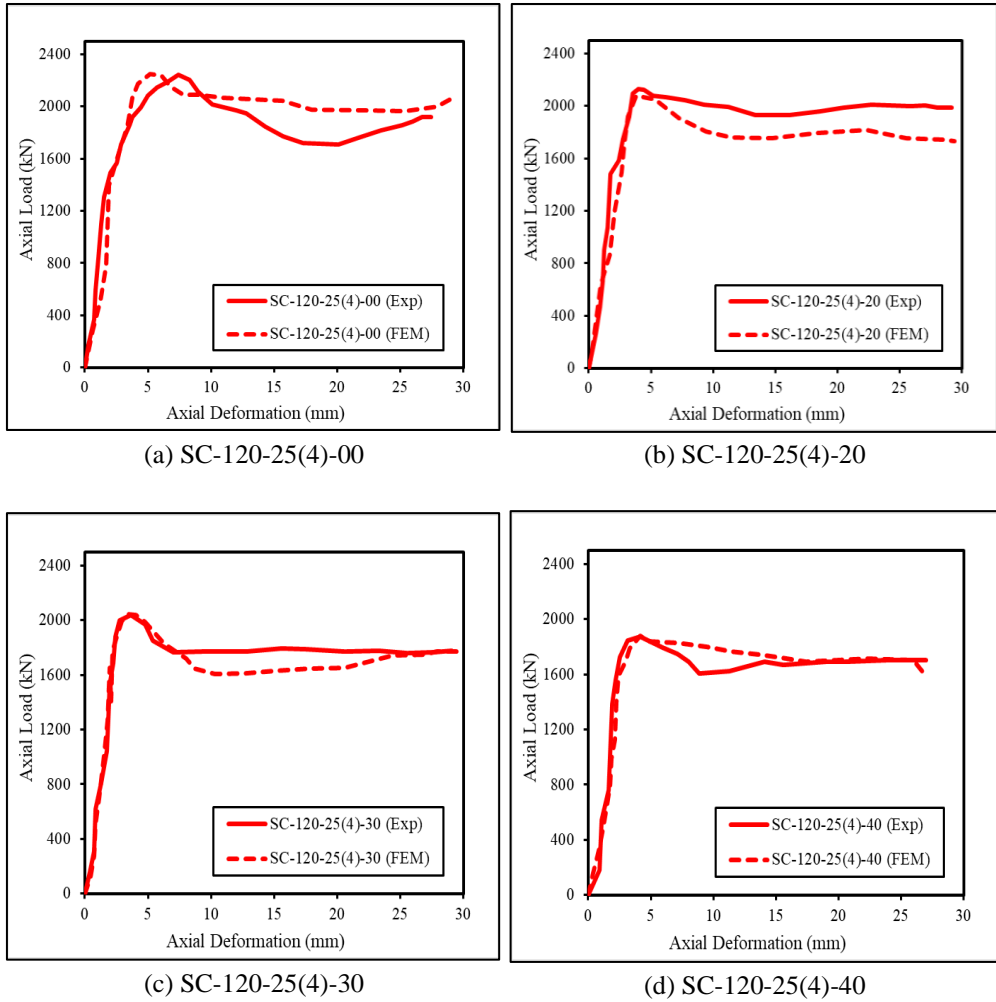
Fig. 7.8 Axial load versus axial deformation relations of square CFMST short columns

Conclusion

8.1. General

The experimental observations and numerical studies were carried out to understand the structural behavior of Concrete-Filled Double skinned Tubular steel (CFDST) and Concrete-Filled Multi-skin Tubular steel (CFMST) columns with different cross-sections under the concentric and eccentric loading been summarized in this chapter, and relevant conclusions have been drawn.

8.2. Influence of Cross-section shape on Failure Mode of CFDST columns

The structural response of CFDST columns under axial and eccentric loads is significantly influenced by the cross-sectional shape as well as the aspect ratio of the outer and inner steel tubes. The effect of CFDST column cross-sectional shape and the aspect ratio of outer and inner steel tubes for the axial and eccentric loads was investigated using experiments and numerical simulation, and the results are presented in the following subsections.

8.1.1. Failure Mode of CFDST columns Under Axial Loads

- Based on the experimental findings, it was concluded that irrespective of shape, CFDST columns under axial loading fail due to outward local buckling in outer steel tubes together with inward buckling in inner steel tubes, and also because of crushing, squeezing, and slipping of the sandwiched concrete at the locations of local buckling in the external tube.

- In the square section CFDST columns, failure was initiated from all four corners of the outer tube due to the non-uniform distribution of

lateral confining pressure being minimum at corners. Moreover, test results indicated that the square section CFDST columns sustain the loads even after reaching their ultimate strength, and the failure of columns was due to the crushing and squeezing of concrete at the corners.

- The failure mode of octagonal section CFDST columns was analogous to square section CFDST columns. Similar to square section CFDST columns, the failure in octagonal section CFDST was observed to initiate from all eight corners of the outer tube.

8.1.2. Failure Mode of CFDST columns Under Eccentric Loads

- Irrespective of the shape of CFDST, for all the CFDST columns considered in this study, the outer steel tube buckling was detected near the column's top portion at the ultimate stage; however, the internal tube buckling was noticed near the column's mid-height.
- In general, the shape of the inner steel tube and magnitude of eccentricity was not found to significantly affect the failure mode of the CFDST column specimens under eccentric loads.
- The failure in CFDST column specimens under eccentric load was observed to initiate mainly due to the outer tube's local buckling, and a subsequent increase in load caused the buckling in an inner tube. The experimental observations as well as the numerical results indicated that CFDST columns under eccentric load display sufficient ductility before the collapse.
- The study revealed that for the CFDST columns with smaller outer dimensions (120 mm), the size of the internal steel tube in eccentrically loaded CFDST columns was more significant in contributing to the strength of the column as compared to axially loaded columns.

- The eccentricity of the load significantly reduces the compressive strength of the CFDST column. Even for the minimum eccentricity considered in this study (20mm), there was a 17 %, 19%, and 14% reduction in strength for circular, square, and octagonal columns, respectively, which indicated that the octagonal sections are the least sensitive to the eccentricity of load.

- For the CFDST columns with circular as well as square external tubes, the eccentric strength-to-axial strength ratio was found to decrease monotonically with the increase in diameter of the internal circular from 40 mm to 55 mm. For the CFDST column with an outer tube octagonal, the eccentric strength-to-axial strength ratio decreased while increasing the inner tube diameter from 40 mm to 44 mm; however, a trend reversal was observed for the 55 mm inner tube diameter.

- The study revealed that the larger inner tube diameter octagonal CFDST columns under eccentric loads possess higher compressive compared to circular and rectangular CFDST columns.

8.3. Behavior of Concrete-Filled Multi-skin Tubular steel (CFMST) column

- The study revealed that there was not much difference in the buckling pattern of the outer steel tube of the CFMST columns under the concentric and eccentric load cases compared to CFDST columns.

- Observations during the test showed that up to approximately 60% of ultimate axial compressive load on the column, there were no significant deformations and bulging on the outer face of CFDST columns.

- The bulging in each of the four internal tubes in the CFMST columns was lower than the (single) steel tube in the CFDST column due to the smaller size tubes; as a result, the internal steel tubes achieved their yield strength before the failure of the CFMST column.

- The outer tube outward bulging in the CFMST columns was found to be lower than that for CFDST columns.

- The magnitude of eccentricity does not directly affect the failure modes of CFMST specimens.

- Pronounced bulge rings (local buckling) were observed on the outer face in the CFMST columns instead of global bulging in the CFDST columns.

- For a given geometry of CFMST columns under the compressive load applied at maximum eccentricity (40 mm), it causes a reduction in strength up to approximately 16% compared to concentric loading, which infers that the CFMST columns are less sensitive to the eccentricity of load.

- CFMST columns did not show significant deviation in the load-deformation curve (ductility) due to an increase in the magnitude of the eccentricity of the load.

8.4. Numerical Analysis of CFDST and CFMST columns

- The numerical simulation carried out in the present study using the ABAQUS is capable of predicting the compressive behavior of circular, square, and octagonal CFDST/CFMST members. The discrepancy between the numerically predicted and experimentally determined ultimate compressive strength of columns was not more than 10%.

- The experimentally observed deformed shape and mode of failure of column specimens at the ultimate load stage-matched well with that predicted numerically.

- In general, there was no significant variation between the numerically predicted axial-load versus axial-deformation curves of CFDST and CFMST columns up to the failure stage.

- The investigation of the elliptical cross-sectional shape of an equal area

of the steel tubes and concrete; showed that the column compressive strength steadily enhanced for a larger size of an external tube of the CFDST column.

- In the case of the elliptical column, the outward buckling was found around the mid-height section; however, the inner tube's failure mode is analogous to the distorted diamond.

- Therefore, the numerical simulation may be considered a reliable tool to predict the axial load versus deformation response of circular CFDST columns up to the failure stage.

8.5. Limitations and Future Scope of the Present Study

- The present study has been limited to a short column of 500mm height with different cross-sections such as circular, square, octagonal, and elliptical.

- The cross-section dimension of CFDST and CFMST columns are limited to 120-140mm only.

- The loading applications of CFDST and CFMST column is limited to axial compression with uniaxial bending.

- The numerical study on confinement pressure in CFDST is still at a very preliminary stage. Cross-sections of different shapes, sizes, and core configurations may be analyzed.

- The effect in reduction of the thickness of steel tubes in actual structures on account of corrosion may be explored in future experimental studies

- The behaviour of beam-column and column footing connections in the field can be investigated

- The behaviour of the CFMST columns with different cross-sections can be performed under the cyclic loading condition.

References

ABAQUS (2014) 'Analysis user's manual 6.14-EF, Dassault Systems Simulia Corp., Providence.

Abed, F., Alhamaydeh, M. and Abdalla, S. (2013) 'Experimental and numerical investigations of the compressive behavior of concrete filled steel tubes (CFSTs)', *Journal of Constructional Steel Research*. Elsevier Ltd, 80, pp. 429–439. doi: 10.1016/j.jcsr.2012.10.005.

Ahmed, M. *et al.* (2020) 'Behavior of circular concrete-filled double steel tubular slender beam-columns including preload effects', *Engineering Structures*. Elsevier, 220(June), p. 111010. doi: 10.1016/j.engstruct.2020.111010.

Alqawzai, S. *et al.* (2020) 'Behavior of octagonal concrete-filled double-skin steel tube stub columns under axial compression', *Journal of Constructional Steel Research*. Elsevier Ltd, 170, p. 106115. doi: 10.1016/j.jcsr.2020.106115.

Attard, M. M. and Setunge, S. (1996) 'Stress-strain relationship of confined and unconfined concrete', *ACI Materials Journal*, 93(5), pp. 432–442. doi: 10.14359/9847.

Australia Standards (AS) (1998) 'AS4100 Steel structures'. Sydney: Standards Australia.

Bardet, J. P. (1990) 'Lode dependences for isotropic pressure-sensitive elastoplastic materials', *Journal of Applied Mechanics, Transactions ASME*, 57(3), p. 498. doi: 10.1115/1.2897051.

Bridge, R. Q. (1976) 'Concrete Filled Steel Tubular Columns', *School of Civil Engineering, University of Sydney, Sydney, Australia,* p. Report No. R283.

British Standard Institute. (1979) 'BS5400, part 5', *concrete and composite bridges.*

Chang, X. *et al.* (2014) 'Analysis of circular concrete-filled steel tube (CFT) support in high ground stress conditions', *Tunnelling and Underground Space Technology*. Elsevier Ltd, 43, pp. 41–48. doi: 10.1016/j.tust.2014.04.002.

Chen, J. *et al.* (2016) 'Behavior of thin-walled dodecagonal section double skin concrete-filled steel tubes under bending', *Thin-Walled Structures*. Elsevier, 98, pp. 293–300. doi: 10.1016/j.tws.2015.10.002.

Chung, K. S., Kim, J. H. and Yoo, J. H. (2013) 'Experimental and analytical investigation of high-strength concrete-filled steel tube square columns subjected to flexural loading', *Steel and Composite Structures*, 14(2), pp. 133–153. doi: 10.12989/scs.2013.14.2.133.

Cicekli, U., Voyiadjis, G. Z. and Abu Al-Rub, R. K. (2007) 'A plasticity and anisotropic damage model for plain concrete', *International Journal of Plasticity*, 23(10–11), pp. 1874–1900. doi: 10.1016/j.ijplas.2007.03.006.

D., P. S. and S. (2012) 'Comparative Study of Concrete Filled Tubes with Hollow Double Skinned Composite Columns in- Filled With Self Compacting Concrete', *Proceedings of International Conference on Advances in Architecture and Civil Engineering (AARCV 2012)*, 1, pp. 195–199.

Dabaon, M. *et al.* (2009) 'Confinement effect of stiffened and unstiffened concrete-filled stainless steel tubular stub columns', *Journal of Constructional Steel Research*. Elsevier Ltd, 65(8–9), pp. 1846–1854. doi: 10.1016/j.jcsr.2009.04.012.

Deng, R. *et al.* (2022) 'Behaviour of tapered CFDST columns with large hollow ratio under combined loads', 196(June). doi: 10.1016/j.jcsr.2022.107388.

Ding, C. *et al.* (2021) 'Cyclic behaviour of prefabricated connections for steel beam to concrete filled steel tube column', *Journal of Constructional Steel Research*. Elsevier Ltd, 176, p. 106422. doi: 10.1016/j.jcsr.2020.106422.

Dong, C. X. and Ho, J. C. M. (2012) 'Concrete-filled Double-skin Tubular Columns with External Steel Rings', *Australian Earthquake Engineering Society 2012 Conference*, pp. 1–9.

Duarte, A. P. C. *et al.* (2016) 'Finite element modelling of short steel tubes filled with rubberized concrete', *Composite Structures*, pp. 28–40. doi: 10.1016/j.compstruct.2016.04.048.

Ekmekyapar, T. and Ghanim, H. (2019) 'The influence of the inner steel tube on the compression behaviour of the concrete filled double skin steel tube (CFDST) columns', *Marine Structures*. Elsevier Ltd, 66(April), pp. 197–212. doi: 10.1016/j.marstruc.2019.04.006.

Elchalakani, M. *et al.* (2016) 'Plastic and yield slenderness limits for circular concrete filled tubes subjected to static pure bending', *Thin-Walled Structures*. Elsevier, 109, pp. 50–64. doi: 10.1016/j.tws.2016.09.012.

Elchalakani, M. *et al.* (2019) 'Finite element simulation of circular short CFDST columns under axial compression', *Structures*. Elsevier, 20(December

2018), pp. 607–619. doi: 10.1016/j.istruc.2019.06.004.

Elchalakani, M., Zhao, X. L. and Grzebieta, R. (2002) 'Tests on concrete filled double-skin (CHS outer and SHS inner) composite short columns under axial compression', *Thin-Walled Structures*, 40(5), pp. 415–441. doi: 10.1016/S0263-8231(02)00009-5.

Ellobody, E. (2013) 'Numerical modelling of fibre reinforced concrete-filled stainless steel tubular columns', *Thin-Walled Structures*. Elsevier, 63, pp. 1–12. doi: 10.1016/j.tws.2012.10.005.

Eurocode 4 (EC4) (2004) '(EC4)', *Design of composite steel and concrete structures, Part 1.1: General rules and rules for buildings*, (Brussels: Commission of European Communities).

Feng, P., Cheng, S. and Yu, T. (2018) 'Seismic Performance of Hybrid Columns of Concrete-Filled Square Steel Tube with FRP-Confined Concrete Core', *Journal of Composites for Construction*, 22(4), p. 04018015. doi: 10.1061/(asce)cc.1943-5614.0000849.

Fujikura, S., Bruneau, M. and Lopez-Garcia, D. (2008) 'Experimental Investigation of Multihazard Resistant Bridge Piers Having Concrete-Filled Steel Tube under Blast Loading', *Journal of Bridge Engineering*, 13(6), pp. 586–594. doi: 10.1061/(asce)1084-0702(2008)13:6(586).

Fujimoto, T. *et al.* (2004) 'Behavior of Eccentrically Loaded Concrete-Filled Steel Tubular Columns', *Journal of Structural Engineering*, 130(2), pp. 203–212. doi: 10.1061/(asce)0733-9445(2004)130:2(203).

Furlong, R. W. (1967) 'Strength of Steel-Encased Concrete Beam Columns', *Journal of the Structural Division*, 93(ST5), pp. 113–124.

Fuyun Huang, X. Y. and B. C. (2012) 'The structural performance of axially loaded CFST columns under various loading conditions', *Steel and Composite Structures*, 13(5), pp. 451–471.

GB 50017 (2003) 'Code for Design of Steel Structures'. 1st Ed., Ministry of Construction of China, Beijing, (China).

Giakoumelis, G. and Lam, D. (2004) 'Axial capacity of circular concrete-filled tube columns', *Journal of Constructional Steel Research*, 60(7), pp. 1049–1068. doi: 10.1016/j.jcsr.2003.10.001.

Goode, C. D., Kuranovas, A. and Kvedaras, A. K. (2010) 'Buckling of slender composite concrete - filled steel columns', 3730. doi: 10.3846/jcem.2010.26.

Grassl, P. and Jirásek, M. (2006) 'Damage-plastic model for concrete failure', *International Journal of Solids and Structures*, 43(22–23), pp. 7166–7196. doi: 10.1016/j.ijsolstr.2006.06.032.

Guerrini, G. *et al.* (2015) 'Seismic Behavior of Posttensioned Self-Centering Precast Concrete Dual-Shell Steel Columns', *Journal of Structural Engineering*, 141(4), p. 04014115. doi: 10.1061/(asce)st.1943-541x.0001054.

Gupta, P. K., Sarda, S. M. and Kumar, M. S. (2007) 'Experimental and computational study of concrete filled steel tubular columns under axial loads', *Journal of Constructional Steel Research*, 63(2), pp. 182–193. doi: 10.1016/j.jcsr.2006.04.004.

Hajjar, J. F. *et al.* (2013) 'Full-Scale Tests of Slender Concrete-Filled Tubes : Axial Behavior', 139(July), pp. 1249–1262. doi: 10.1061/(ASCE)ST.1943-541X.0000784.

Han, L.-H., Zhao, X.-L. and Tao, Z. (2001) 'Tests and mechanics model for concrete-filled SHS stub columns, columns and beam-columns', *Steel and Composite Structures*, 1(1), pp. 51–74. doi: 10.12989/scs.2001.1.1.051.

Han, L. H. (2002) 'Tests on stub columns of concrete-filled RHS sections', *Journal of Constructional Steel Research*, 58(3), pp. 353–372. doi: 10.1016/S0143-974X(01)00059-1.

Han, L. H. *et al.* (2004) 'Concrete-filled double skin (SHS outer and CHS inner) steel tubular beam-columns', *Thin-Walled Structures*, 42(9), pp. 1329–1355. doi: 10.1016/j.tws.2004.03.017.

Han, L. H. *et al.* (2006) 'Concrete-filled double skin steel tubular (CFDST) beam-columns subjected to cyclic bending', *Engineering Structures*, 28(12), pp. 1698–1714. doi: 10.1016/j.engstruct.2006.03.004.

Han, L. H., Li, Y. J. and Liao, F. Y. (2011) 'Concrete-filled double skin steel tubular (CFDST) columns subjected to long-term sustained loading', *Thin-Walled Structures*. Elsevier, 49(12), pp. 1534–1543. doi: 10.1016/j.tws.2011.08.001.

Han, L. H., Ren, Q. X. and Li, W. (2010) 'Tests on inclined, tapered and STS concrete-filled steel tubular (CFST) stub columns', *Journal of Constructional Steel Research*. Elsevier Ltd, 66(10), pp. 1186–1195. doi: 10.1016/j.jcsr.2010.03.014.

Han, L. H., Ren, Q. X. and Li, W. (2011) 'Tests on stub stainless steel concrete carbon steel double-skin tubular (DST) columns', *Journal of Constructional*

Steel Research. Elsevier Ltd, 67(3), pp. 437–452. doi: 10.1016/j.jcsr.2010.09.010.

Han, L. H. and Yang, Y. F. (2003) 'Analysis of thin-walled steel RHS columns filled with concrete under long-term sustained loads', *Thin-Walled Structures*, 41(9), pp. 849–870. doi: 10.1016/S0263-8231(03)00029-6.

Han, L. H. and Yao, G. H. (2004) 'Experimental behaviour of thin-walled hollow structural steel (HSS) columns filled with self-consolidating concrete (SCC)', *Thin-Walled Structures*, 42(9), pp. 1357–1377. doi: 10.1016/j.tws.2004.03.016.

Han, L. H., Yao, G. H. and Tao, Z. (2007) 'Behaviors of concrete-filled steel tubular members subjected to combined loading', *Thin-Walled Structures*, 45(6), pp. 600–619. doi: 10.1016/j.tws.2007.04.008.

Han, T. H., Stallings, J. M. and Kang, Y. J. (2010) 'Nonlinear concrete model for double-skinned composite tubular columns', *Construction and Building Materials*. Elsevier Ltd, 24(12), pp. 2542–2553. doi: 10.1016/j.conbuildmat.2010.06.001.

Hasan, H. G., Ekmekyapar, T. and Shehab, B. A. (2019) 'Mechanical performances of stiffened and reinforced concrete-filled steel tubes under axial compression', *Marine Structures*. Elsevier Ltd, 65(July 2018), pp. 417–432. doi: 10.1016/j.marstruc.2018.12.008.

Hassanein, M. F. *et al.* (2018) 'Behaviour of Concrete-filled Double-skin Short Columns Under Compression Through Finite Element Modelling: SHS Outer and SHS Inner Tubes', *Structures*. Elsevier Ltd on behalf of Institution of Structural Engineers, 14, pp. 358–375. doi: 10.1016/j.istruc.2018.04.006.

Hassanein, M. F., Kharoob, O. F. and Liang, Q. Q. (2013) 'Circular concrete-filled double skin tubular short columns with external stainless steel tubes under axial compression', *Thin-Walled Structures*. Elsevier, 73, pp. 252–263. doi: 10.1016/j.tws.2013.08.017.

Hillerborg, A., Modéer, M. and Petersson, P. E. (1976) 'Analysis of crack formation and crack growth in concrete by means of fracture mechanics and finite elements', *Cement and Concrete Research*, 6(6), pp. 773–781. doi: 10.1016/0008-8846(76)90007-7.

Le Hoang, A. and Fehling, E. (2017) 'Analysis of circular steel tube confined UHPC stub columns', *Steel and Composite Structures*, 23(6), pp. 669–682. doi: 10.12989/scs.2017.23.6.669.

Hu, H.-T. *et al.* (2003) 'Nonlinear Analysis of Axially Loaded Concrete-Filled Tube Columns with Confinement Effect', *Journal of Structural Engineering*, 129(10), pp. 1322–1329. doi: 10.1061/(asce)0733-9445(2003)129:10(1322).

Huang, H. *et al.* (2010) 'Analytical behaviour of concrete-filled double skin steel tubular (CFDST) stub columns', *Journal of Constructional Steel Research*. Elsevier Ltd, 66(4), pp. 542–555. doi: 10.1016/j.jcsr.2009.09.014.

İpek, S., Erdoğan, A. and Güneyisi, E. M. (2021) 'Compressive behavior of concrete-filled double skin steel tubular short columns with the elliptical hollow section', *Journal of Building Engineering*, 38(January). doi: 10.1016/j.jobe.2021.102200.

IS 1608 (2005) 'Metallic materials - Tensile testing at ambient temperature', *Bureau of Indian Standards*.

IS 456 (2000) 'Plain Concrete and Reinforced', *Bureau of Indian Standards,New Dehli*, pp. 1–114.

J. Tang, S.-I. Hino, I. Kuroda, T. O. (1996) 'Modeling of Stress - Strain Relationships for Steel and Concrete in Concrete Filled Circular Steel Tubular Columns', *Steel Construction Engineering*, 3, pp. 35–46.

J.W. Roderick and D.F. Rogers (1969) 'Load Carrying Capacity of Simple Composite Columns', *Journal of the Structural Division*, 95(2), pp. 209–228.

Jinan Chung, Keigo Tsuda, C. M. (1999) 'Strength of Slender Square Tube Columns Filled with High-Strength Concrete', *Steel Construction Engineering*, 6(21), pp. 25–32.

V. K. Kloppel and W. Goder (1957) 'An investigation of the load carrying capacity of concrete-filled steel tubes and development of design formula', *Der Stahlbau*, 26(1), pp. 1–10.

Karthik, M. M. and Mander, J. B. (2011) 'Stress-Block Parameters for Unconfined and Confined Concrete Based on a Unified Stress-Strain Model', *Journal of Structural Engineering*, 137(2), pp. 270–273. doi: 10.1061/(asce)st.1943-541x.0000294.

Kawaguchi, J. *et al.* (no date) 'TICS OF PORTAL FRAMES CONSISTING OF SQUARE CFT , io'.

Kim Jin-KookKwak, Hyo-Gyoung, Kwak, J.-H. (2013) 'Behavior of Hybrid Double Skin Concrete Filled Circular Steel Tube Columns', *Steel and Composite Structures*, 14(2), pp. 191–204.

Knowles, R. B. and Park, R. (1969) 'Strength of Concrete Filled Steel Tubular Columns', *Journal of the Structural Division*, 95(ST12), pp. 2565–2587.

Kuranovas, A. and and Kvedaras, A. K. (2007) 'Centrifugally manufactured hollow concrete-filled steel tubular columns', *Journal of Civil Engineering and Management*, 13(4), pp. 297–306.

Lai, M. H. and Ho, J. C. M. (2014) 'Experimental and theoretical studies of confined HSCFST columns under uni-axial compression', *Earthquake and Structures*, 7(4), pp. 527–552. doi: 10.12989/eas.2014.7.4.527.

Li, W. *et al.* (2012) 'Behaviour of tapered concrete-filled double skin steel tubular (CFDST) stub columns', *Thin-Walled Structures*. Elsevier, 57, pp. 37–48. doi: 10.1016/j.tws.2012.03.019.

Li, W. and Cai, Y. X. (2019) 'Performance of CFDST stub columns using high-strength steel subjected to axial compression', *Thin-Walled Structures*. Elsevier Ltd, 141(January), pp. 411–422. doi: 10.1016/j.tws.2019.04.021.

Li, W., Han, L. H. and Zhao, X. L. (2012) 'Axial strength of concrete-filled double skin steel tubular (CFDST) columns with preload on steel tubes', *Thin-Walled Structures*. Elsevier, 56, pp. 9–20. doi: 10.1016/j.tws.2012.03.004.

Li, W., Han, L. and Zhao, X. (2012) 'Thin-Walled Structures Axial strength of concrete-filled double skin steel tubular (CFDST) columns with preload on steel tubes', *Thin Walled Structures*. Elsevier, 56, pp. 9–20. doi: 10.1016/j.tws.2012.03.004.

Liang, Q. Q. (2009) 'Performance-based analysis of concrete-filled steel tubular beam-columns, Part I: Theory and algorithms', *Journal of Constructional Steel Research*. Elsevier Ltd, 65(2), pp. 363–372. doi: 10.1016/j.jcsr.2008.03.007.

Liang, Q. Q. and Uy, B. (2000) 'Theoretical study on the post-local buckling of steel plates in concrete- ® lled box columns', 75.

Liang, W., Dong, J. and Wang, Q. (2019) 'Thin-Walled Structures Mechanical behaviour of concrete- fi lled double-skin steel tube (CFDST) with sti ff eners under axial and eccentric loading', *Thin Walled Structures*. Elsevier Ltd, 138(February), pp. 215–230. doi: 10.1016/j.tws.2019.02.002.

Lu, F. W., Li, S. P. and Sun, G. (2007) 'Nonlinear equivalent simulation of mechanical properties of expansive concrete-filled steel tube columns', *Advances in Structural Engineering*, 10(3), pp. 273–281. doi: 10.1260/136943307781422271.

Lubliner, J. *et al.* (1989) 'A Plastic-Damage Model', *International Journal of Solids and Structures*, 25(3), pp. 299–326.

MacRae, G. *et al.* (2004) 'Brace-Beam-Column Connections for Concentrically Braced Frames with Concrete Filled Tube Columns', *Journal of Structural Engineering*, 130(2), pp. 233–243. doi: 10.1061/(asce)0733-9445(2004)130:2(233).

Martin D. O'Shea and Russell Q. Bridge (2000) 'Design of Circular Thin-Walled Concrete-Filled Steel Tubes', *Journal of Structural Engineering*, 126(11), pp. 1295–1303.

Matsui C., Mitani I., K. A. and T. K. (1997) 'AIJ Design Method for Concrete Filled Steel Tubular Structures', *ASCCS Seminar Report, ASCCS Seminar Report*, Innsbruck(93–116).

Mohammad Shams and M. Ala Saadeghvaziri (1197) 'State of the Art of Concrete-Filled Steel Tubular Columns', *ACI Structural Journal*, 94(5), pp. 558–571.

Montague (1975) 'A Simple Composite Construction for Cylindrical Shells Subjected to External Pressure', *Journal of Mechanical Engineering Science,* 17(2), pp. 105–113.

Morino, S. and Tsuda, K. (2015) 'Behavior of Concrete-Filled Steel Tubular Three-Dimensional Subassemblages', (January 1993).

Morino, S. and Tsuda, K. (2002) 'Design and construction of concrete-filled steel tube column system in Japan', *Earthquake Engineering and Engineering Seismology*, 4(1), pp. 51–73.

Nassirnia, M. *et al.* (2016) 'Innovative hollow columns comprising corrugated plates and ultra high-strength steel tubes', *Thin-Walled Structures*. Elsevier, 101, pp. 14–25. doi: 10.1016/j.tws.2015.12.020.

Nassirnia, M. *et al.* (2018) 'Hybrid corrugated members subjected to impact loading: Experimental and numerical investigation', *International Journal of Impact Engineering*, 122(September), pp. 395–406. doi: 10.1016/j.ijimpeng.2018.09.009.

O'Shea, M. D. and Bridge, R. Q. (1994) 'Tests of thin-walled concrete-filled steel tubes', *International Specialty Conference on Cold-Formed Steel Structures: Recent Research and Developments in Cold-Formed Steel Design and Construction*, pp. 399–419.

Ouyang, Y. *et al.* (2017) 'Finite element analysis of concrete-filled steel tube (CFST) columns with circular sections under eccentric load', *Engineering Structures*, 148, pp. 387–398. doi: 10.1016/j.engstruct.2017.06.064.

P.K. Neogi, H.K., Sen and J.C. Chapman (1969) 'Concrete-filled tubular steel columns under eccentric loading', *The Structural Engineer*, 47(5), pp. 187–195.

Pi, T. *et al.* (2019) 'Study on circular CFST stub columns with double inner square steel tubes', *Thin-Walled Structures*. Elsevier Ltd, 140(September 2018), pp. 195–208. doi: 10.1016/j.tws.2019.03.028.

Richart, F. E., Brandtzaeg, A. and Brown, R. L. (1928) 'A study of the failure of concrete under combined compressive stresses', *Bulletin No. 185 Engineering Experiment Station*, pp. 7–92. Available at: http://www.ideals.illinois.edu/handle/2142/4277%0Ahttps://www.ideals.illinois.edu/handle/2142/4277.

Sakino, K. *et al.* (2004) 'Behavior of centrally loaded concrete-filled steel-tube short columns', *Journal of Structural Engineering*, 130(2), pp. 180–188. doi: 10.1061/(ASCE)0733-9445(2004)130:2(180).

Schneider, S. P. (1998) 'Axially loaded concrete-filled steel tubes', *Journal of Structural Engineering (United States)*, 10(124), pp. 1125–1138. doi: https://doi.org/10.1061/(ASCE)0733-9445(1998)124:10(1125).

Shakir-Khalil and Mouli (1990) 'Further test on concrete-filled rectangular hollow-section columns', *Journal of Structural Engineering*, 68(20), pp. 405–413.

Shakir-Khalil H and eghiche J. (1989) 'Experimental behaviour of concrete-filled rolled rectangular hollow-section columns', *The Structural Engineer*, 67(19), pp. 346–353.

Shi, Y. *et al.* (2022) 'Axial compressive behaviour of tapered CFDST stub columns with large void ratio', *Journal of Constructional Steel Research*. Elsevier Ltd, 191(January), p. 107206. doi: 10.1016/j.jcsr.2022.107206.

Shinji Toda, Ryuta Hataya, Shintaro Abe, K. M. (1995) 'The 1995 Kobe earthquake and problems of evaluation of active faults in Japan', *Engineering Geology*, 43(3), pp. 151–167.

Su, R. *et al.* (2021) 'Axial behavior of novel CFDST columns with outer welded corrugated steel tubes', *Structures*. Elsevier Ltd, 34(July), pp. 2708–2720. doi: 10.1016/j.istruc.2021.09.039.

Susantha, K. A. S., Ge, H. and Usami, T. (2001) 'Uniaxial stress-strain relationship of concrete confined by various shaped steel tubes', *Engineering Structures*, 23(10), pp. 1331–1347. doi: 10.1016/S0141-0296(01)00020-7.

Tao, Z. *et al.* (2008) 'Design of concrete-filled steel tubular members according to the Australian Standard AS 5100 model and calibration', *Australian Journal of Structural Engineering*, 8(3), pp. 197–214. doi: 10.1080/13287982.2008.11464998.

Tao, Z. *et al.* (2011) 'Nonlinear analysis of concrete-filled square stainless steel stub columns under axial compression', *Journal of Constructional Steel Research*. Elsevier Ltd., 67(11), pp. 1719–1732. doi: 10.1016/j.jcsr.2011.04.012.

Tao, Z., Han, L. H. and Zhao, X. L. (2004) 'Behaviour of concrete-filled double skin (CHS inner and CHS outer) steel tubular stub columns and beam-columns', *Journal of Constructional Steel Research*, 60(8), pp. 1129–1158. doi: 10.1016/j.jcsr.2003.11.008.

Tao, Z., Wang, Z. Bin and Yu, Q. (2013) 'Finite element modelling of concrete-filled steel stub columns under axial compression', *Journal of Constructional Steel Research*. Elsevier Ltd, 89, pp. 121–131. doi: 10.1016/j.jcsr.2013.07.001.

Uenaka, K., Kitoh, H. and Sonoda, K. (2010) 'Concrete filled double skin circular stub columns under compression', *Thin-Walled Structures*. Elsevier, 48(1), pp. 19–24. doi: 10.1016/j.tws.2009.08.001.

Ukanwa, K. U. *et al.* (2018) 'Numerical analysis of plain and steel fiber reinforced concrete filled steel tubular slender column', *Advanced Steel Construction*, 14(2), pp. 308–323. doi: 10.18057/IJASC.2018.4.2.10.

Uy, B., Tao, Z. and Han, L. H. (2011) 'Behaviour of short and slender concrete-filled stainless steel tubular columns', *Journal of Constructional Steel Research*. Elsevier Ltd, 67(3), pp. 360–378. doi: 10.1016/j.jcsr.2010.10.004.

Vernardos, S. and Gantes, C. (2019) 'Experimental behavior of concrete-filled double-skin steel tubular (CFDST) stub members under axial compression : A comparative review', *Structures*. Elsevier, 22(October), pp. 383–404. doi: 10.1016/j.istruc.2019.06.025.

Vrcelj, Z. and Uy, B. (2002) 'Strength of slender concrete-filled steel box columns incorporating local buckling', 58, pp. 275–300.

Wai-Fah Chen (1982) *Plasticity in reinforced concrete*. New York: McGraw-Hill.

Wang, F. cheng, Han, L. hai and Li, W. (2018) 'Analytical behavior of CFDST stub columns with external stainless steel tubes under axial compression', *Thin-Walled Structures*. Elsevier Ltd, 127(January), pp. 756–768. doi: 10.1016/j.tws.2018.02.021.

Wang, F., Young, B. and Gardner, L. (2020) 'Compressive behaviour and design of CFDST cross-sections with stainless steel outer tubes', *Journal of Constructional Steel Research*. Elsevier Ltd, 170, p. 105942. doi: 10.1016/j.jcsr.2020.105942.

Wang, F. and Zhao, H. (2020) 'Experimental investigation on blast furnace slag aggregate concrete fi lled double skin tubular (CFDST) stub columns under sustained loading', *Structures*. Elsevier, 27(May), pp. 352–360. doi: 10.1016/j.istruc.2020.05.046.

Wang, J. *et al.* (2019) 'Analytical behavior of dodecagonal concrete- fi lled double skin tubular (CFDST) columns under axial compression', *Journal of Constructional Steel Research*. Elsevier Ltd, 162, p. 105743. doi: 10.1016/j.jcsr.2019.105743.

Wang, R. *et al.* (2016) 'Analytical behavior of concrete filled double steel tubular (CFDST) members under lateral impact', *Thin-Walled Structures*. Elsevier, 101, pp. 129–140. doi: 10.1016/j.tws.2015.12.006.

Wang, W. *et al.* (2019) 'Experimental study and numerical simulation of replaceable corrugated steel plate-concrete composite shear walls', *Soil Dynamics and Earthquake Engineering*. Elsevier Ltd, 127(April), p. 105827. doi: 10.1016/j.soildyn.2019.105827.

Wang, Y., Cao, M. and Sun, H. (2014) 'Time-dependent reliability analysis of circular CFST stub columns under environmental corrosion', *Pacific Science Review*. Elsevier Ltd, 16(3), pp. 201–206. doi: 10.1016/j.pscr.2015.04.002.

Wei, S. *et al.* (1995) 'Performance of New Sandwich Tube under Axial Loading: Experiment', *Journal of Structural Engineering*, 121(12), pp. 1806–1814. doi: 10.1061/(asce)0733-9445(1995)121:12(1806).

Yamamoto, T., Kawaguchi, J. and Morino, S. (2000) 'Experimental study of scale effects on the compressive behavior of short concrete-filled steel tube columns', *Proceedings of the Conference: Composite Construction in Steel and Concrete IV*, pp. 879–890. doi: 10.1061/40616(281)76.

Yan, X. F. and Zhao, Y. G. (2020) 'Compressive strength of axially loaded circular concrete-filled double-skin steel tubular short columns', *Journal of Constructional Steel Research*. Elsevier Ltd, 170, p. 106114. doi:

10.1016/j.jcsr.2020.106114.

Yan, X. F., Zhao, Y. G. and Lin, S. (2021) 'Compressive behaviour of circular CFDST short columns with high- and ultrahigh-strength concrete', *Thin-Walled Structures*. Elsevier Ltd., 164(April), p. 107898. doi: 10.1016/j.tws.2021.107898.

Yang, Y. *et al.* (2015) 'Thin-Walled Structures Investigation on square concrete fi lled double-skin steel tube (CFDST) subjected to local bearing force : Experiments', *Thin Walled Structures*. Elsevier, 94, pp. 394–409. doi: 10.1016/j.tws.2015.04.026.

Yang, Y. *et al.* (2021) 'Axial compressive behaviour of CFDST stub columns with large void ratio', *Journal of Constructional Steel Research*. Elsevier Ltd, 186(July), p. 106892. doi: 10.1016/j.jcsr.2021.106892.

Yin, F. *et al.* (2022) 'Seismic behavior of multi-cell steel reinforced concrete columns : Experimental study', *Journal of Building Engineering*. Elsevier Ltd, 47(June 2021), p. 103883. doi: 10.1016/j.jobe.2021.103883.

Yu, Z. wu, Ding, F. xing and Cai, C. S. (2007) 'Experimental behavior of circular concrete-filled steel tube stub columns', *Journal of Constructional Steel Research*, 63(2), pp. 165–174. doi: 10.1016/j.jcsr.2006.03.009.

Zhang, F. *et al.* (2015) 'Numerical Modeling of Concrete-Filled Double-Skin Steel Square Tubular Columns under Blast Loading', *Journal of Performance of Constructed Facilities*, 29(5), pp. 1–12. doi: 10.1061/(asce)cf.1943-5509.0000749.

Zhang, S. *et al.* (2005) 'Behavior of steel tube and confined high strength concrete for concrete-filled RHS tubes', *Advances in Structural Engineering*, 8(2), pp. 101–116. doi: 10.1260/1369433054037976.

Zhang, Y., Han, L. and Li, W. (2017) 'Analytical behaviour of tapered CFDST stub columns under axially partial compression', *Journal of Constructional Steel Research*. Elsevier Ltd, 139, pp. 302–314. doi: 10.1016/j.jcsr.2017.09.023.

Zhao, H. *et al.* (2021) 'Behaviours of circular CFDST with stainless steel external tube: Slender columns and beams', *Thin-Walled Structures*. Elsevier Ltd, 158(September 2020), p. 107172. doi: 10.1016/j.tws.2020.107172.

Zhao, X.-L., Grzebieta, R. and Elchalakani, M. (2002) 'Tests of concrete-filled double skin CHS composite stub columns', *Steel and Composite Structures*, 2(2), pp. 129–146. doi: 10.12989/scs.2002.2.2.129.

Zhao, X. L. and Grzebieta, R. (2002) 'Strength and ductility of concrete filled double skin (SHS inner and SHS outer) tubes', *Thin-Walled Structures*, 40(2), pp. 199–213. doi: 10.1016/S0263-8231(01)00060-X.

List of Publications

Journals

1. Manigandan R, and Manoj Kumar (2022), '**Shape effect on axially loaded CFDST columns**'', *Steel and Composite Structures,* 43(6), 735-757. https://doi.org/10.12989/scs.2022.43.6.759

2. Manigandan R, Manoj Kumar, and Hrishikesh N. Shedge (2022), '**Experimental and numerical behavior of circular concrete-filled double skin steel tubular short columns under eccentric loads**'', *Asian Journal of Civil Engineering.* https://doi.org/10.1007/s42107-022-00473-5.

3. Manigandan R, Manoj Kumar and Hrishikesh N. Shedge (2022), '**Investigation on circular and octagonal concrete-filled double skinned steel tubular short columns under axial compression**'', *Steel and Composite Structures.* 44(1), 141-154. https://doi.org/10.12989/scs.2022.44.1.141

4. Manigandan R, Manoj Kumar, and Hrishikesh N. Shedge (2022), '**Behavior of circular concrete-filled double skin steel tubular columns under eccentric loads**'', *Structural Engineering and Mechanics. (Accepted).*

5. Manigandan R, Manoj Kumar, and Hrishikesh N. Shedge (2022), '**Tests and Numerical Analyses on Octagonal Concrete-Filled Double Skinned Steel Tubular Short Columns Under Axial Compression**'',*Steel and Composite Structures*, *(Accepted).*

6. Manigandan R, and Manoj Kumar (2022), '**Experimental and numerical behavior of Octagonal concrete-filled double skin steel tubular short columns under eccentric loads**'', *Steel and Composite Structures.* (Under review)

7. Manigandan R, and Manoj Kumar (2022), '**Investigation on Square Concrete-Filled Double Skinned Steel Tubular short columns under axial compression**'', *Steel and Composite Structures.* (Under review)

Conferences

1. Manigandan R, and Manoj Kumar (2022) "**Effect of the Imperfection on the Axial Loaded Rectangular CFST Column**," *Indian Structural Steel Conference - ISSC 2020*, in Indian Institute of Technology (IIT-Hyderabad), Hyderabad. January 2022.

2. Manigandan R, and Manoj Kumar (2022) "**Finite Element Analysis of Axially Loaded Octagonal CFDST Short Columns**," *12th Structural Engineering Convention - SEC2022*, in Malaviya National Institute of Technology (MNIT-Jaipur), Jaipur. 2022 **(Accepted)**.

3. Manigandan R, and Manoj Kumar (2022) "**Effect of Debonding on Axial Response of Concrete Filled Steel Tubular Columns**," *12th Structural Engineering Convention - SEC2022*, in Malaviya National Institute of Technology (MNIT-Jaipur), Jaipur. 2022 **(Accepted)**.

Brief biography of the candidate

Mr. Manigandan R is a Research Scholar in the Department of Civil Engineering at BITS Pilani. He received his B.E in Civil Engineering and M.E in Structural Engineering from the College of Engineering Guindy (CEG) Anna University, Tamil Nadu, in 2016 and 2018. His research interests are the analysis of concrete-filled steel tubular structures, non-linear analysis, and failure of composite structures. He has five journals and three conference publications.

Brief biography of the Supervisor

Dr. Manoj Kumar is an Associate Professor of Structural Engineering at the Department of Civil Engineering, BITS Pilani (Rajasthan). He received his B.E. (Civil Engineering), M.E. (Structural Engineering), and Ph.D. degrees from IIT Roorkee (erstwhile University of Roorkee) in the years 1994, 1997, and 2002 respectively. He was awarded the Senior Research Fellowship from CSIR, New Delhi, for pursuing his Ph.D. After completing his Ph.D., he joined the BITS, Pilani, as a lecturer and was subsequently promoted to Assistant Professor and Associate Professor in 2005 and 2013, respectively.

His research interests include Non-linear finite element analysis of concrete structures, Behavior of concrete box-girder bridges in the post-peak regime, Seismic analysis of shear-walled structures, Thermal analysis of concrete structures, and analysis of concrete-filled steel tubular structures. He has supervised two Ph.D. thesis and more than 25 M.E. Dissertations. He was the co-editor of the Proceedings of the National Conference on Structural Engineering and Mechanics-2004 (SEM-04) and has authored the chapters in five books. He visited USA, UK, and Singapore to present his research papers at international conferences. He has published more than 40 research papers in Journals and conferences. He is a reviewer for the Journal of Bridge Engineering (ASCE), Engineering structures (Elsevier), and the Indian Concrete Journal (ICJ). He has been the Head of the Civil Engineering Department of BITS Pilani during 2012-2016. He is a Fellow of the Institution of Engineers (India) and a Life Member of the Indian Road Congress and Indian Concrete Institute.